A Shallow Water Acoustic Model for an Ocean Stratified in Range and Depth. Volume II

Naval Underwater Systems Center

June 30, 1976

NUSC Technical Report 4887–II

A Shallow Water Acoustic Model For an Ocean Stratified in Range and Depth Volume II

WILLIAM G. KANABIS
Ocean Sciences and Technology Department

30 June 1976

NAVAL UNDERWATER SYSTEMS CENTER
New London Laboratory

PREFACE

This work was accomplished under NUSC Project No. A-650-09 and Navy Subproject and Task No. SF 52 552 702-14054, "Shallow Water Acoustic Theory and Measurements for Sonar System Design and Operation" (U), Principal Investigator, Dr. L. A. King (Code TA112). The sponsoring activity is Naval Sea Systems Command (Code SEA 06H1-4), Program Manager, A. Franceschetti.

The Technical Reviewer for this report was G. A. Leibiger (Code PA323).

REVIEWED AND APPROVED: 30 June 1976

R. W. Hasse
Associate Director for Sonar Research

The author of this report is located at the New London Laboratory, Naval Underwater Systems Center, New London, Connecticut 06320.

UNCLASSIFIED

SECURITY CLASSIFICATION OF THIS PAGE (When Data Entered)

REPORT DOCUMENTATION PAGE		READ INSTRUCTIONS BEFORE COMPLETING FORM
1. REPORT NUMBER TR 4887-II	2. GOVT ACCESSION NO.	3. RECIPIENT'S CATALOG NUMBER
4. TITLE (and Subtitle) A SHALLOW WATER ACOUSTIC MODEL FOR AN OCEAN STRATIFIED IN RANGE AND DEPTH VOLUME II		5. TYPE OF REPORT & PERIOD COVERED 6. PERFORMING ORG. REPORT NUMBER
7. AUTHOR(s) William G. Kanabis		8. CONTRACT OR GRANT NUMBER(s)
9. PERFORMING ORGANIZATION NAME AND ADDRESS Naval Underwater Systems Center New London Laboratory New London, Connecticut 06320		10. PROGRAM ELEMENT, PROJECT, TASK AREA & WORK UNIT NUMBERS A-650-09 SF 52 552 702-14054
11. CONTROLLING OFFICE NAME AND ADDRESS Naval Sea Systems Command (SEA 06H1-4) Washington, D.C. 20362		12. REPORT DATE 30 June 1976 13. NUMBER OF PAGES 130
14. MONITORING AGENCY NAME & ADDRESS(if different from Controlling Office)		15. SECURITY CLASS. (of this report) UNCLASSIFIED 15a. DECLASSIFICATION/DOWNGRADING SCHEDULE

16. DISTRIBUTION STATEMENT (of this Report)

Approved for public release; distribution unlimited.

17. DISTRIBUTION STATEMENT (of the abstract entered in Block 20, if different from Report)

18. SUPPLEMENTARY NOTES

19. KEY WORDS (Continue on reverse side if necessary and identify by block number)

Acoustic models
Shallow water theory
Shallow water measurements
BIFI range measurements
Mode theory
A Shallow Water Acoustic Model (Volume I)

20. ABSTRACT (Continue on reverse side if necessary and identify by block number)

Volume II describes the procedures by which the validity of the shallow water acoustic model was tested. The testing was performed in two ways. First, predictions obtained by using the model were compared against those obtained by using other models in standard cases. Second, comparisons were made between theoretical predictions obtained by using the model and experimental results under a wide variety of environmental conditions.

DD FORM 1 JAN 73 1473 EDITION OF 1 NOV 65 IS OBSOLETE
S/N 0102-014-6601

UNCLASSIFED

SECURITY CLASSIFICATION OF THIS PAGE (When Data Entered)

TABLE OF CONTENTS

	Page
LIST OF TABLES	ii
LIST OF ILLUSTRATIONS	ii
INTRODUCTION	1
COMPARISONS WITH OTHER MODELS	1
COMPARISONS WITH EXPERIMENTAL DATA	10
Tests Using Explosives in BIFI Range	10
Tests Using CW Sources in BIFI Range	23
Tests Using Explosives In Baltic Sea.	36
Tests Using Explosives In Deep Water	62
Tests Using CW Sources Over Sloping Bottom	71
Tests Using Array of CW Sources in BIFI Range	81
CONCLUSIONS	117
REFERENCES	119

LIST OF TABLES

Table		Page
1	Comparison of Calculated α_m	2
2	Test Case 3A	2
3	Time Smear Analysis at 127 Hz	24
4	Typical Sound-Velocity Profile for January 1973 in the BIFI Range	81
5	Element Amplitudes and Phases for Modes 1 Through 6	83
6	Cosine Weighting of Array Elements	86
7	Phases of Array Elements in Steering	87
8	Typical Sound-Velocity Profile for August 1972 in the BIFI Range	88
9	Relative Levels of Modes During August-September Test	91
10	Relative Levels of Modes During November-December Test	91

LIST OF ILLUSTRATIONS

Figure		Page
1	Velocity Profile, Test Case	4
2	Propagation Loss Versus Range, Test Case, Shallow Water Model	5
3	Propagation Loss Versus Range, Test Case, FFP Program	5
4	Case 3A, Predictions of Kanabis (NUSC)	6
5	Case 3A, Predictions of Bartberger (NADC)	7
6	Case 3A, Predictions of DiNapoli (NUSC)	8
7	Case 3A, Predictions of Ingenito (NRL)	9
8	BIFI Range	13
9	Depth Profile, BIFI Range	14
10	Velocity Profile, 8 August 1967	14
11	Ray Equivalent, Frequency 70 Hz, Mode 1	15
12	Ray Equivalent, Frequency 112 Hz, Mode 1	16
13	Ray Equivalent, Frequency 141 Hz, Mode 1	17
14	Ray Equivalent, Frequency 224 Hz, Mode 1	17
15	Propagation Loss Versus Frequency, August 1967	18
16	Velocity Profile, 30 January 1968	19
17	Propagation Loss Versus Frequency, January 1968 and August 1967	20
18	Velocity Profiles, 2 October 1968	21
19	Propagation Loss Versus Frequency, August 1967 and September 1968	22
20	Outline of Analysis	27
21	Typical Sound-Velocity Profile, August 1970	28
22	Amplitude Versus Depth, Frequency 127 Hz, Mode 1, August 1970	29
23	Propagation Loss Versus Range, Frequency 127 Hz, Source Depth 55 ft, Receiver Depth 100 ft, Mode 1, August 1970	30

LIST OF ILLUSTRATIONS (Cont'd)

Figure		Page
24	Standard Deviation of Signal Level Versus Range, Frequency 127 Hz	31
25	Typical Sound-Velocity Profile, October 1970	32
26	Amplitude Versus Depth, Frequency 127 Hz, Mode 1, October 1970	33
27	Propagation Loss Versus Range, Frequency 127 Hz, Source Depth 55 ft, Receiver Depth 100 ft, Mode 1, October 1970	34
28	Propagation Loss Versus Range, Change in C_B from 2.5- to 3.5-mile Ranges, Frequency 127 Hz, Source Depth 55 ft, Receiver Depth 100 ft, Mode 1, October 1970	34
29	Bottom Structure in BIFI Range	35
30	Typical Sound-Velocity Profiles in Baltic Sea	40
31	Operating Area	41
32	Bornholm Summer, Sound-Velocity Profile	42
33	Bornholm Summer, Ray Equivalent, Mode 1, at 50 and 100 Hz	43
34	Bornholm Summer, Propagation Loss Versus Frequency Range 0.56 nmi, Source Depth 10 m, Receiver Depth 12 m, Water Depth 45 m	44
35	Eckernforde Summer, Sound-Velocity Profile	45
36	Eckernforde Summer, Ray Equivalent, Mode 1, at 100, 200, and 800 Hz	46
37	Eckernforde Summer, Propagation Loss Versus Frequency, Range 1.16 nmi, Source Depth 5 m, Receiver Depth 6 m, Water Depth 24 m	47
38	Eckernforde Summer Versus Bornholm Summer, Propagation Loss Versus Frequency, Range 1.1 nmi	48
39	Bornholm Winter, Sound-Velocity Profile	49
40	Bornholm Winter, Ray Equivalent, Mode 1, at 50, 100, and 200 Hz	50
41	Bornholm Winter, Propagation Loss Versus Frequency, Range 0.60 nmi, Source Depth 12 m, Receiver Depth 10 m, Water Depth 45 m	51
42	Bornholm Winter Versus Bornholm Summer, Propagation Loss Versus Frequency, Range 0.6 nmi	52
43	Eckernforde Winter, Sound-Velocity Profile	53
44	Eckernforde Winter, Ray Equivalent, Mode 1, at 100, 200, and 800 Hz	54
45	Eckernforde Winter, Propagation Loss Versus Frequency, Range 2.75 nmi, Source Depth 6 m, Receiver Depth 5 m, Water Depth 24 m	55
46	Eckernforde Winter Versus Eckernforde Summer, Propagation Loss Versus Frequency, Range 1.1 nmi	56
47	Eckernforde Winter Versus Bornholm Winter, Propagation Loss Versus Frequency, Range 0.6 nmi	57

LIST OF ILLUSTRATIONS (Cont'd)

Figure		Page
48	Bornholm Summer, Propagation Loss Versus Range, Theory Versus Experiment, Source Depth 20 m, Receiver Depth 20 m, Frequency 315 Hz, Mode 1	58
49	Bornholm Summer, Propagation Loss Versus Range, Theory Versus Experiment, Source Depth 20 m, Receiver Depth 20 m, Frequency 315 Hz, Modes 1-3	59
50	Bornholm Summer, Sound-Velocity Profile Showing Deterioration of the Sound Channel	60
51	Bornholm Summer, Propagation Loss Versus Range for Three Receiver Depths, Theory Versus Experiment, Source Depth 20 m, Frequency 1000 Hz, Modes 1-8	61
52	Velocity Profiles Along Deep Water Tract	63
53	Comparison of Two Velocity Profiles Along Tract	64
54	Propagation Loss Versus Range, Source Depth 18 m, Receiver Depth 4300 m, Frequency 50 Hz	65
55	Propagation Loss Versus Range, Theory (Single Profile), and Experiment, Source Depth 18 m, Receiver Depth 4300 m, Frequency 50 Hz	65
56	Propagation Loss Versus Range, Theory (Actual Stratification), and Experiment, Source Depth 18 m, Receiver Depth 4300 m, Frequency 50 Hz	66
57	Received Pulse, Predicted at 100 nmi for 100-msec Pulse Transmitted at 50 Hz	67
58	Received Pulse, Predicted at 200 nmi for 100-msec Pulse Transmitted at 50 Hz	68
59	Received Pulse, Predicted at 300 nmi for 100-msec Pulse Transmitted at 50 Hz	69
60	Propagation Loss Versus Range, Theory (Time-Limited Signal and Actual Stratification), and Experiment, Source Depth 18 m, Receiver Depth 4300 m, Frequency 50 Hz	70
61	Bottom Profile (First Tract)	72
62	Typical Velocity Profile (First Tract)	73
63	Experimental Results Showing Propagation Loss Versus Range (First Tract)	74
64	Propagation Loss Versus Range, Comparison Between Experiment and Theory (No Mode Conversion)	75
65	Propagation Loss Versus Range, Comparison Between Experiment and Theory (Considering Mode Conversion)	76
66	Bottom Profile (Second Tract)	77
67	Typical Velocity Profile (Second Tract)	78
68	Experimental Results Showing Propagation Loss Versus Range (Second Tract)	79
69	Propagation Loss Versus Range, Comparison Between Experiment and Theory	80
70	BIFI Range Showing Array of Projectors	93
71	Loss Profile, Comparison Between Experiment and Theory, Range 0.968 nmi, Winter, Modes 1-6	94

LIST OF ILLUSTRATIONS (Cont'd)

Figure		Page
72	Loss Profile, Comparison Between Experiment and Theory, Range 0.968 nmi, Winter, Modes 1-12	95
73	Loss Profile, Comparison Between Experiment and Theory, Range 3.14 nmi, Winter	96
74	Loss Profile, Comparison Between Experiment and Theory, Range 4.42 nmi, Winter	97
75	Loss Profile, Comparison Between Experiment and Theory, Range 5.46 nmi, Winter	98
76	Loss Profile, Comparison Between Experiment and Theory, Range 6.57 nmi, Winter	99
77	Loss Profile, Comparison Between Experiment and Theory, Range 7.84 nmi, Winter	100
78	Loss Profile, Comparison Between Experiment and Theory, Range 8.66 nmi, Winter	101
79	Loss Profile, Cosine Weighting, Comparison Between Experiment and Theory, Range 0.97 nmi, Winter	102
80	Loss Profile, Cosine Weighting, Comparison Between Experiment and Theory, Range 3.14 nmi, Winter	103
81	Loss Profile, Cosine Weighting, Comparison Between Experiment and Theory, Range 4.42 nmi, Winter	104
82	Loss Profile, Steering, Comparison Between Experiment and Theory, Range 0.97 nmi, Winter	105
83	Loss Profile, Steering, Comparison Between Experiment and Theory, Range 3.14 nmi, Winter	106
84	Loss Profile, Steering, Comparison Between Experiment and Theory, Range 4.42 nmi, Winter	107
85	Loss Profile, Comparison Between Experiment and Theory, Range 1.0 nmi, Summer	108
86	Loss Profile, Comparison Between Experiment and Theory, Range 1.08 nmi, Summer	109
87	Loss Profile, Comparison Between Experiment and Theory, Range 1.98 nmi, Summer	110
88	Loss Profile, Comparison Between Experiment and Theory, Range 2.18 nmi, Summer	111
89	Loss Profile, Comparison Between Experiment and Theory, Range 3.10 nmi, Summer	112
90	Loss Profile, Comparison Between Experiment and Theory, Range 3.23 nmi, Summer	113
91	Temperature Sensors on Tower Near Block Island	114
92	Time History of Oceanographic Measurements, from 1433 on 30 August 1972 to 0942 on 14 September 1972	115
93	Time History of Oceanographic Measurements, from 1100 on 27 November 1972 to 1210 on 1 December 1972	116

REVERSE BLANK

A SHALLOW WATER ACOUSTIC MODEL FOR AN OCEAN STRATIFIED IN RANGE AND DEPTH VOLUME II

INTRODUCTION

Volume I of this report discussed the shallow water acoustic model. The theoretical basis underlying the model and the implementation of the model through a computer program were described. Volume II will describe the present status of the validation procedure for the model. First comparisons with other models through the use of standard cases are described; second comparisons are made with actual data. The primary purpose of the comparisons with other models is to test the mathematics of the calculations employed in the model. The primary purpose of the comparisons with actual data is to test the physical assumptions inherent in the model.

COMPARISONS WITH OTHER MODELS

Comparisons with other models by matching the results of standard cases is a fundamental step in model validation. For the validation of the shallow water model described herein, such comparisons were first made against the model of Bartberger and Ackler (reference 1) and the Fast Field Program (FFP) model of DiNapoli (reference 2). These results have been described previously in reference 3. Later similar comparisons were made at an Acoustic Environmental Support Detachment (AESD) Workshop on Acoustic-Propagation Modeling by Non-Ray-Tracing Techniques (reference 4) on 22-25 May 1973 against 16 different models. The results of both comparisons are summarized below.

Comparisons with the FFP and Bartberger and Ackler models were made by using a test case illustrated in figure 1. The stratification was assumed to be constant with range and the stratification at any given range is illustrated in the figure. The velocity of sound in the water decreases linearly with depth from 5000 to 4982 ft/sec over the 360-ft water depth. The velocity of sound in the homogeneous semi-infinite bottom is 5006 ft/sec. The density is the same in both water and bottom. The frequency is 1000 Hz.

Since each mode is defined by a unique horizontal wave number κ_m, the values of κ_m obtained by using each model were compared. Such a comparison is shown in table 1. In the table, the values of κ_m obtained by Bartberger and Ackler are compared with the values obtained by using the model described in this report. It can be seen that the results agree to the fourth decimal place, and hence tend to support the validity of the two procedures for determination of eigenvalues (normal modes). Furthermore, similar good agreement was obtained for this test case by using the FFP model, where the eigenvalues were derived from the peaks of a plot of the Green's function as a function of horizontal wave number.

Table 1. Comparison of Calculated κ_m

Mode	κ_m (Kanabis)	κ_m (Bartberger and Ackler)
1	3.78104	3.78105
2	3.77896	3.77896
3	3.77725	3.77725
4	3.77574	3.77575
5	3.77436	3.77437
6	3.77309	3.77309
7	3.77186	3.77187
8	3.77063	3.77065
9	3.76932	3.76933
10	3.76782	3.76784
11	3.76617	3.76618

Another theoretical result tested was the calculation of propagation loss as a function of range for the test case. The depths of the point source and receiver were taken to be 36 and 10 ft, respectively. The comparison of results with those of the FFP is shown in figures 2 and 3. It can be seen from the figures that the mean levels are the same at all ranges and the interference patterns are virtually identical at all ranges, except those very near the source. The differences near the source result from the inclusion in FFP of the continuous spectrum in the sound field. This component contributes to the field significantly at short ranges but is attenuated rapidly so that it is usually insignificant at longer ranges. The procedure described in this report neglects the continuous spectrum and considers only energy corresponding to angles of incidence which exceed the critical angle, so that there is "total" reflection at the boundaries.

Similarly, comparisons were made with 16 different models at the AESD workshop on Acoustic-Propagation Models by Non-Ray-Tracing Techniques in May 1973. Comparisons were made with other models for three basic test cases. In all these cases, the stratification was assumed to be constant with range. Two of the cases were used to predict propagation loss as a function of range in deep water environments. A third case was used to predict propagation loss in a shallow water environment. More than 50 predictions were generated by 17 different models, in these cases. The plots of the predicted loss as a function of range are contained in reference 4. Generally speaking, in both the deep and shallow water cases, the predictions obtained from the model described herein were consistent with those of the majority of the other models.

To illustrate the type of agreement obtained between this model and others presented at the AESD workshop, the discussion of a shallow water test case (case 3A described in reference 4) considered at that meeting follows. This is a case which describes a typical shallow water situation and thus can be considered a representative standard case. In this case, the stratification, assumed to be constant with range, is

given in table 2. In addition, the assumed source and receiver depths and the frequency of the transmitted signal are given in the table. All depths are measured down from the ocean's surface.

Table 2. Test Case 3A

Depth (ft)	Sound Velocity (ft/sec)	ρ (g/cm^3)
0	5000	1.0
50	4990	1.0
150	4980	1.0
150+	5056.8	1.4
Source depth	20 ft	
Receiver depth	40 ft	
Frequency	500 Hz.	

Ten models in the non-ray-tracing category were exercised against this case. Eight of the ten agreed closely with respect to mean level. The predictions of four models which agreed closely are shown in figures 4 through 7. Figure 4 shows the predictions obtained by using the model described herein. Figures 5 and 6 show the predictions obtained from the models used for the purpose of comparison in the first case described above. Figure 5 is obtained from the model of Bartberger and Ackler. Figure 6 is obtained from the model of DiNapoli. Figure 7 shows predictions obtained by using the shallow water model developed at the Naval Research Laboratory (NRL) (reference 5). In all four predictions, the transmission loss increases, as expected, in a manner corresponding to cylindrical spreading. At a range of 1 nautical mile (nmi) the mean loss is roughly 55 dB. The loss increases to 68 dB at a range of 20 nmi. The size of the fluctuations in loss about the mean differ, but this may be due to the fact that the standard increment in range between the loss calculations was not specified to the modelers. The models of Leibiger, Weinberg, Cybulski, and Blatstein, Uberall, and Newman yielded essentially the same predictions.

Besides the eight models showing consistent results, there were two others presented at the AESD workshop which did not agree with the majority. In one case, the noted differences were due to computer programming error (reference 6) and in the other, range step size used in the numerical integration required in the model may have been chosen poorly (reference 7). Therefore, all results which differ from the majority of tested models appear to have a logical explanation, which lends appreciable credibility to the larger group.

The comparisons cited in this section build confidence in the validity of the model when stratification is constant with range. However, no such comparisons are available when the stratification varies with range, mostly because of the difficulty in fabricating a good standard case. This difficulty stems from the inability to obtain an exact solution for the sound field, when the stratification varies with range. Work is under way by Deavenport to obtain exact solutions for an isovelocity sound velocity profile in a wedge. Similarly, it is hoped that confidence in the validity of the model can be increased for more complicated cases.

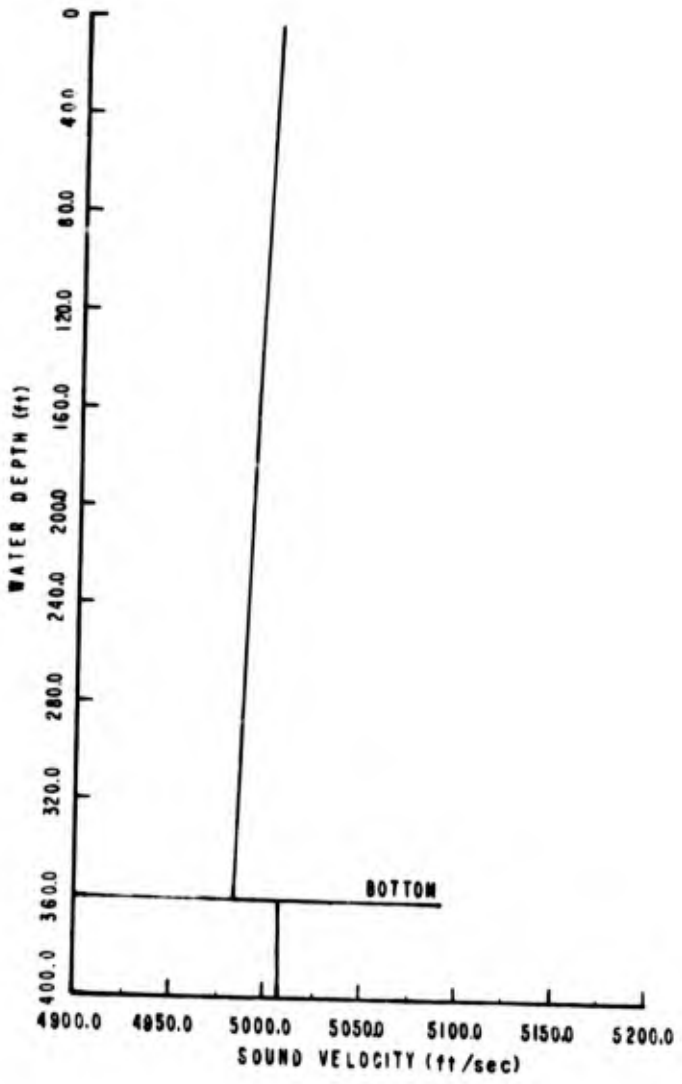

Figure 1. Velocity Profile, Test Case

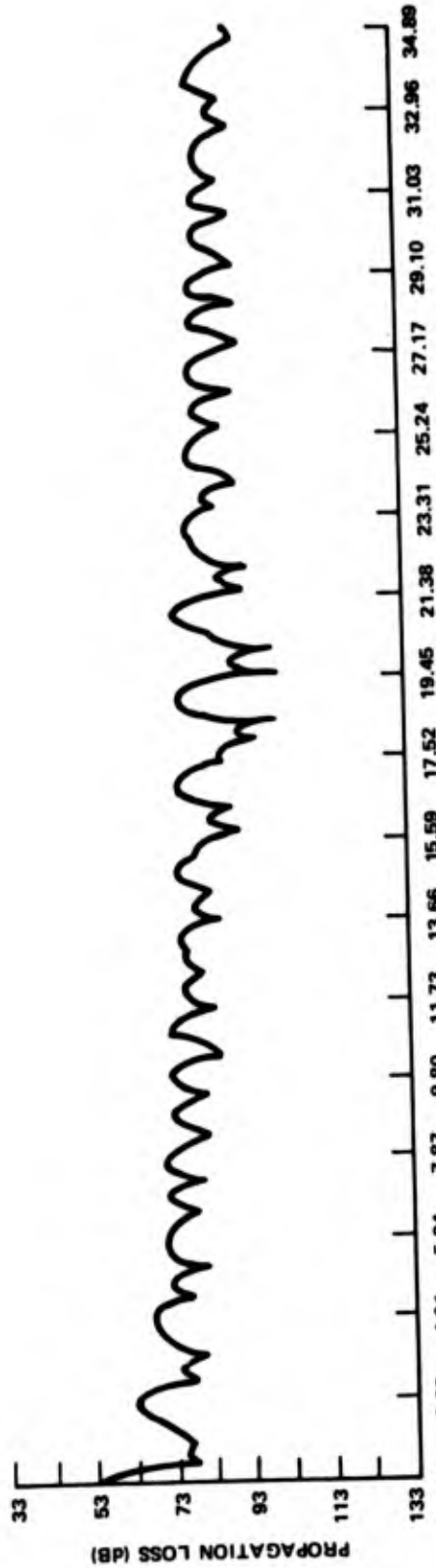

Figure 2. Propagation Loss Versus Range, Test Case, Shallow Water Model

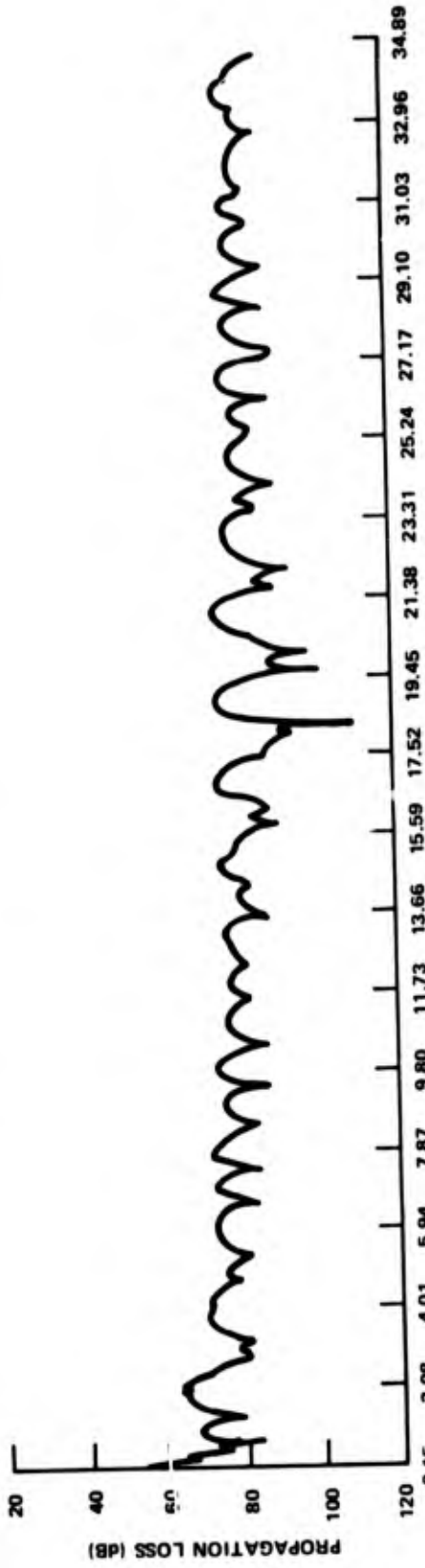

Figure 3. Propagation Loss Versus Range, Test Case, FFP Program

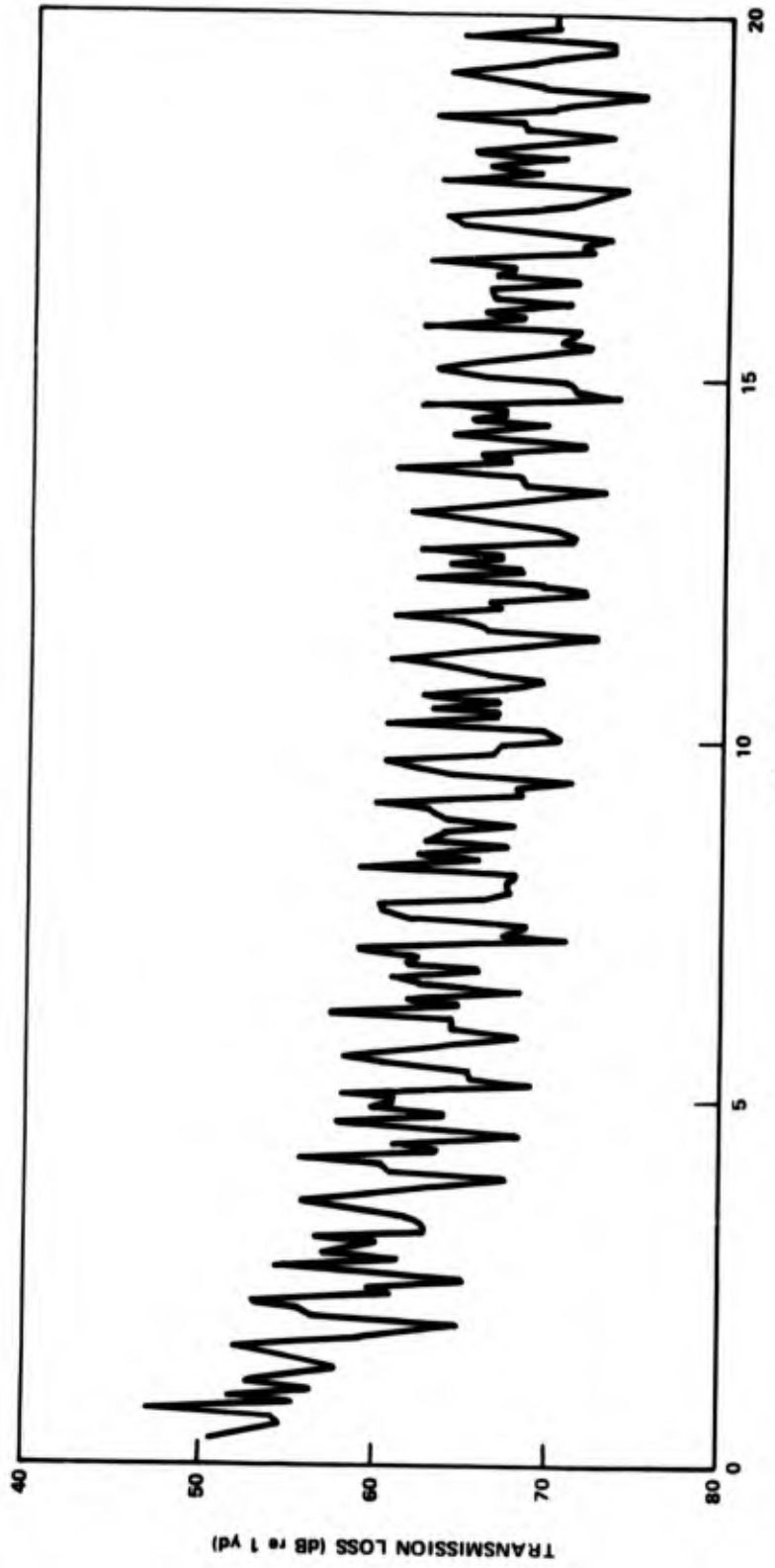

Figure 4. Case 3A, Predictions of Kanabis (NUSC)

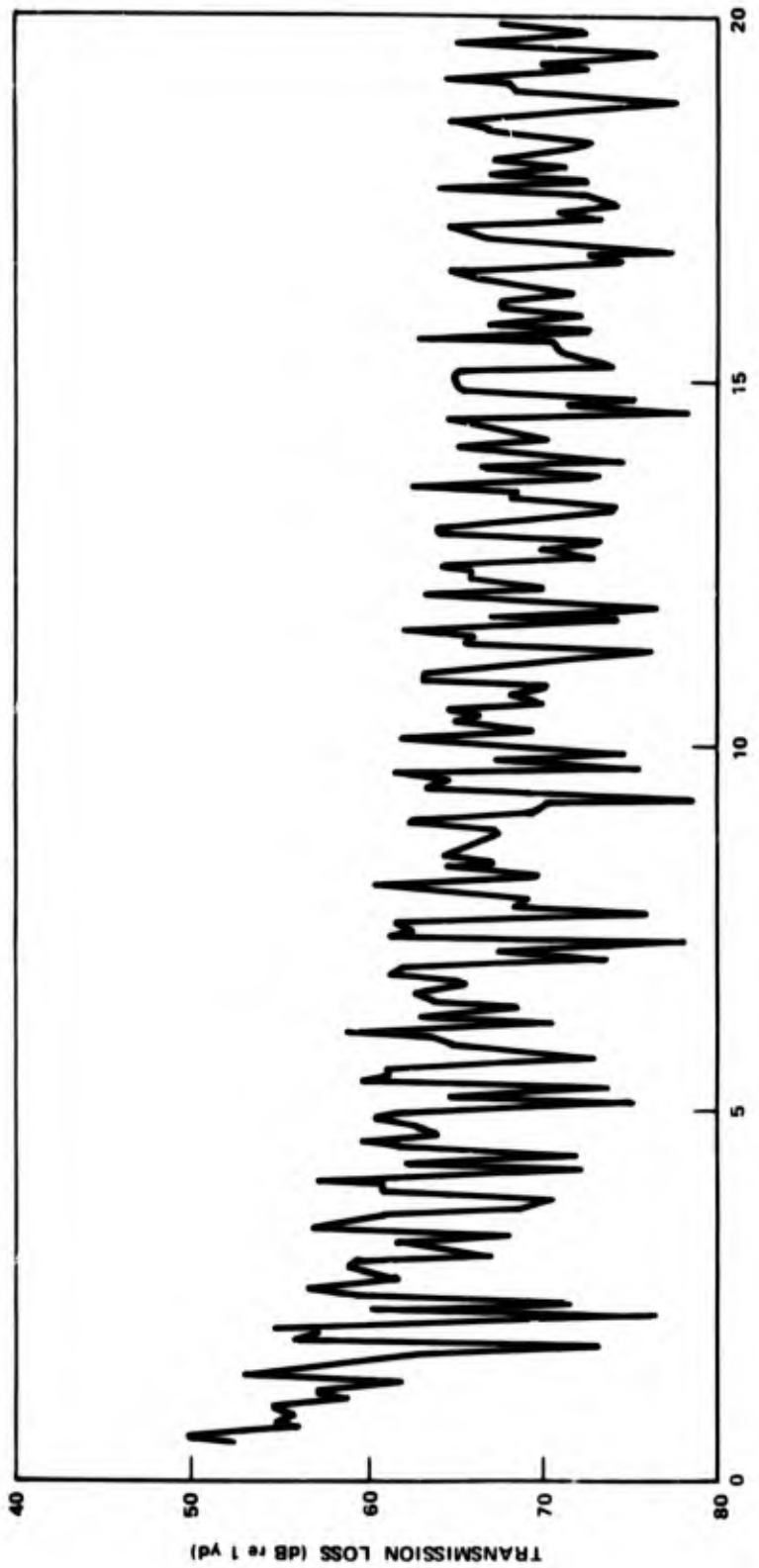

Figure 5. Case 3A, Predictions of Bartberger (NADC)

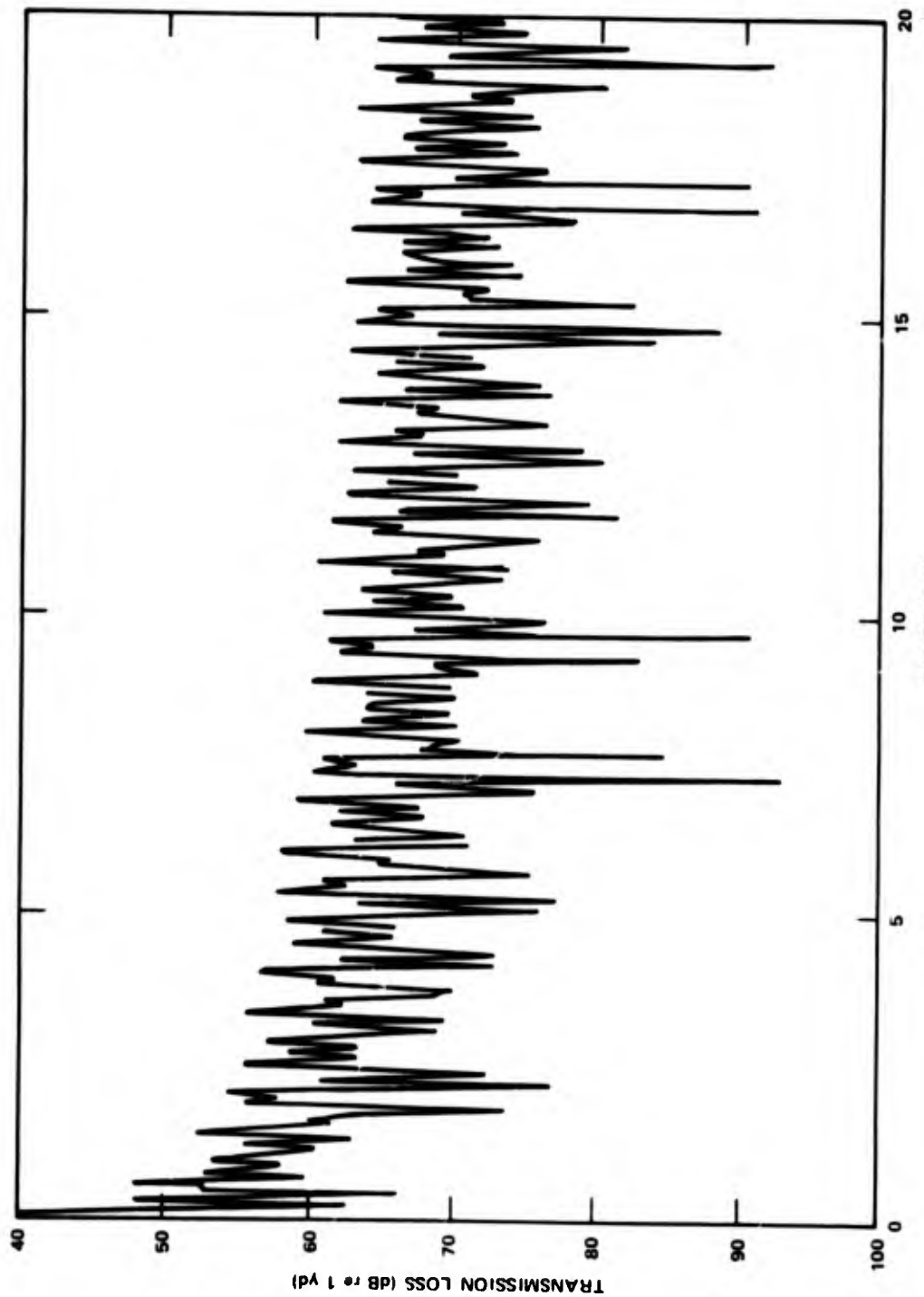

Figure 6. Case 3A, Predictions of DiNapoli (NUSC)

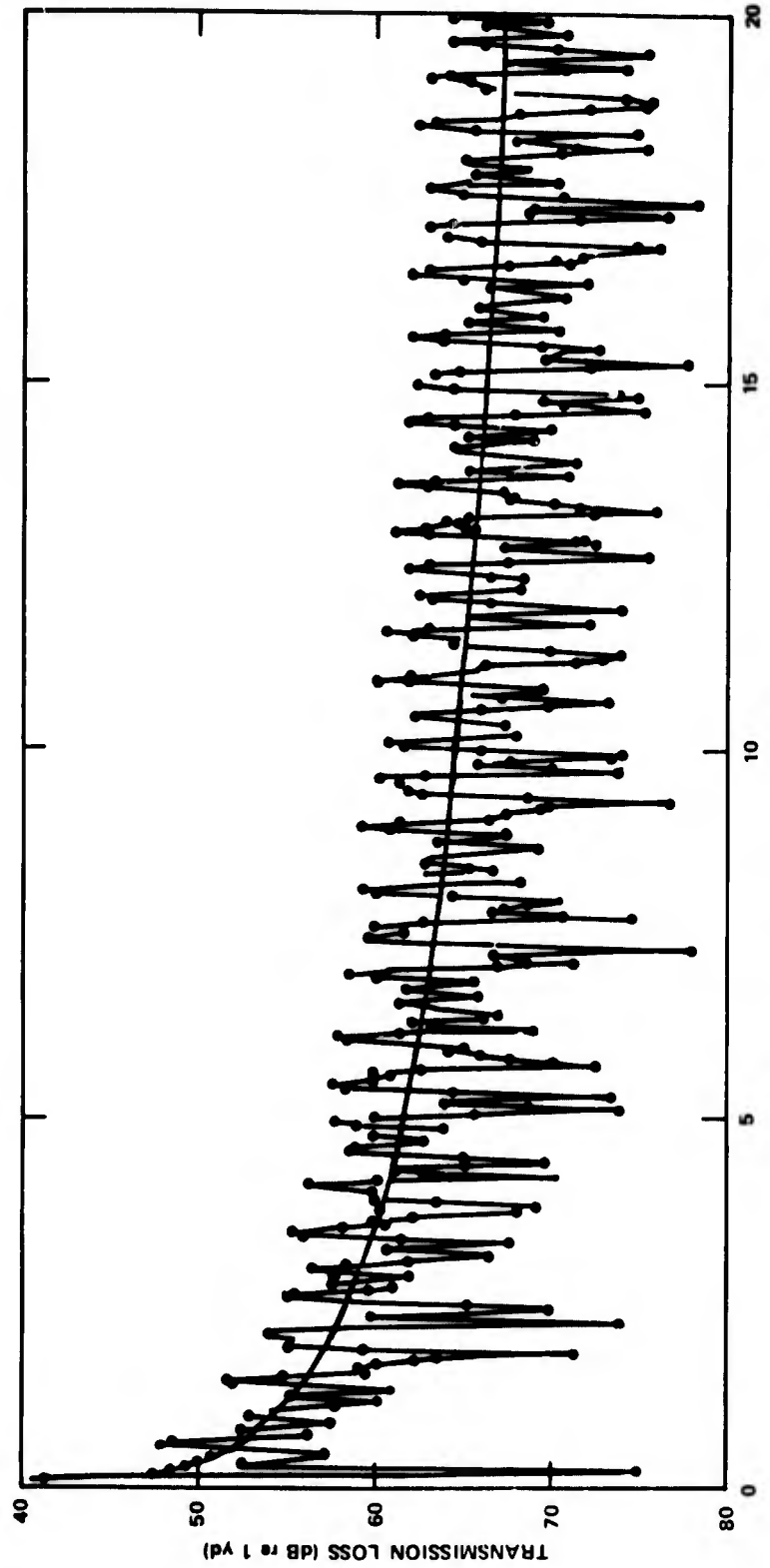

Figure 7. Case 3A, Predictions of Ingenito (NRL)

COMPARISONS WITH EXPERIMENTAL DATA

Another step in model validation is the comparison of experimental results with theoretical predictions under a wide variety of environmental conditions. In this section, such comparisons are described. The order of presentation of the comparisons roughly follows the chronological order of the experiments which, in turn, parallels the growth in sophistication of the model. It should be noted by the reader that the predictions reflect the capabilities of the model at the time of the analysis. Although these capabilities may have increased with time, the law of diminishing returns has discouraged any effort to recompute the predictions by using more powerful capabilities in the analysis.

Comparisons between theoretical and experimental results will be described for six sets of data. The first set, which spurred our first major effort in comparisons of this type, was obtained from tests conducted in the BIFI range, using explosive sources. This work has been described previously in detail in references 8 through 10. These tests with explosive sources provided a broad overview of acoustic propagation. Thereafter, tests that used CW sources allowed examination of the fine structure of propagation in the BIFI range (reference 11). The model was tested in another geographic location after tests using explosives were conducted in the Baltic Sea (reference 12). Although this model has been used primarily to predict acoustic propagation in shallow water, a deep water experiment provided data which first tested the capability of the model to accommodate changes in stratification with range as well as with depth, without excessive difficulties due to the bottom (reference 13). Later comparisons were made for sound propagated in a medium in which there was a sloping bottom in the Norwegian Sea. Finally, back at the BIFI range, tests using an array of sources allowed an evaluation of the model in predicting the sound field produced by an array.

TESTS USING EXPLOSIVES IN BIFI RANGE

A series of tests with explosives as sources was conducted in the BIFI range, shown in figure 8, between August 1967 and October 1968. In these tests, referred to as "Experiment 2" in reference 14, propagation loss was measured under a wide variety of sound velocity profile conditions. For all these tests, explosives were detonated at depths of 50 and 75 ft at point A in figure 9, near Block Island. Signals were received by a bottom-mounted hydrophone located at a depth of 155 ft at point B off Fishers Island. The explosive charges used were 0.5- and 1-lb blocks of TNT. Propagation loss as a function of frequency was determined by finding the energy content of each received shot for a 1-Hz band of logit frequencies from 56 to 562 Hz. The levels thus derived were subtracted from the source levels for the explosives as given by Weston (reference 15). To gain further insight into what happens in the sound channel, a dispersion analysis by means of the Kay Missilyzer was done on the signals received from the explosive sources. As a result of this analysis, it was concluded that at the frequencies considered in these tests, the first mode dominates in the signals received at point B in figure 9. Therefore, it has been assumed in all

the theoretical calculations of propagation loss in the experiment, that the pressure field at the receiver consists only of the first mode.

Comparisons were made between theoretical predictions and experimental results. However, one difficulty in the analysis, common to all analyses of shallow water acoustic propagation, was evident. This difficulty can result when there is a strong interaction of the acoustic field with the ocean bottom, and as a result there is observed loss beyond that predicted under the assumption of a sound field composed of unattenuated modes. Although this excess loss is due to the effect of the bottom, the exact loss mechanism is rarely determined with any degree of certainty. Useful results can still be obtained from analysis under these conditions. For instance, in the case of these explosive experiments, bottom loss was determined as a function of frequency and angle of incidence of sound hitting the bottom per unit distance and per bounce. These results are tabulated in reference 3, which shows the necessity of incorporating bottom loss determined empirically.

It is possible to test the consistency of the theoretical predictions with the theoretical results. This can be done by comparing qualitatively the measured propagation loss as a function of frequency against that expected due to theoretical considerations based upon the characteristics of the ray equivalents of modes, as defined in the first volume of this report.

Three major factors account for the relationship between propagation loss and frequency, for a given mode. First, excitation pressure (defined in volume I of this report) generally decreases with increasing frequency, which has the effect of increasing propagation loss with increasing frequency. Second, skip distance, in general, increases with frequency, if the ray equivalent strikes both boundaries, thereby decreasing propagation loss with increasing frequency. At frequencies of 100 Hz and below, the first mode strikes the bottom on the order of 100 times, while propagating from Block Island to Fishers Island under all thermal conditions. Hence, in the BIFI range, these two effects seem to cause a minimum of propagation loss at a frequency of around 100 to 200 Hz. This minimum is either enhanced or depressed by a third factor, the frequency at which vertexing of the ray equivalent commences. If vertexing occurs near the minimum frequency, the minimum is enhanced; if it occurs away from the minimum, the minimum is rendered less pronounced and relatively less loss occurs at frequencies close to the frequency of the maximum skip distance.

This effect is illustrated in the following examples. The August 1967 tests were conducted when the velocity profile possessed a large negative gradient, as shown in figure 10. At low frequencies, the skip distance increases with frequency, as shown in figures 11 and 12. This increase continues until a frequency is reached at which the ray vertexes near the surface (figure 13). Thus the skip distance is a maximum at 141 Hz, when the angle at which energy strikes the surface first becomes 90°. Thereafter, as shown in figure 14, the ray vertexes at increasing depth for higher frequencies, and the skip distance decreases. As a result, as shown in figure 15, the measured propagation loss as a function of frequency shows a deep minimum at 141 Hz.

The tests in January 1968 were conducted when the typical velocity profile had a small positive gradient. All five profiles taken over the range were similar to that shown in figure 16 (taken from reference 16). For comparison, figure 17 exhibits plots of measured propagation loss as a function of frequency for both the January 1968 and the August 1967 tests. It can be seen that propagation loss was much less in January than in August. This may be attributed to the fact that for a positive gradient, energy tends to concentrate higher in the water column, and so interacts less with the bottom. The maximum skip distance does not occur until about 700 Hz, and hence the minimum in loss is less pronounced and the decrease in propagation loss is largest at the highest frequencies measured in January.

The September 1968 tests were performed when the velocity profiles* taken over the range exhibited moderately negative gradients, as shown in figure 18 (taken from reference 16). Figure 19 gives plots of measured propagation loss as a function of frequency for the August 1967 and September 1968 tests. In September, the maximum skip distance occurred at 315 Hz, as opposed to 141 Hz in August. Hence, in September, the minimum is less pronounced and the propagation loss is lower in August at low frequencies and lower in September at the higher frequencies, in accordance with the distribution of skip distances as a function of frequency.

For all tests, two sets of predictions were made: first predictions were made while assuming that the stratification of the medium was constant with range, second predictions were made while approximating the actual range-dependent stratification that existed at the time of the tests. For the tests in which negative gradients obtained, the predicted field at the bottom-mounted receiver was similar for both sets of predictions. However, for the January 1968 tests, the differences were considerable, with the predictions using the range-dependent stratification physically more plausible. Therefore, the inclusion of the range-dependent stratification appears to be an improvement over the simpler assumption of constant stratification with range. This conclusion has been borne out in similar comparisons described later in this report.

*These profiles were obtained two days after the tests were performed.

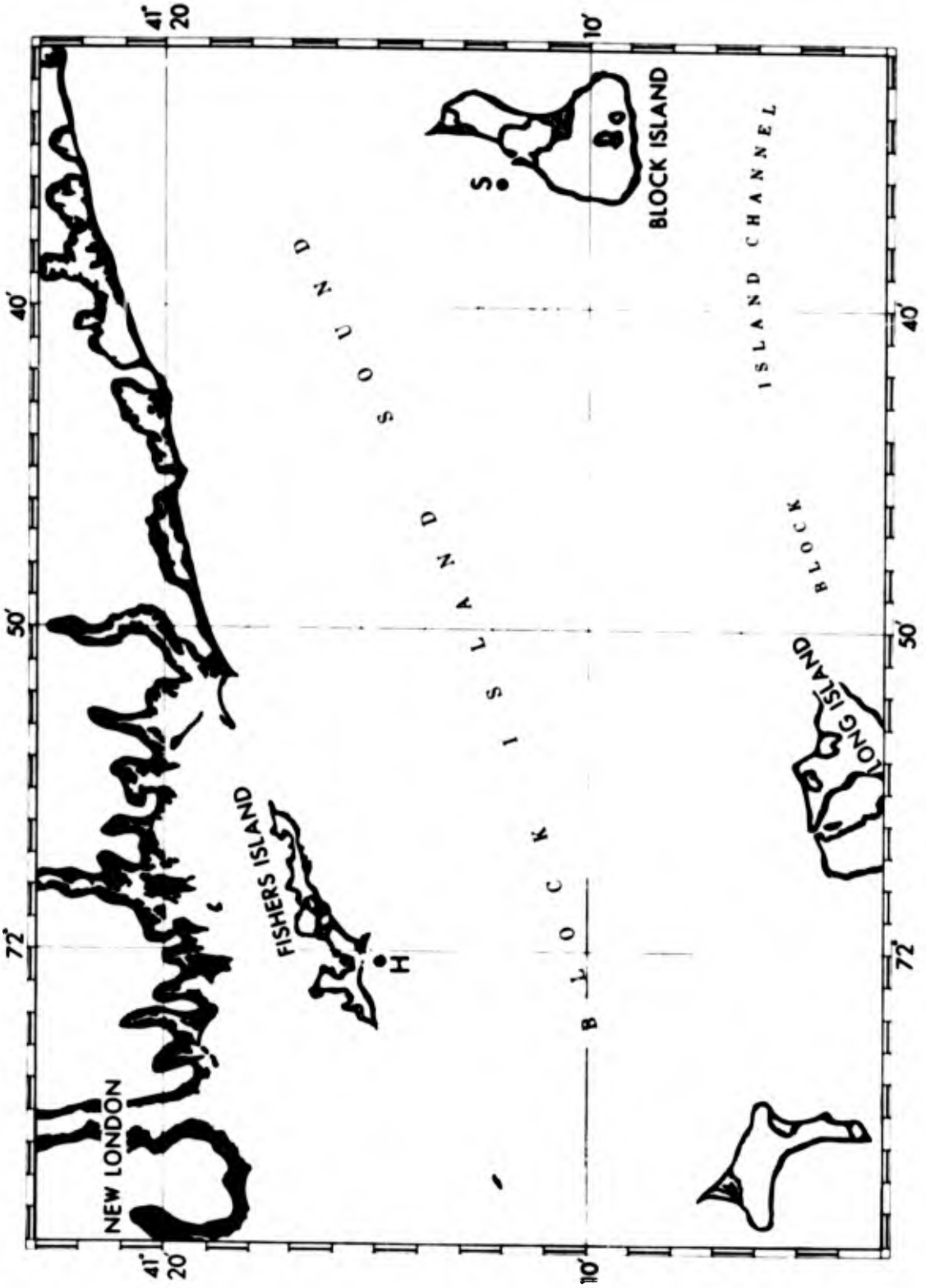

Figure 8. BIFI Range

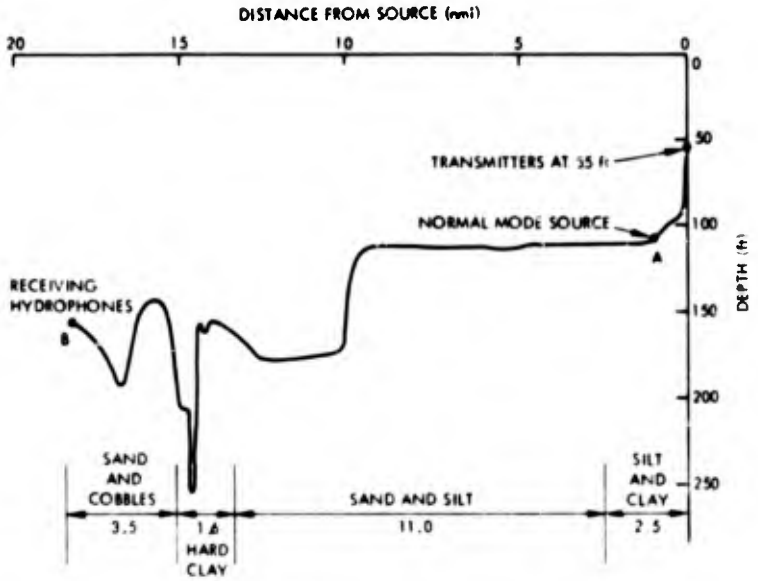

Figure 9. Depth Profile, BIFI Range

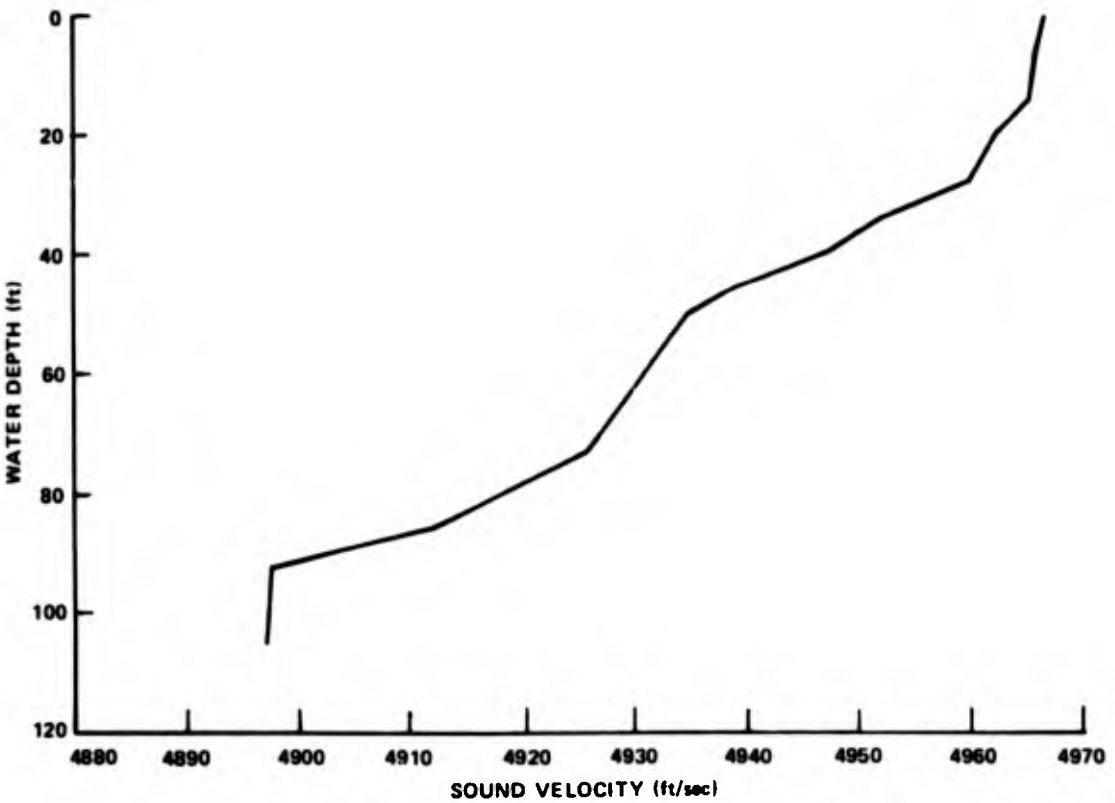

Figure 10. Velocity Profile, 8 August 1967

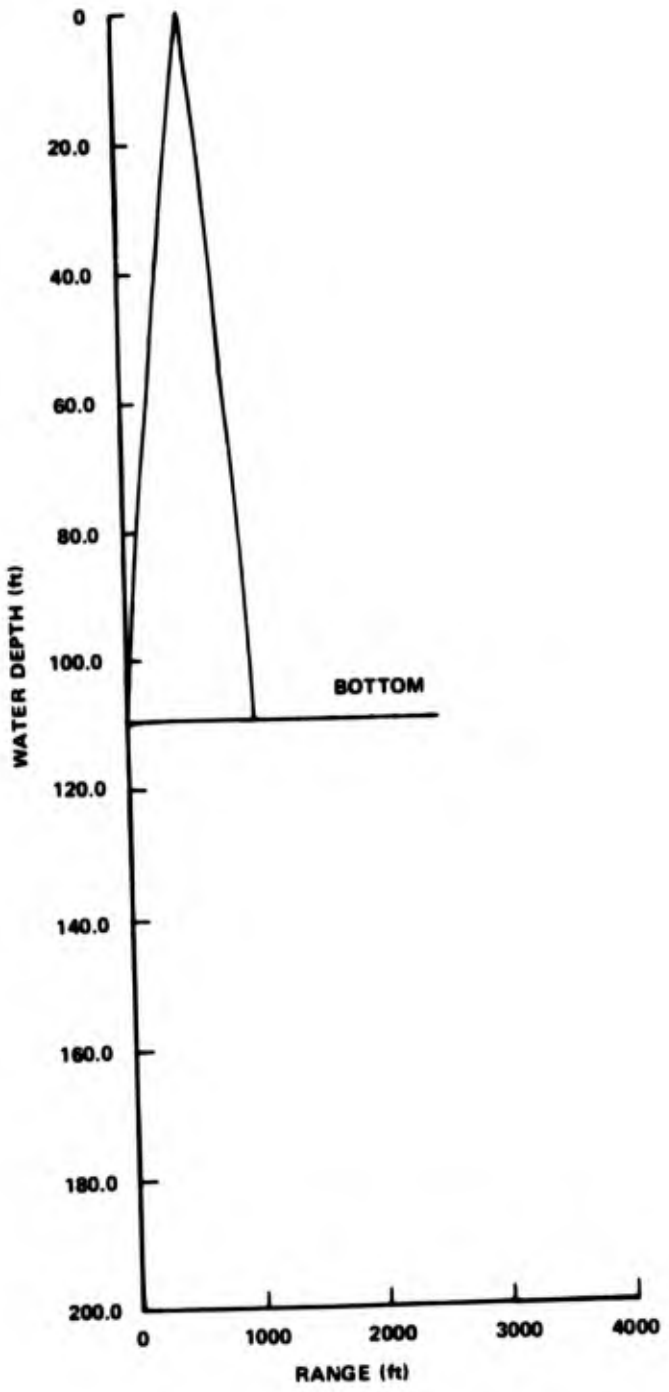

Figure 11. Ray Equivalent, Frequency 70 Hz, Mode 1

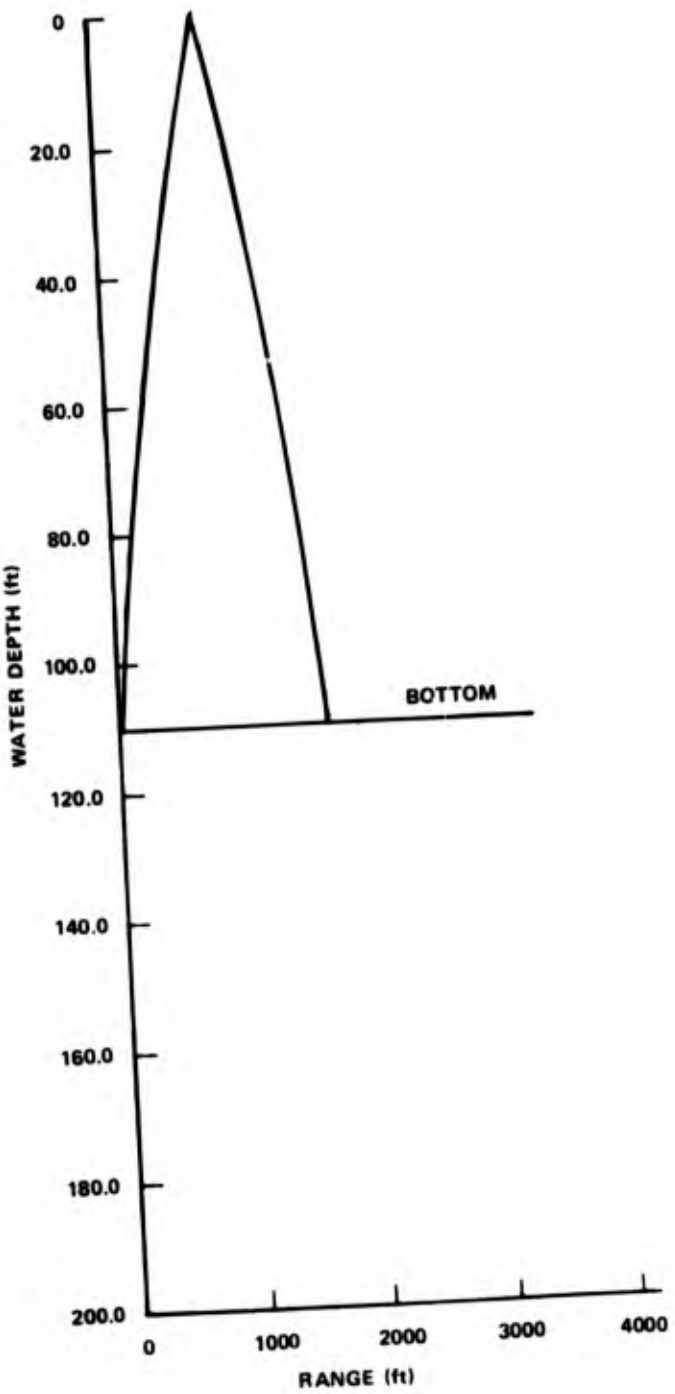

Figure 12. Ray Equivalent, Frequency 112 Hz, Mode 1

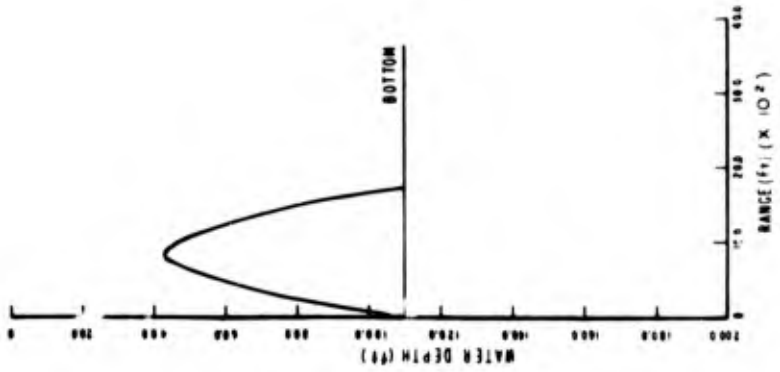

Figure 14. Ray Equivalent, Frequency 224 Hz, Mode 1

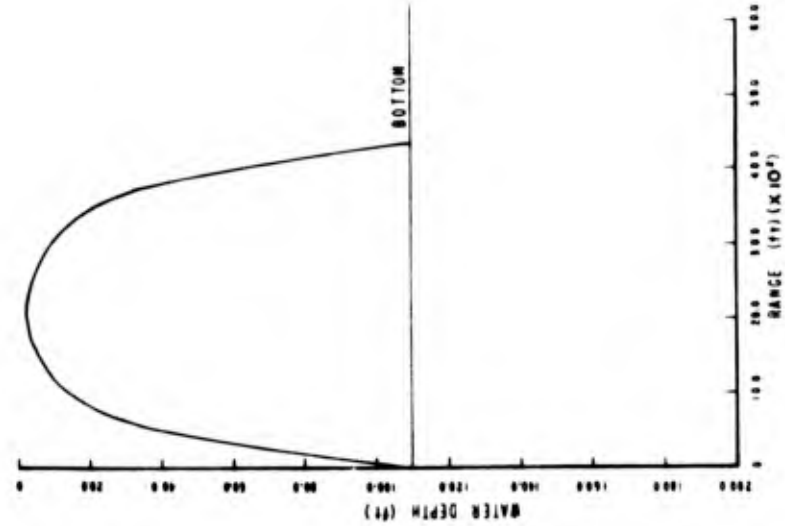

Figure 13. Ray Equivalent, Frequency 141 Hz, Mode 1

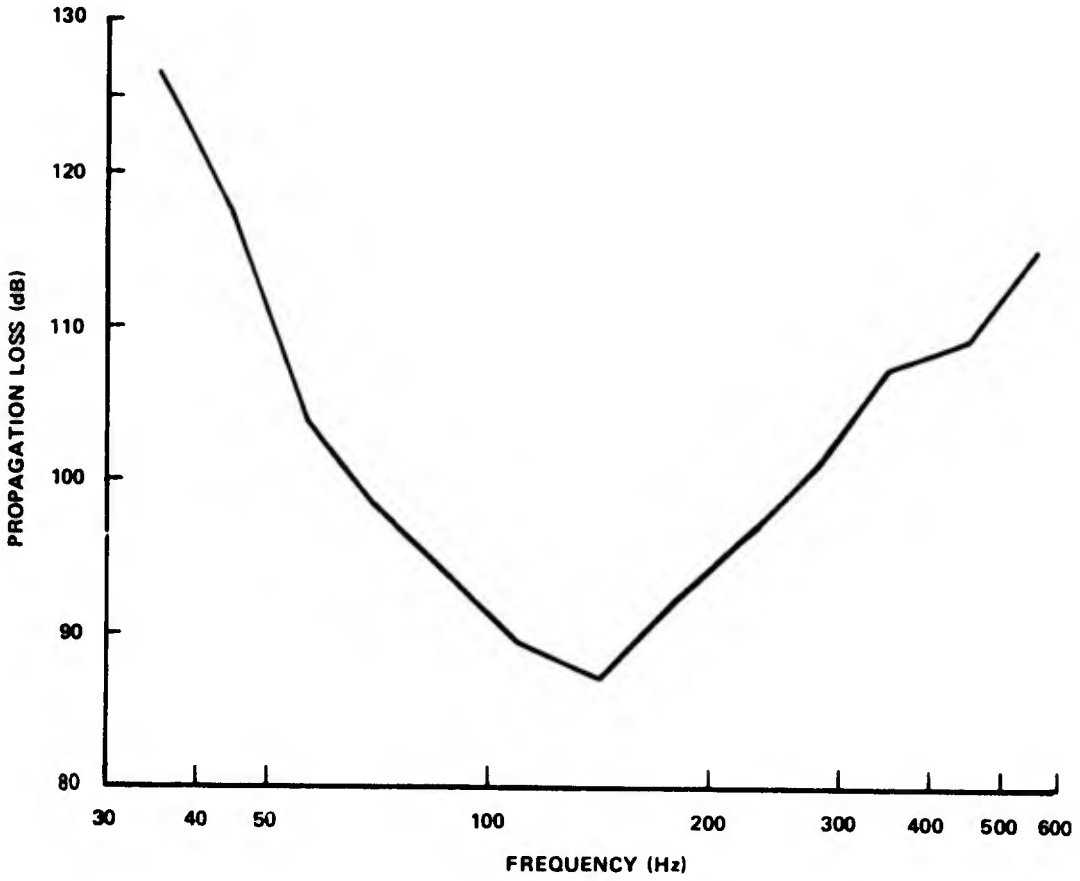

Figure 15. Propagation Loss Versus Frequency, August 1967

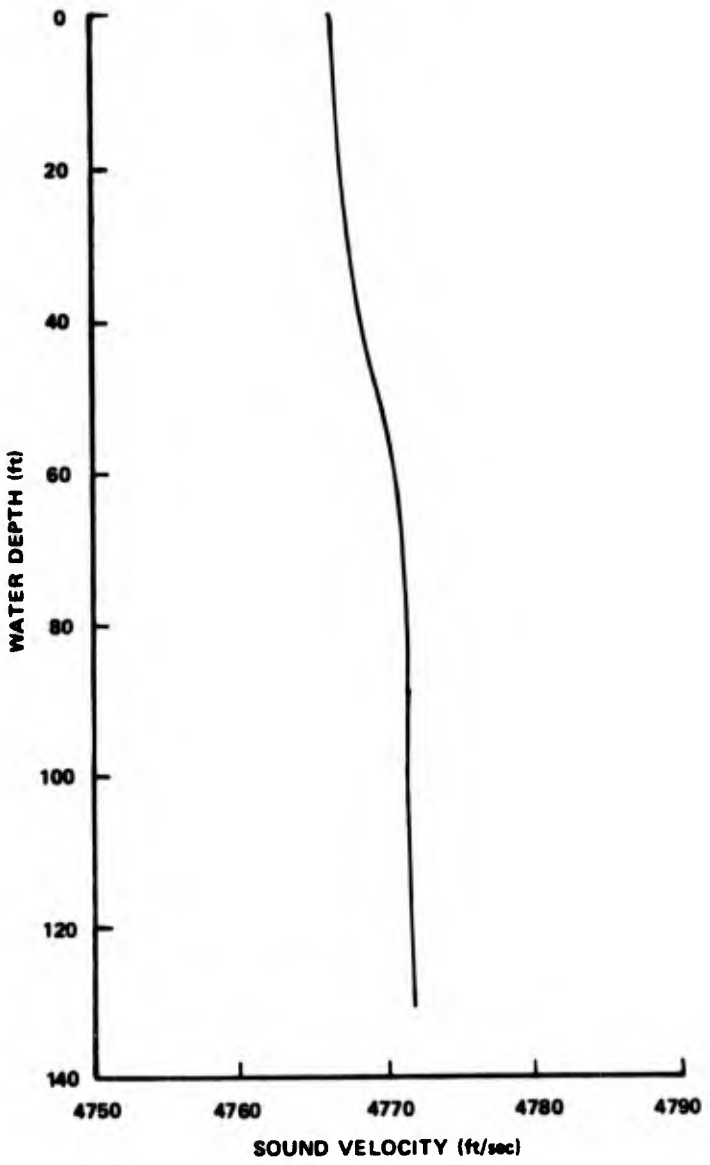

Figure 16. Velocity Profile, 30 January 1968

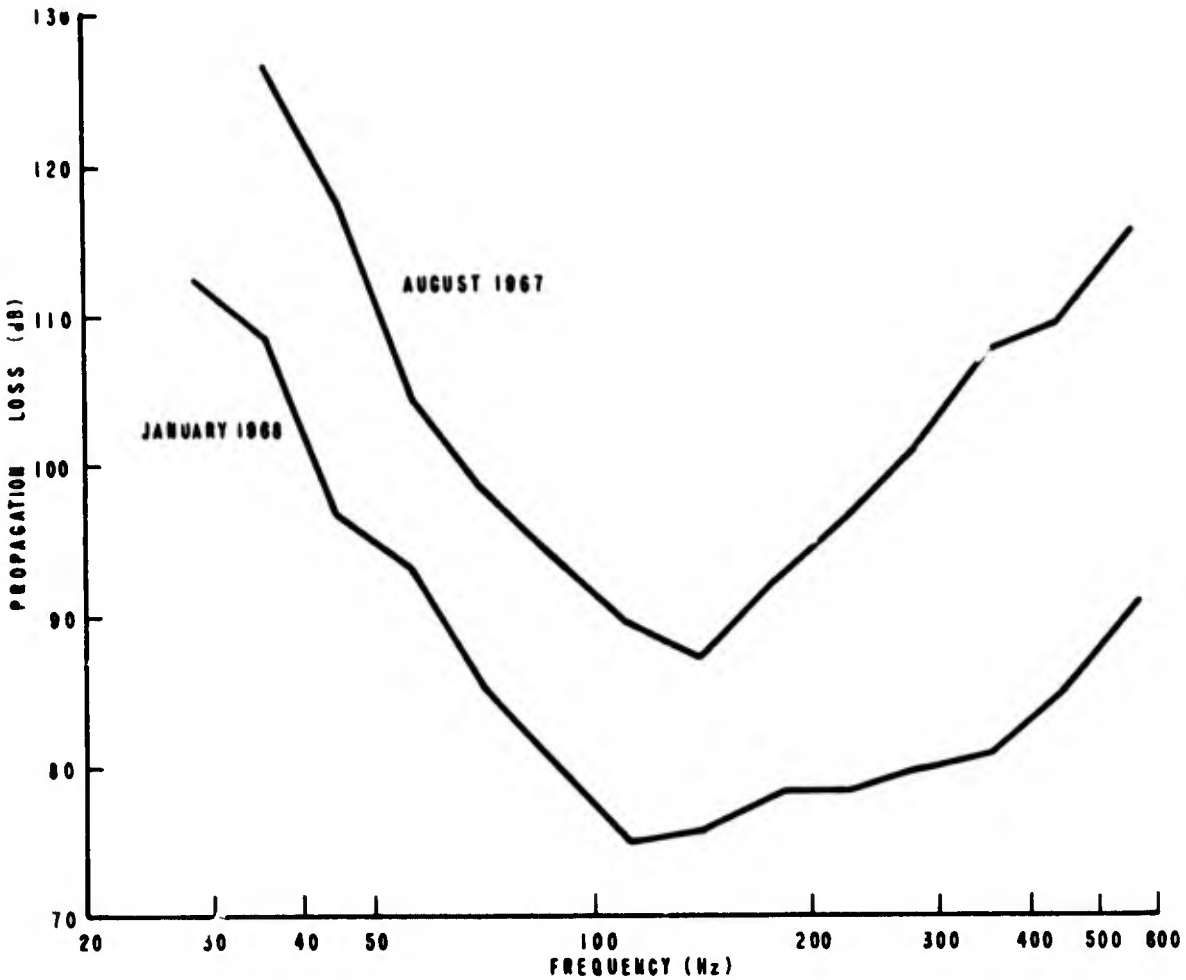

Figure 17. Propagation Loss Versus Frequency, January 1968 and August 1967

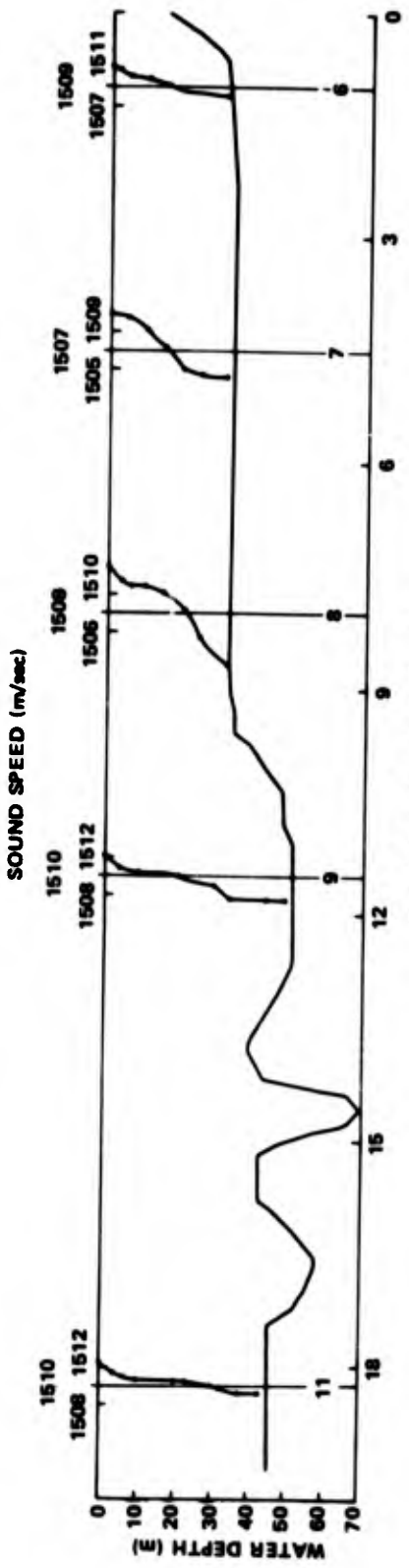

Figure 18. Velocity Profiles, 2 October 1968

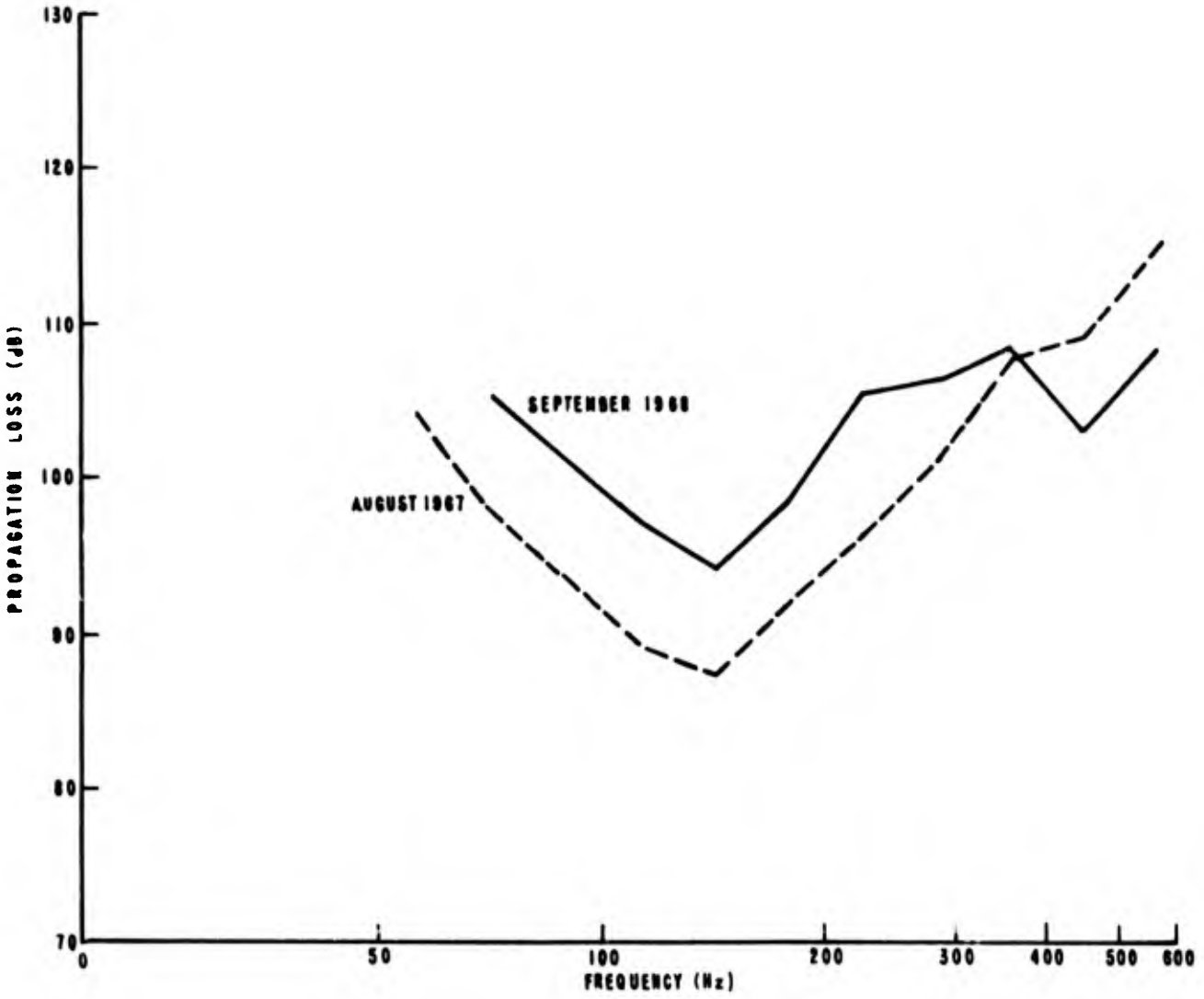

Figure 19. Propagation Loss Versus Frequency, August 1967 and September 1968

TESTS USING CW SOURCES IN BIFI RANGE

Although acoustic tests using explosive sources are useful in determining the broad characteristics of acoustic propagation, it is usually necessary to resort to CW sources for the study of the fine structure of acoustic propagation. A series of tests using fixed, CW sources and fixed receivers has been conducted over the BIFI range and these tests are described in references 17 through 19. Tests using a towed 400-Hz source and a fixed receiver were conducted in the Fishers Island area and are described in reference 20. Here we will confine our attention to a series of tests conducted near Block Island, using fixed, CW sources. These tests serve as a good test of the model, because signals were transmitted over a wide frequency range (127, 400, and 1700 Hz) and were received in locations which probed the sound field in both range and depth. Signals were transmitted by the three fixed sources at Block Island (point S in figure 8) and received by a 3-element array suspended from a ship at a large number of discrete ranges from about 0.5 to 6 miles from the source. The course followed was the line between S and H in figure 8. The maximum 6-mile range is about one-third the distance between S and H. At the ranges considered, the bottom depth is nearly a constant 110 ft.

The tests were conducted in August and October 1970. The basic experimental procedure and method of analysis were the same in both experiments. The computer-oriented analysis is outlined in figure 20. The analysis may be broken down into three steps. First, time smear analysis of short pulses, employing the procedure discussed in references 19 and 21, is used to measure the relative strength of the modes. This is possible because there is a different group velocity associated with each mode, and hence each arrival in the received signal corresponds to a particular mode. At the time of the tests, geological studies of the area were preliminary and rather inconsistent. The estimates of the velocity of sound in the bottom varied from 4900 to 5500 ft/sec. Therefore, in the second step of the analysis, C_B, the velocity of sound in the bottom, is determined by comparing the measured vertical amplitude distribution to the theoretical distributions obtained by assuming different values of C_B and the proper relative strength of the modes. Third, bottom loss is determined by comparing the measured loss to theoretical loss obtained by assuming different values of bottom loss and the proper C_B and relative strength of the modes. The theoretical and experimental values of propagation loss can be compared for all receiver depths, with the caution that many of the acoustic parameters have been obtained from the data.

In August 1970, tests were conducted when a typical velocity profile showed a large negative gradient, as shown in figure 21. Time smear measurements were made at several ranges by recording short pulses at frequencies of 127, 400, and 1700 Hz. The results at 127 Hz are shown in table 3. Most of the energy in the received signal was contained in the first arrival, i.e., mode 1. The median fraction of energy in the tail, F(tail), which is a measure of the relative energy in the modes of order higher than 1, is listed as a function of range. Even at a range of only 1.6 miles, the median value of F(tail) indicates that less than 8 percent of the total

energy in the received signal can be attributed to modes higher than the first order. It can also be seen that the higher order modes are attenuated extremely rapidly with range. Thus at a range of 3.7 miles, less than 1 percent of the total energy in the received signal is in the tail. As a result of these measurements, one can conclude that at 127 Hz, the first mode is the main contributor to the sound field even at short range, and that higher order modes may be neglected. The validity of this approximation increases as the range from the source is increased. The measurements of F(tail) also indicate that at 400 and 1700 Hz, like 127 Hz, higher order modes can be neglected at similar ranges.

Table 3. Time Smear Analysis at 127 Hz

Run	Range (nmi)	Median Value of F (Tail)
1	1.6	0.079
2	2.5	0.020
3	3.7	<0.010

If one can neglect higher order modes, it is relatively easy to determine C_B, the velocity of sound in the bottom. Most of the data appropriate for determining C_B were taken at a frequency of 127 Hz. Also, the single mode approximation is most accurate at this frequency. Therefore, data taken at 127 Hz were used to determine C_B. These data consisted of pulses 45 seconds long, which were transmitted near Block Island and received by means of three hydrophones suspended from the receiving ship at depths of 35, 68, and 100 ft. Several pulses were received at each of 23 stations located at ranges from about 1 to 6 miles. A computer program (reference 22) was used to obtain the median normalized vertical amplitude distribution from the measurements. In figure 22 on the left, the measured amplitude distribution is compared with the theoretical distribution for the first mode, assuming C_B to be 6000 ft/sec. The measured amplitude distribution indicates that energy is actually much lower in the channel than the theoretical distribution predicts. As the assumed value of C_B is decreased, energy is theoretically located lower in the channel. The best fit to the measured data is shown on the right in the figure, where C_B is assumed to be 5000 ft/sec. Thus one can conclude that C_B in the vicinity of Block Island is approximately 5000 ft/sec.

By making use of the previously determined C_B and relative strength of modes, it is possible to determine D(r), the bottom loss suffered by the first mode as a function of range. The measured loss was compared with theoretical loss curves. The assumed value of D(r) was varied, and comparisons between theoretical and measured loss were made at the three receiver depths. The value of D(r) which provided the best fit to the data at all depths was 4.0 dB/mile and hence was considered the best

estimate of D(r). Assuming this value of D(r), good agreement is obtained between theory and experiment as shown, for example, in figure 23 for a receiver depth of 100 ft. It can be seen that from a range slightly greater than 2 to 3.5 miles, the measured propagation loss values are, in general, not only higher than the predicted loss but also higher than in most measured values of loss at ranges from 3.5 to 5 miles. Since one arrival dominates the sound field, this anomalous effect cannot be attributed to interference of multipaths. Oceanographic measurement indicated that in the test area, there was no significant variation with range in the velocity profile in the water column and in the bottom profile. It is most likely that a difference in stratification occurs in the bottom composition, and hence in C_B. The data taken at stations within the region 3 miles from the source indicate that the vertical amplitude distribution is extremely variable with range in this region. The method of determining C_B outlined previously is dependent upon the formation of standing waves in the region analyzed. Although this method cannot be applied, it is probable that the C_B in this region is much larger than the C_B of 5000 ft/sec in nearby sections, because of the drop in measured loss below predicted loss, beyond 3.5 miles.

The long pulses were also used to determine fluctuations in signal level. Figure 24 shows the standard deviation of the envelope at 127 Hz plotted as a function of range. As expected from time smear measurements, there is little signal fluctuation. The standard deviation is less than 1 dB at all but a few ranges. The largest fluctuations occur at ranges from about 2 to 3.5 miles, where it was shown previously that there was unstable propagation.

In October 1970, tests were conducted in which a typical velocity profile possessed a small positive gradient, as shown in figure 25. Data were taken only at 127 Hz. Time smear analysis indicated that as in August, the first mode dominated the sound field.

It was hoped to determine C_B in the area about 3 miles from the source at Block Island. The decrease in the velocity of sound in the water column due to seasonal cooling would effectively decrease the relative change in the velocity discontinuity at the bottom interface as a function of range. This occurs because the effect of this decrease in the relative change of the bottom velocity contrast is nonlinear with respect to the sound field. (Details are contained in reference 11.) The median vertical amplitude distribution was found for two sets of data. One set contained data from 3 stations from 2.5 to 3.5 miles from the source. The vertical amplitude distribution at these ranges was fairly constant. Therefore, it is likely that standing waves were set up in this section. The other data set was taken at the five remaining stations at other ranges. In figure 26 on the left, the median amplitude distributions of the two sets of data are compared with the theoretical distribution, assuming C_B to be 5600 ft/sec. This provides the best fit to the data in the section about 3 miles from the source. The energy at other ranges is located at a lower depth in the channel, and hence the best fit is obtained for C_B equal to 5000 ft/sec, as shown on the right. Because of the relatively small amount of data, neither

fit is as close as that obtained for the August data, but the results are consistent with the results in the August tests.

In figure 27, a comparison of theoretical and measured propagation loss is made, assuming D(r) to be 3.6 dB/mile. This value of D(r) corresponds to the three theoretical distributions which provide the best estimate of D(r). The 3.6-dB/mile value of D(r) is slightly less than D(r) in August, because the penetration of energy into the bottom decreases as the velocity of sound in the water decreases. The value of C_B assumed in the theoretical calculations was 5000 ft/sec. In figure 28, the comparison is improved by assuming C_B to be 5600 ft/sec in the region 2.5 to 3.5 miles from the source, and assuming that the sound field conforms to the local stratification at the receiver.

Subsequent to this analysis, a geological survey of the area was completed. As a result, the bottom characteristics along the experimental tract were determined as shown in figure 29 (from reference 23). It can be seen that there is a soft, low velocity (around 5000 ft/sec) bottom layer composed of silty sand overlying a hard, high velocity (around 5600 ft/sec) layer composed of coarse sand. This hard layer is well below the ocean bottom at all ranges, except in the 2- to 3-mile area where it extends nearly up to the interface of the water and bottom. These geological results confirm the bottom characteristics derived from the acoustic experiment. Hence not only has a possibly useful tool for determining acoustic parameters been developed, but also the sensitivity of the model at predicting the vertical sound field has been demonstrated. The analysis described was simplified, because one mode dominated the sound field. When several modes are important (as, for example, over a hard bottom), it would be necessary to simplify the sound field by using optimum source or receiver placement, or by using mode enhancement techniques as described in volume I of this report. Thus it appears that such an extension to more general conditions should be investigated.

In the August experiment, apparently an abrupt change in bottom properties resulted in a sound field which was extremely unstable. This is probably due, in large part, to mode conversion processes. As a result, this experiment stimulated the work which resulted in the inclusion of mode conversion effects in the acoustic model. However, given the bottom loss characteristics, good agreement was generally obtained between theory and experiment, as evidenced in figures 23 and 28.

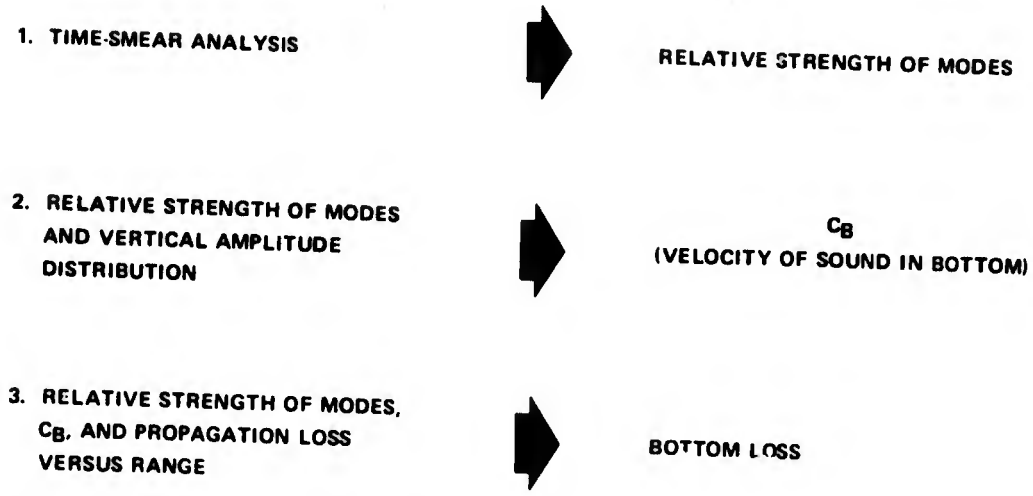

Figure 20. Outline of Analysis

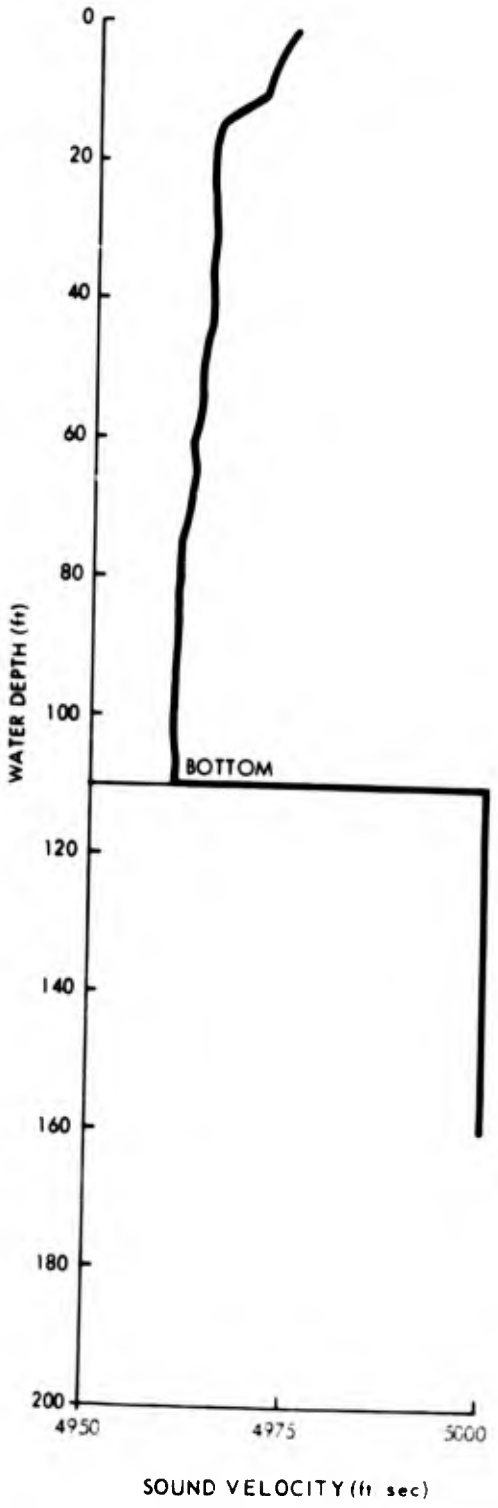

Figure 21. Typical Sound-Velocity Profile, August 1970

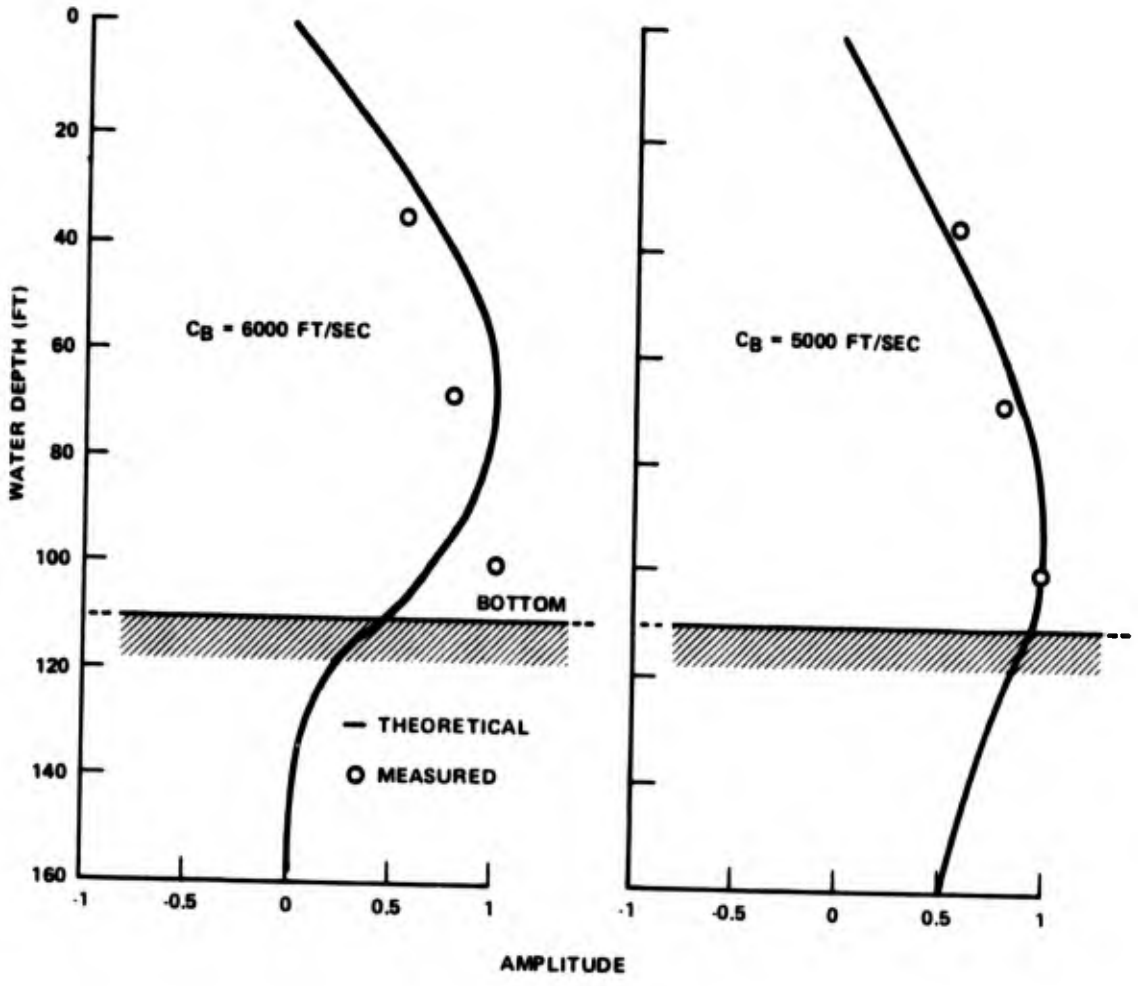

Figure 22. Amplitude Versus Depth, Frequency 127 Hz, Mode 1, August 1970

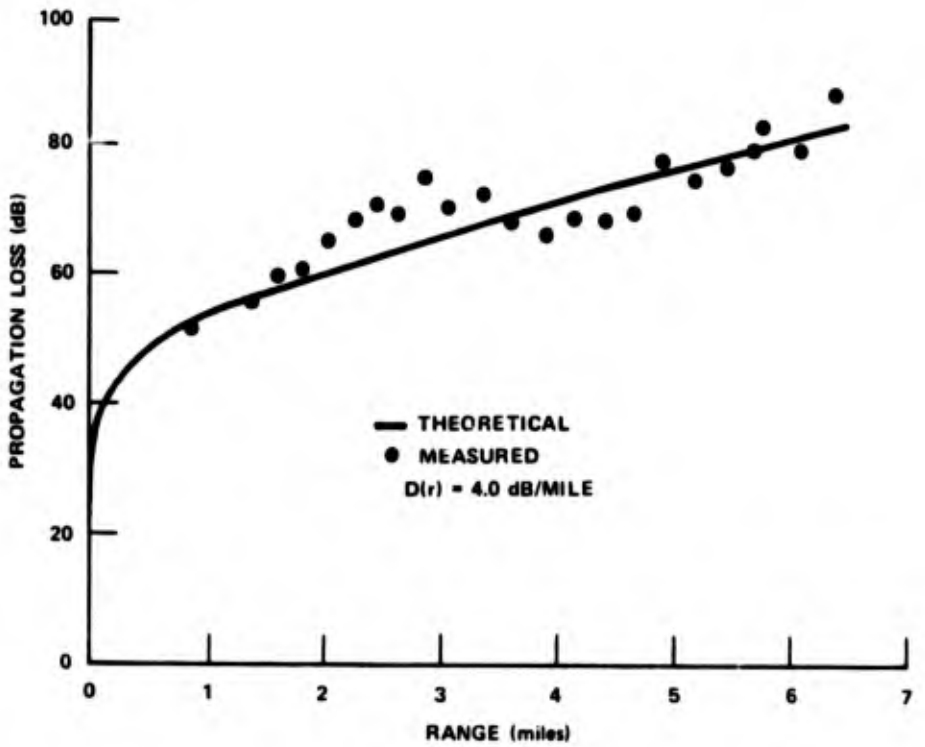

Figure 23. Propagation Loss Versus Range, Frequency 127 Hz, Source Depth 55 ft, Receiver Depth 100 ft, Mode 1, August 1970

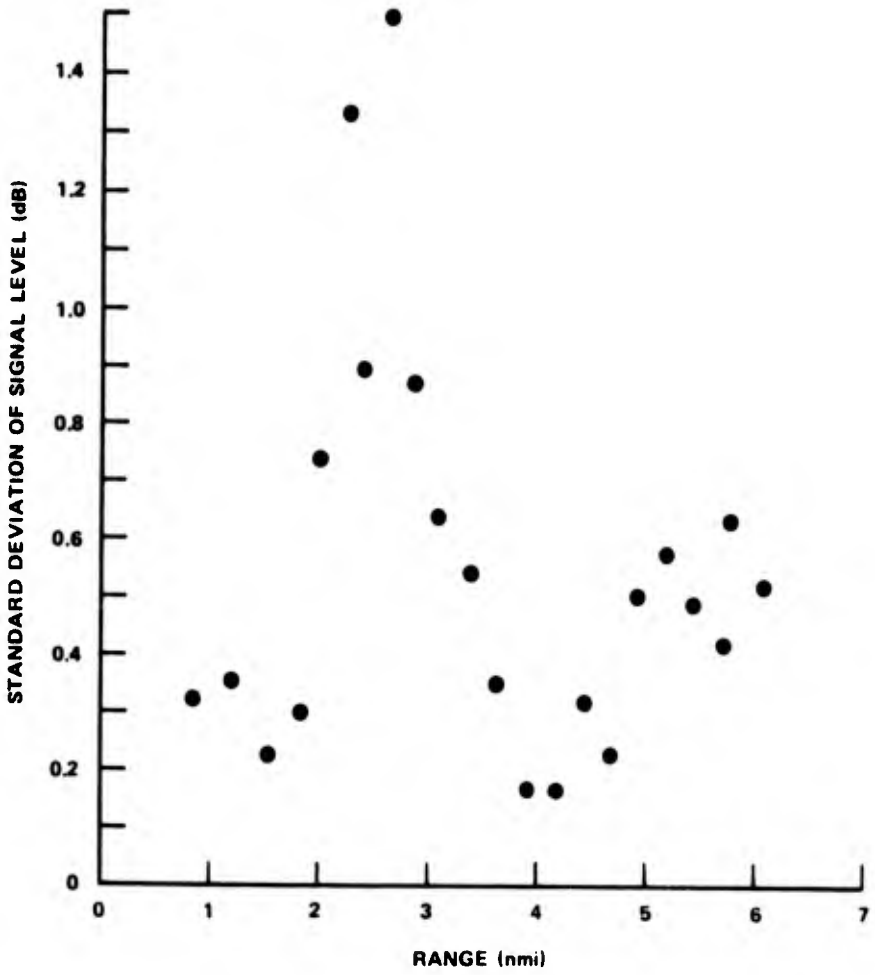

Figure 24. Standard Deviation of Signal Level Versus Range, Frequency 127 Hz

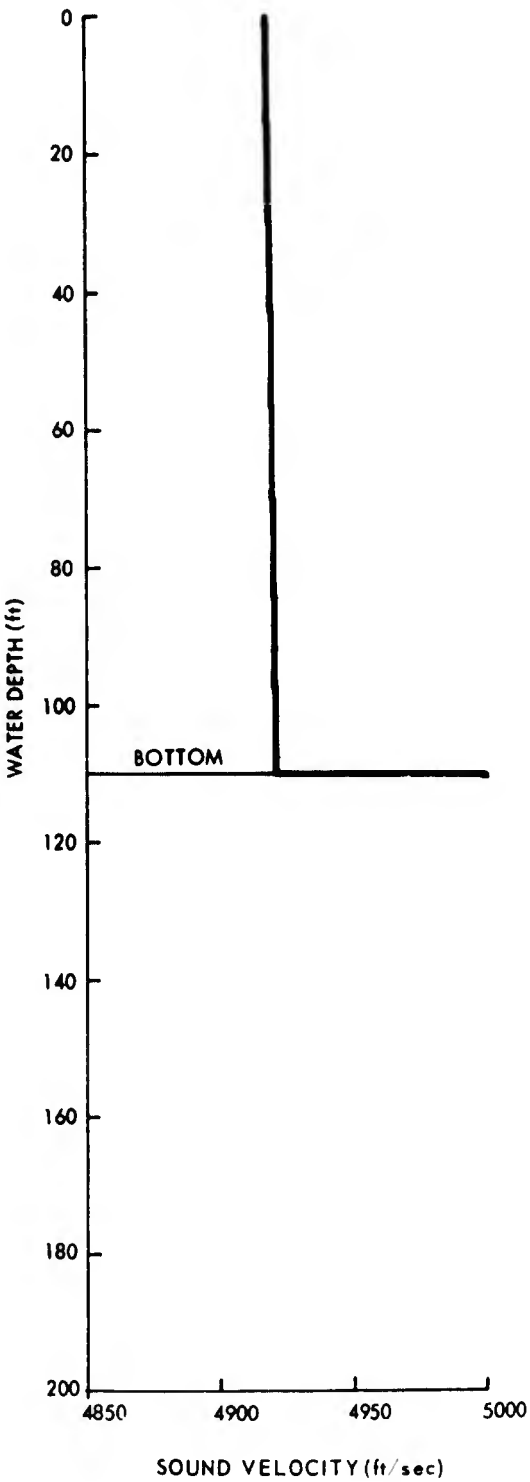

Figure 25. Typical Sound-Velocity Profile, October 1970

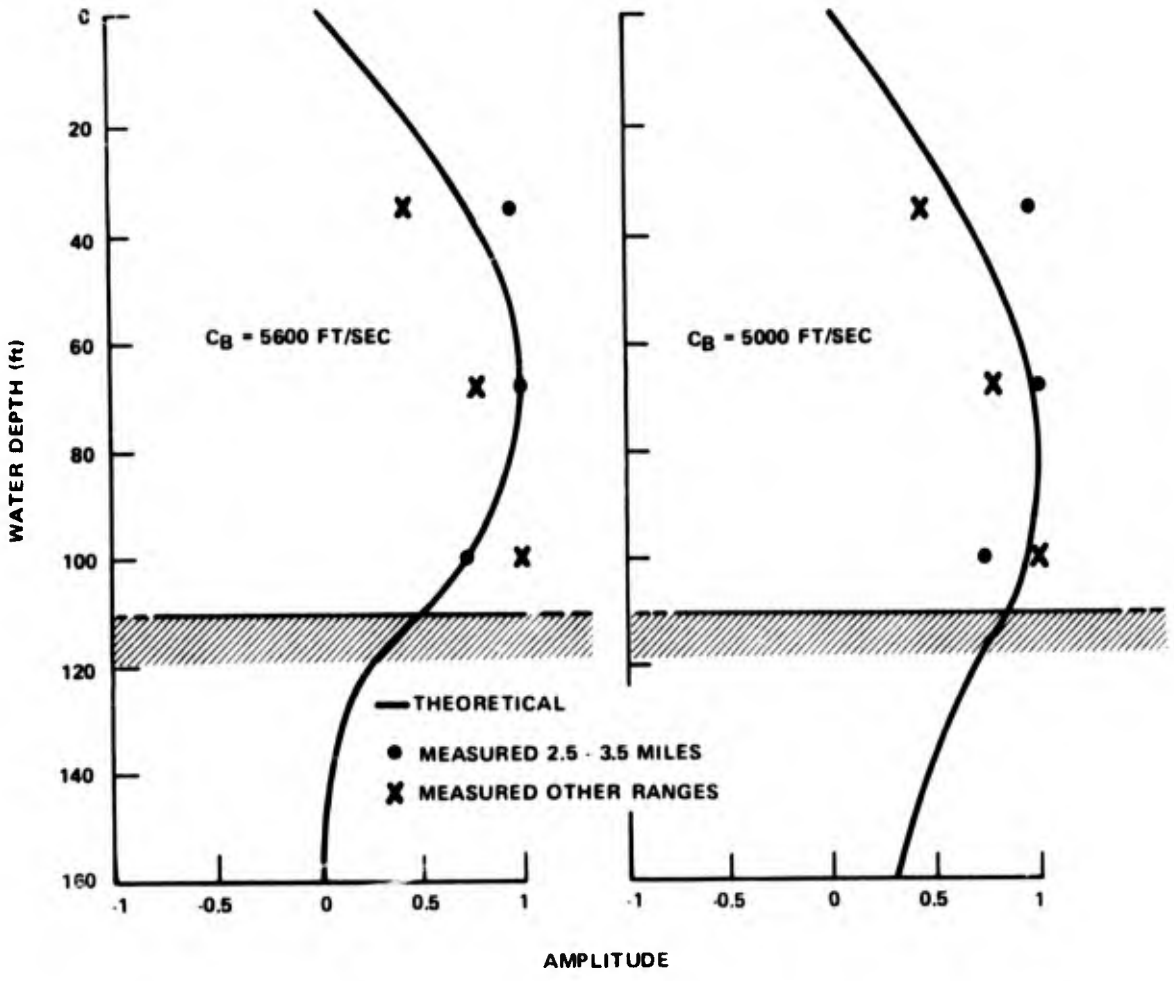

Figure 26. Amplitude Versus Depth, Frequency 127 Hz, Mode 1, October 1970

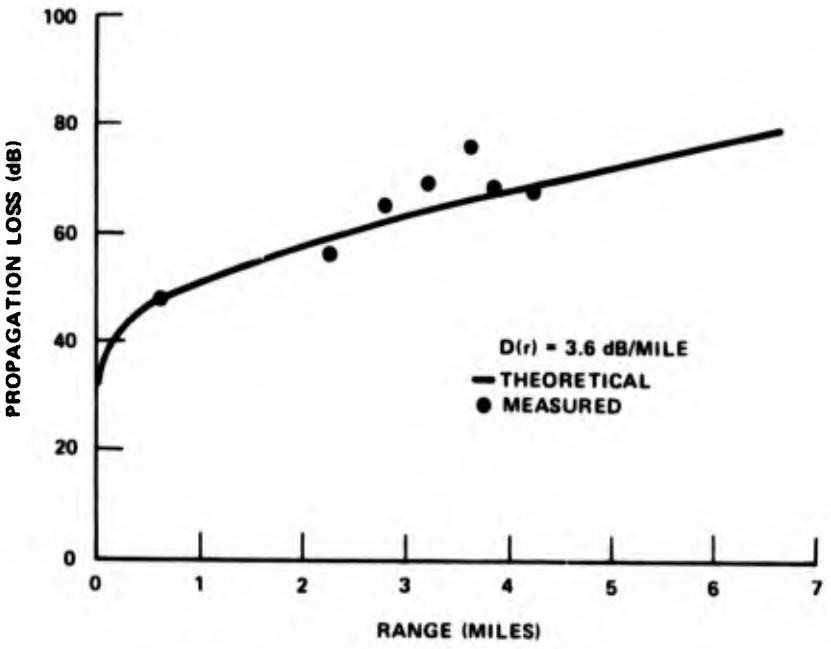

Figure 27. Propagation Loss Versus Range, Frequency 127 Hz, Source Depth 55 ft, Receiver Depth 100 ft, Mode 1, October 1970

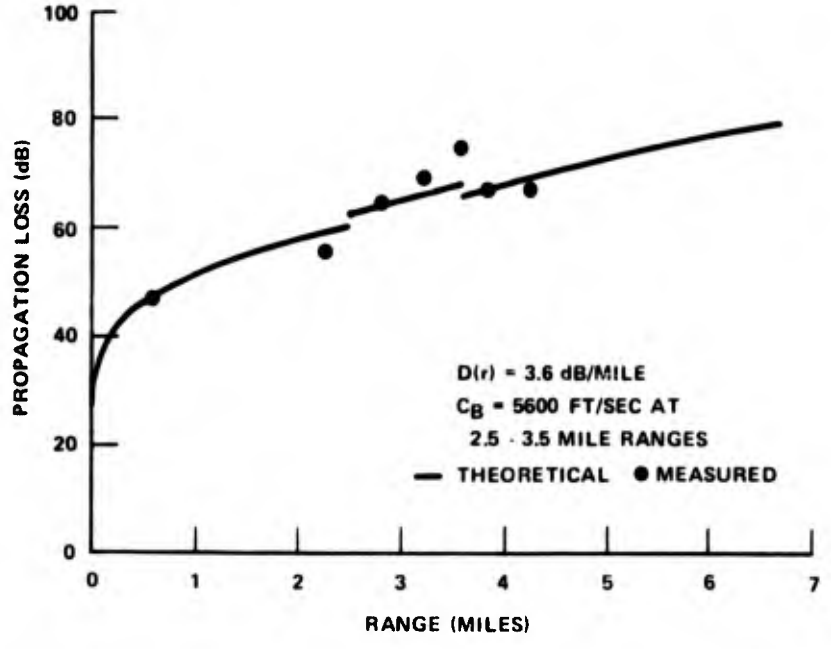

Figure 28. Propagation Loss Versus Range, Change in C_B from 2.5- to 3.5-mile Ranges, Frequency 127 Hz, Source Depth 55 ft, Receiver Depth 100 ft, Mode 1, October 1970

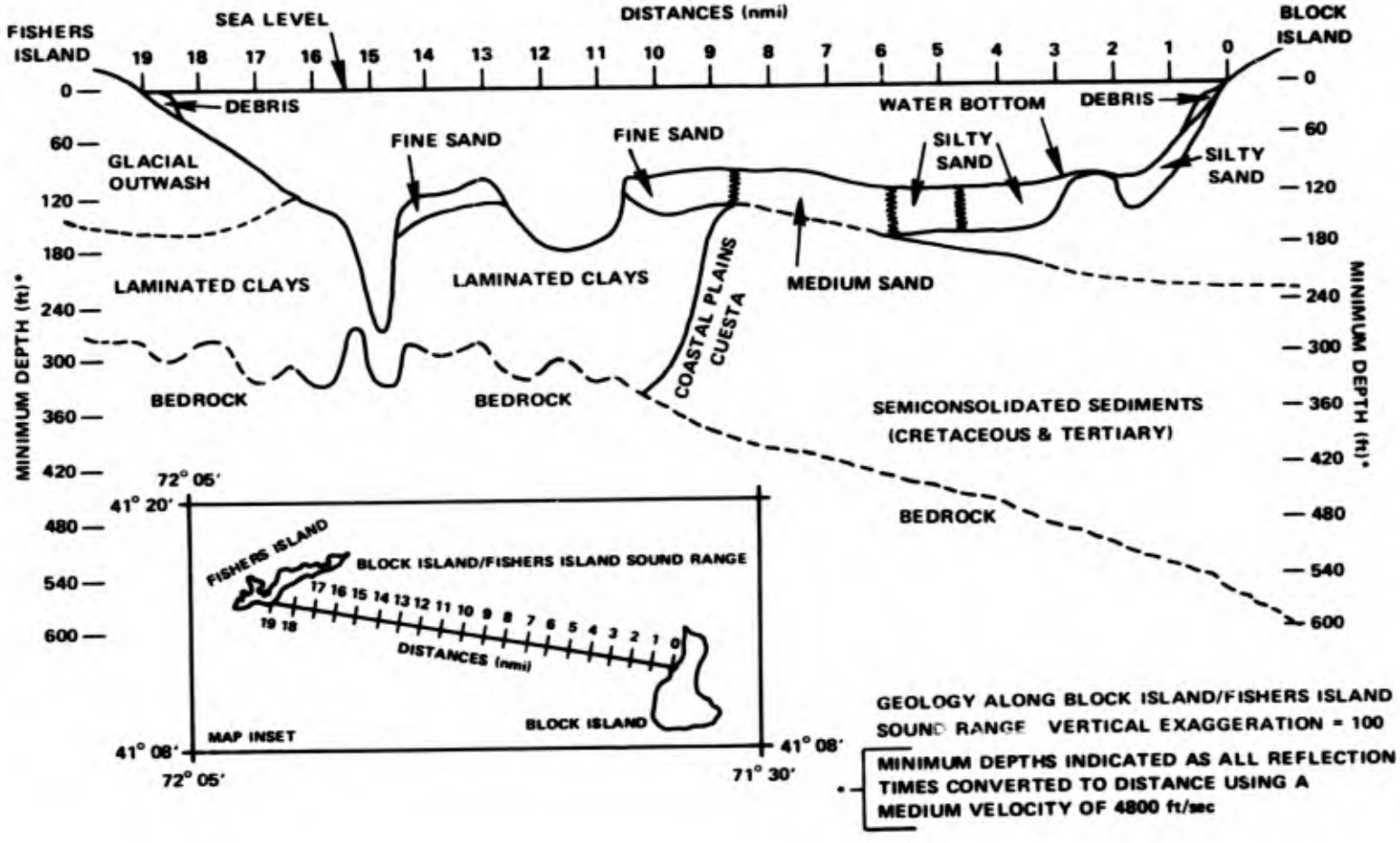

Figure 29. Bottom Structure in BIFI Range

TESTS USING EXPLOSIVES IN BALTIC SEA

After several years of study on the BIFI range, it was desirable to test the applicability of the model to other shallow water ranges. This was made possible when, in 1971-1972, shallow water acoustic tests were conducted jointly under the auspices of a data exchange agreement by the United States Naval Underwater Systems Center (NUSC) and West Germany's Erprobungstelle 71 (E-71) in the western portion of the Baltic Sea.

Tests were conducted at two stations under both summer (June - July 1971) and winter (February - March 1972) conditions. This permitted comparison of acoustic propagation under the extreme differences in the stratification of the water column encountered during the seasonal cycle. A typical summer sound velocity profile (figure 30A) has a rather strong sound channel approximately at middepth, whereas a typical winter profile (figure 30B) has a weak surface channel. Operations were conducted in the two areas shown in figure 31. At station 1, near Eckernforde Bay, the water depth was a nearly constant 24 m over all tracts in which tests were conducted. At station 2, near the island of Bornholm, the water depth was a nearly-constant 45 m, almost twice the depth near Eckernforde. The bottom is extremely soft at both stations. A sound velocity of 1521 m/sec in the bottom was assumed in all calculations.

Because the velocity profiles at the two stations are similar, the tests provided an opportunity to examine the effect of water depth upon acoustic propagation by comparing the test results. Explosive sources were used in all tests, and hence the frequency of acoustic propagation was measured over a wide range of frequencies (about 31.5 Hz to 5 kHz). The results were obtained by determining the energy content of each received explosive shot for one-third-octave bands of frequencies. These energy levels were computed by the Ambilog system (reference 24). To obtain the propagation loss, the received energy levels were subtracted from the explosive source levels provided by L. C. Maples of the NUSC, New London Laboratory (these levels are listed in reference 12). The sound field was measured at three source and receiver depths (near the surface, midwater depth, and near the bottom), and at ranges from about 0.5 nmi (1000 m) to a maximum of about 10 nmi (20,000 m) in increments of about 0.5 nmi.

The first qualitative test of this model was to explain, in terms of the ray equivalent of modes, propagation loss as a function of frequency. This proved to be no great problem.

Tests were conducted in the Bornholm area (station 2 in figure 31) on 7 July 1971. A typical velocity profile for the area, taken during the tests, is shown in figure 32. A strong sound channel, evident at about middepth in the profile, is created by a combination of the summer heating of the upper water column and the highly saline water present in the lower part of the water column.

Calculations of ray equivalents show that sound is trapped in the water column, even at relatively low frequencies. At 50 Hz, the ray equivalent of the first mode reflects from both boundaries (figure 33A); however, at 100 Hz, the ray equivalent shows trapping of energy far from the boundaries (figure 33B). Hence one would expect relatively small propagation loss — other than geometrical spreading — at the frequencies analyzed. This is borne out by a typical plot of measured propagation loss versus frequency (figure 34), in which the loss is relatively small at the frequencies analyzed. The slight increase in propagation loss with frequency can be attributed to the form of the excitation function, which generally decreases with increasing frequency.

Tests were conducted in the Eckernforde area (station 1 in figure 31) on 30 June and 1 July 1971. A typical velocity profile in the area, taken during the tests, is shown in figure 35. A strong sound channel is evident in the profile at about middepth (14 m). This channel, like the similar channel near Bornholm, is produced by a combination of summer heating and saline deep water. Although the general characteristics of the summer profiles near Eckenforde and Bornholm are similar, the difference in water depth profoundly affects the nature of sound propagation in the two areas.

Calculations of ray equivalents show that in the shallower water near Eckernforde, sound is trapped in the water column only at relatively high frequencies. In figure 36A it can be seen that at 100 Hz, the ray equivalent of the first mode reflects from both boundaries. At 200 Hz, the ray equivalent (figure 36B) shows that the first mode still interacts significantly with the boundaries. The first mode becomes trapped in the channel at a frequency of about 400 Hz. At 800 Hz (figure 36C), the ray equivalent shows trapping of energy far from the boundaries. Hence one expects relatively large propagation loss — other than geometrical spreading — at frequencies below 400 Hz and decreasing loss at frequencies greater than 400 Hz, as energy becomes increasingly concentrated in the sound channel. This is borne out by a typical plot of measured propagation loss versus frequency presented in figure 37. It can be seen that the loss is greatest at frequencies below 300 Hz. As trapping of energy in the channel begins at about 400 Hz, the loss decreases rapidly with frequency. After energy becomes trapped far from the boundaries (beyond 800 Hz), the measured loss is at a relatively constant low level.

Figure 38 provides a comparison of propagation loss versus frequency at Eckernforde and Bornholm during the summer tests. It can be seen that at low frequencies, propagation loss is much higher near Eckernforde because of loss at the boundaries. At frequencies beyond 1000 Hz, when sound is fully trapped in the sound channels at both locations, the values of loss near Eckernforde approach those measured near Bornholm.

Tests were conducted in the Bornholm area on 2-3 March 1972. A typical velocity profile in the area, taken during the tests, is shown in figure 39. The profile displays an approximately isovelocity structure from the surface to a depth of 30 m, and a rather sharp positive gradient from 30 m to the bottom. This positive gradient is caused by the saline deep water in the Baltic.

Calculations of ray equivalents show that sound is trapped above the bottom only at moderate and high frequencies. In figure 40A it can be seen that at 50 Hz, the ray equivalent of the first mode reflects from both boundaries. At 100 Hz (figure 40B), the ray equivalent still interacts significantly with both boundaries. However, at 200 Hz (figure 40C), the trapping of energy prevents the ray equivalent from striking the bottom. Hence one expects relatively large propagation loss — aside from geometrical spreading — at frequencies of 100 Hz and less, and smaller loss at frequencies greater than 200 Hz. This is borne out by a typical plot of measured propagation loss versus frequency (figure 41). At frequencies below 100 Hz, the loss is so high that the signal does not exceed ambient noise at several frequencies. At frequencies above 200 Hz, the loss declines rapidly as sound becomes more fully trapped above the bottom. Above 1000 Hz, the loss is at a relatively constant low level, since energy at these frequencies is strongly trapped.

Figure 42 presents a comparison of summer and winter propagation loss versus frequency near Bornholm. It can be seen that the weaker trapping of energy in winter results in extremely high loss at low frequencies, whereas the stronger summer channel traps sound even at these low frequencies. Because sound is strongly trapped at high frequencies in both summer and winter, these losses are very close in level.

Tests were conducted in the Eckernforde area on 24-25 February and 7-8 March 1972. A velocity profile, typical of profiles taken in the area in February and March is shown in figure 43. The profile displays an isovelocity structure (approximately) from the surface to a depth of 20 m and a positive gradient from 20 m to the bottom. This positive gradient is caused by the saline deep water in the Baltic.

Calculation of ray equivalents shows that sound is trapped above the bottom only at relatively high frequencies. At 100 Hz (figure 44A), the ray equivalent of the first mode reflects from both boundaries. At 200 Hz (figure 44B), the ray equivalent of the first mode reflects from both boundaries. However, at 800 Hz (figure 44C), the ray equivalent indicates that energy strikes the surface but does not strike the bottom. Hence one expects relatively large propagation loss — aside from geometrical spreading — at frequencies of 200 Hz, and less and smaller loss at frequencies greater than 800 Hz. This is borne out by a typical plot of measured propagation loss versus frequency (figure 45). At frequencies below 200 Hz, the loss is extremely high, and as a result, at many frequencies below 200 Hz, the signal does not exceed ambient noise. At frequencies above 800 Hz, the loss decreases rapidly as sound becomes more fully trapped above the bottom. Above 2000 Hz, the loss is at a relatively constant low level, since energy at these frequencies is strongly trapped.

Figure 46 presents a comparison of summer and winter propagation loss versus frequency near Eckernforde. It can be seen that the weaker trapping of energy in winter results in extremely high loss at low frequencies, whereas the stronger summer channel traps sound at lower frequencies than in winter. Because sound is strongly trapped at high frequencies in both summer and winter, these losses are very close in level.

Figure 47 provides a comparison of propagation loss versus frequency at Eckernforde and Bornholm during the winter tests. It can be seen that near Bornholm, loss begins to decrease rapidly as trapping begins at relatively low frequencies. However, near Eckernforde, trapping occurs at higher frequencies because of the smaller positive gradient and shallower water depth, and the decrease in propagation loss begins at higher frequencies. At the highest frequencies measured, sound is strongly trapped in both areas, and the levels of propagation loss are nearly the same for both areas.

However, in contrast to the success of the analysis of the characteristics of propagation loss as a function of frequency, the quantitative analysis of propagation loss versus range was permeated with one major problem. This problem is illustrated in figure 48. It can be seen that theory and experiment differ by about 8 dB at all ranges. Good agreement can be reached only by shifting values by 8 dB, as shown in figure 49. Similar discrepancies occur at nearly all frequencies, with the differences in level being a function of frequency. The source of this discrepancy has not been located. However, a recent experiment, using both explosive and CW sources in the Baltic, has been performed to examine possible reasons for the discrepancy: (1) inaccuracy of the explosive source levels, (2) possible oversimplification of the oceanography when, for example, as shown in figure 50, a deterioration in the sound channel results in an abrupt increase in loss at a range of 12 m in figure 49; or (3) lack of validity of some of the assumptions in the theoretical model.

More success was obtained in predicting the relative propagation loss as a function of depth, as shown in figure 51. Here, after 10 dB has been subtracted from all experimental results, the comparison is good. The variation in loss with depth is very significant, since it varies as much as 20 dB at a given range. Thus the model has shown the ability to predict the variation of propagation loss with depth over a wide range interval. Although a large unexplainable discrepancy exists in matching absolute levels with measurements, it is conceivable that this is due to errors in source level estimation of the explosive charges.

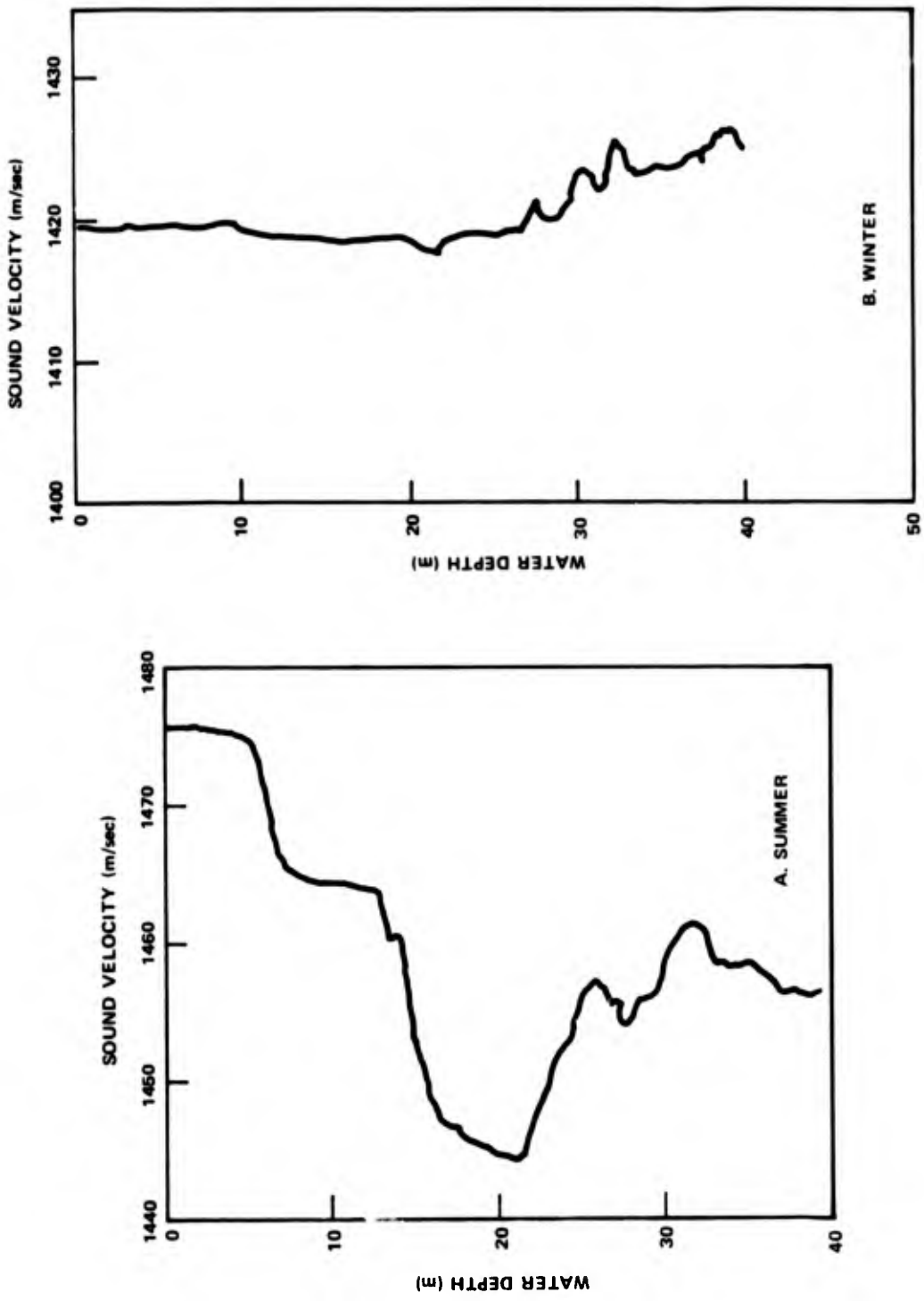

Figure 30. Typical Sound-Velocity Profiles in Baltic Sea

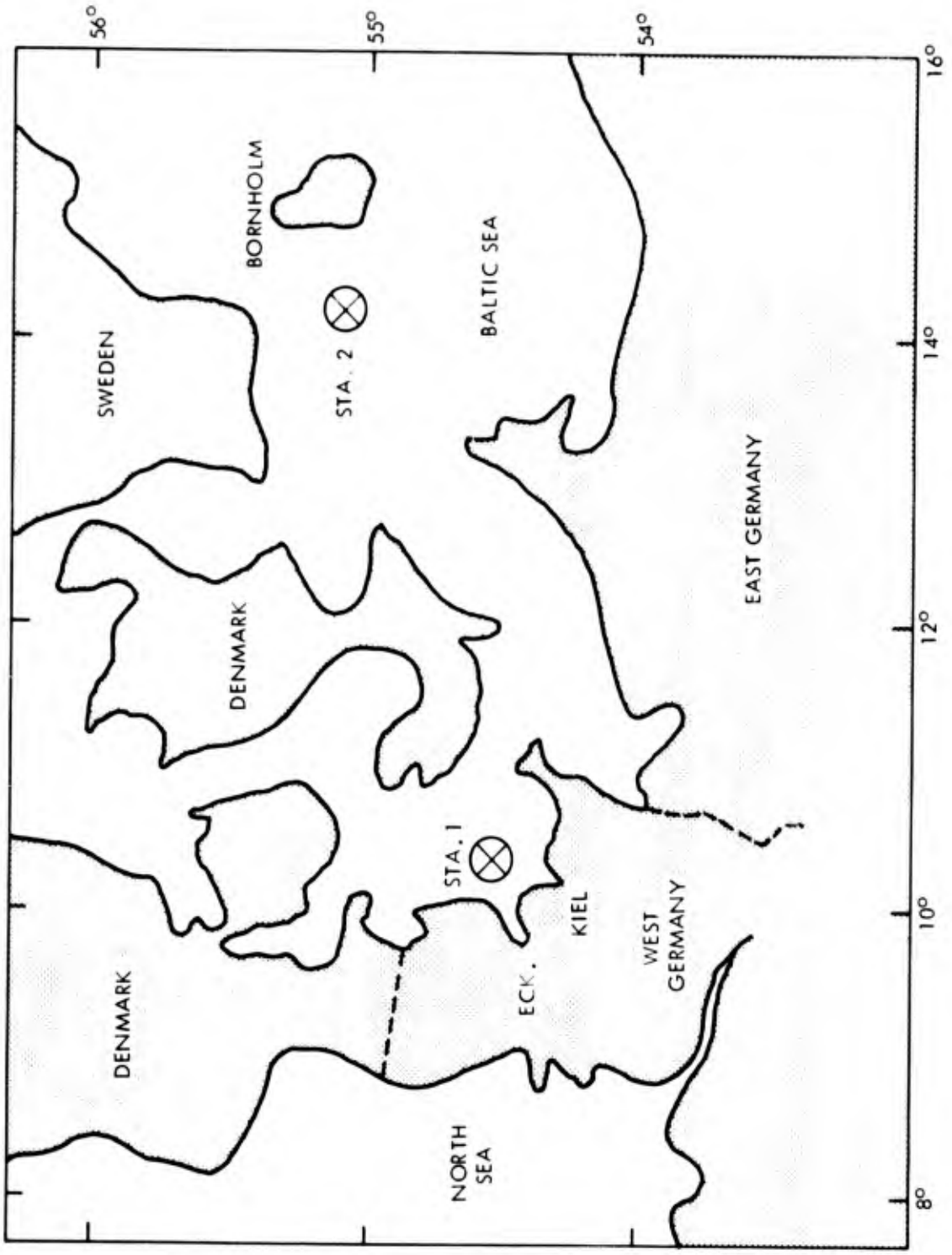

Figure 31. Operating Area

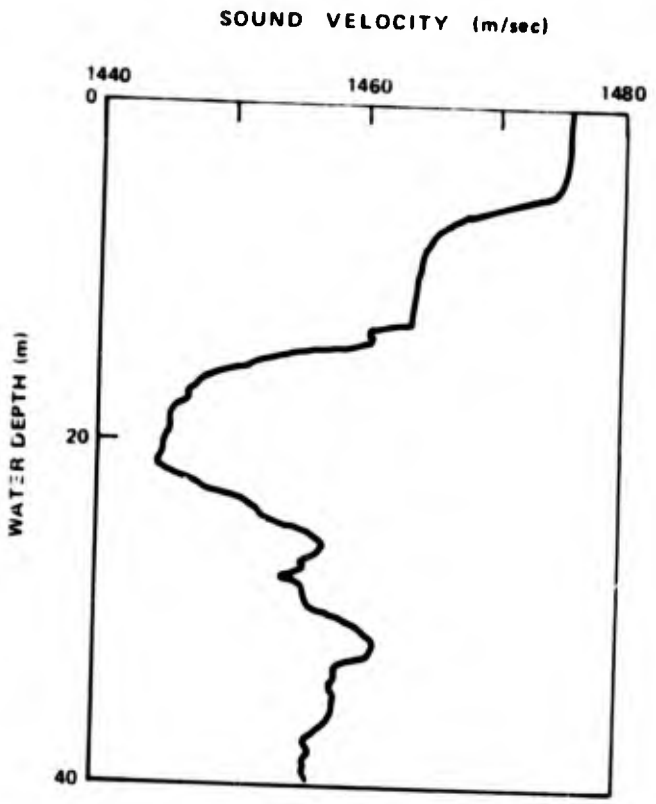

Figure 32. Bornholm Summer, Sound-Velocity Profile

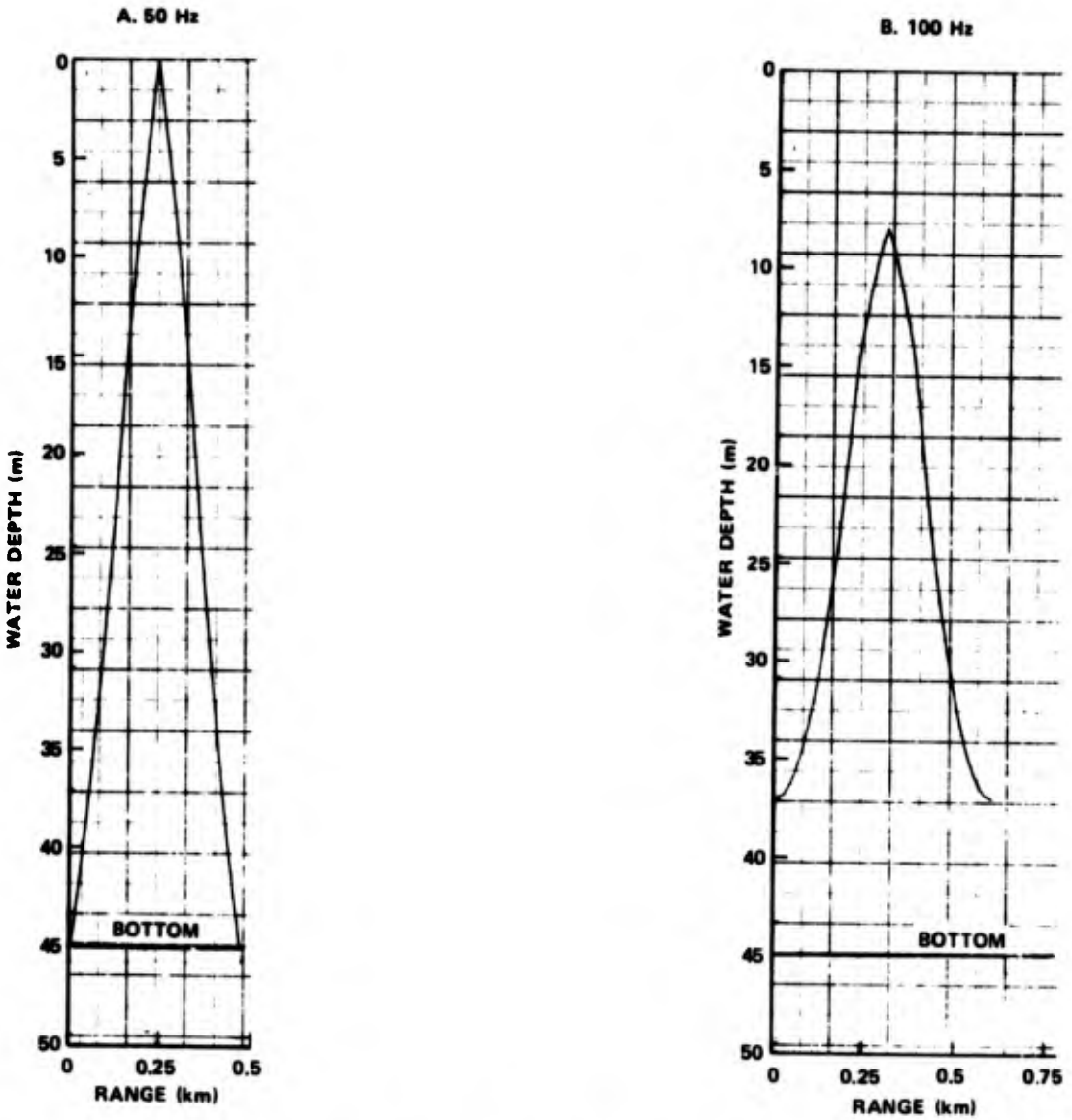

Figure 33. Bornholm Summer, Ray Equivalent, Mode 1, at 50 and 100 Hz

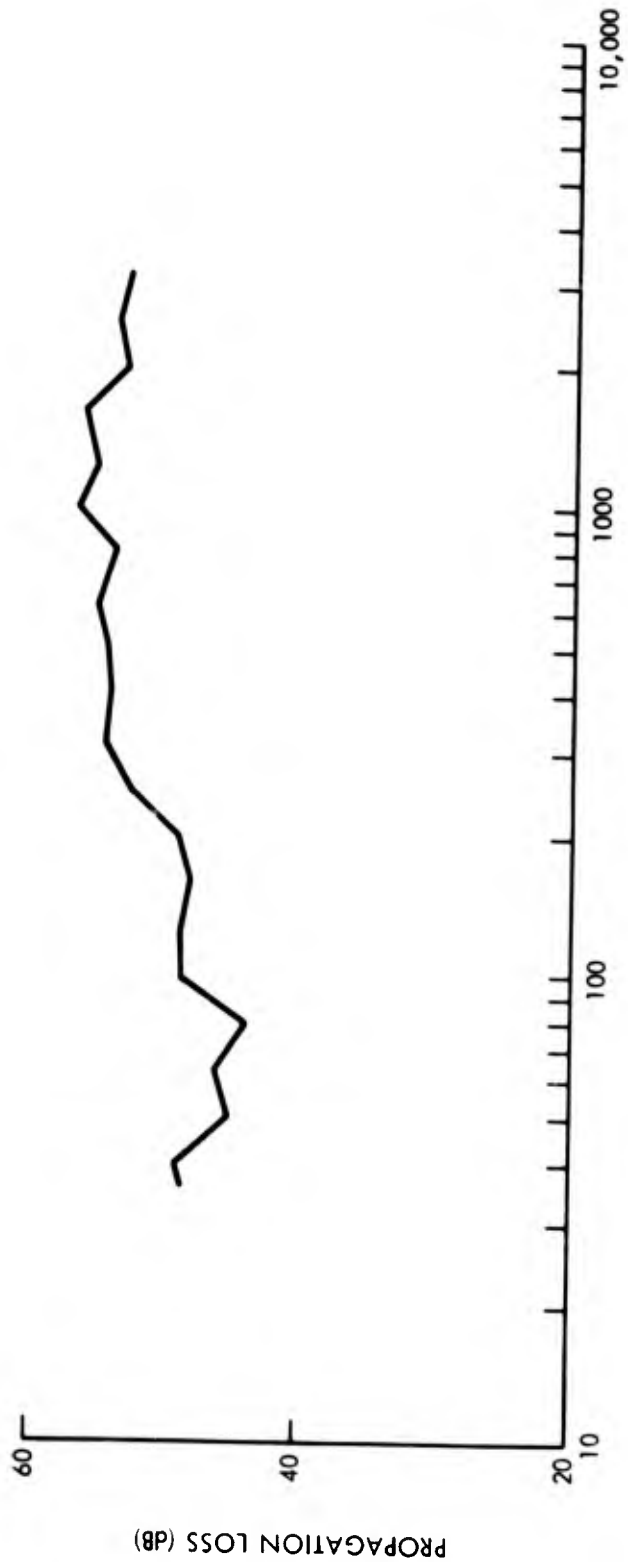

Figure 34. Bornholm Summer, Propagation Loss Versus Frequency Range 0.56 nmi, Source Depth 10 m, Receiver Depth 12 m, Water Depth 45 m

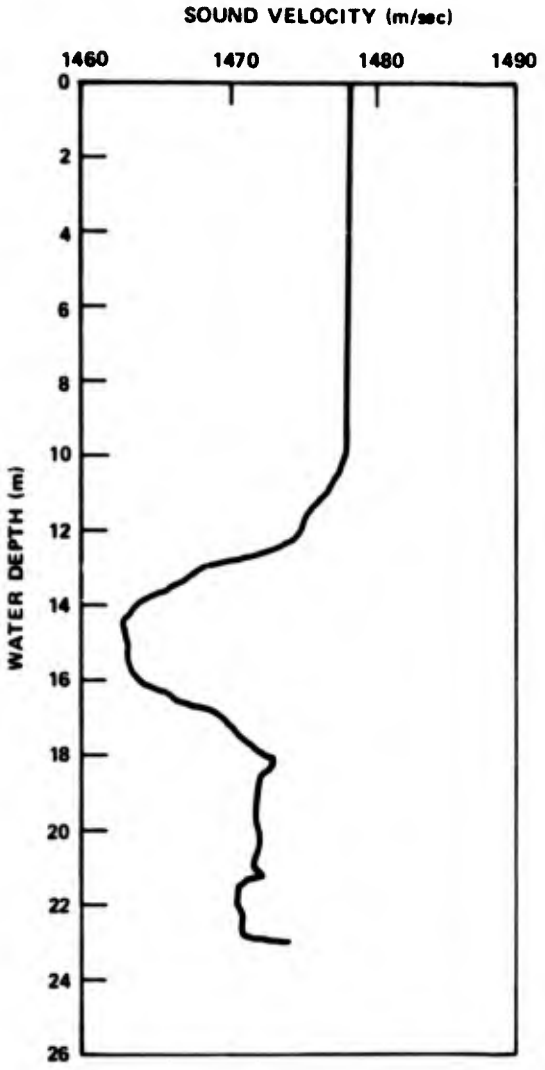

Figure 35. Eckernforde Summer, Sound-Velocity Profile

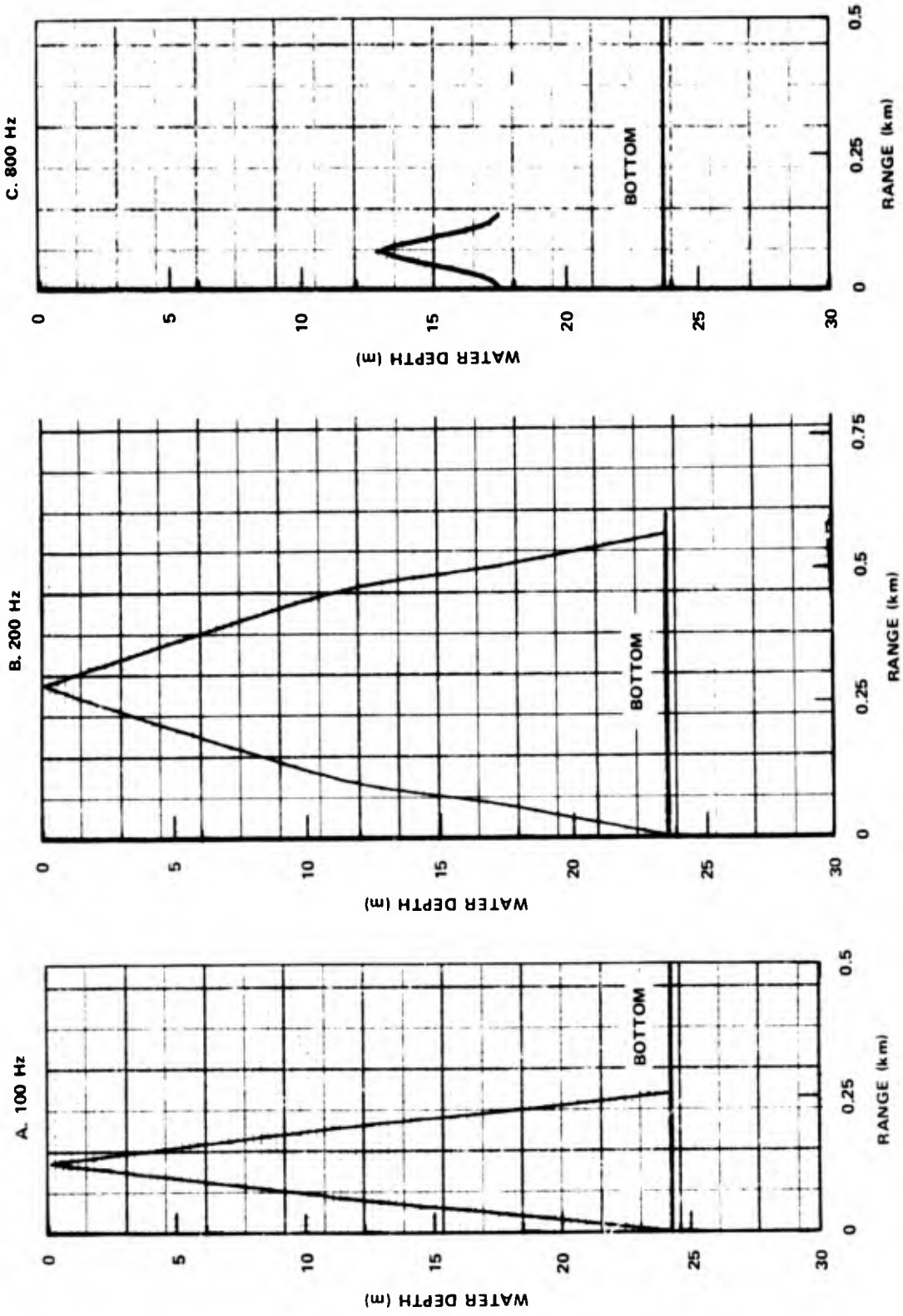

Figure 36. Eckernforde Summer, Ray Equivalent, Mode 1, at 100, 200, and 800 Hz

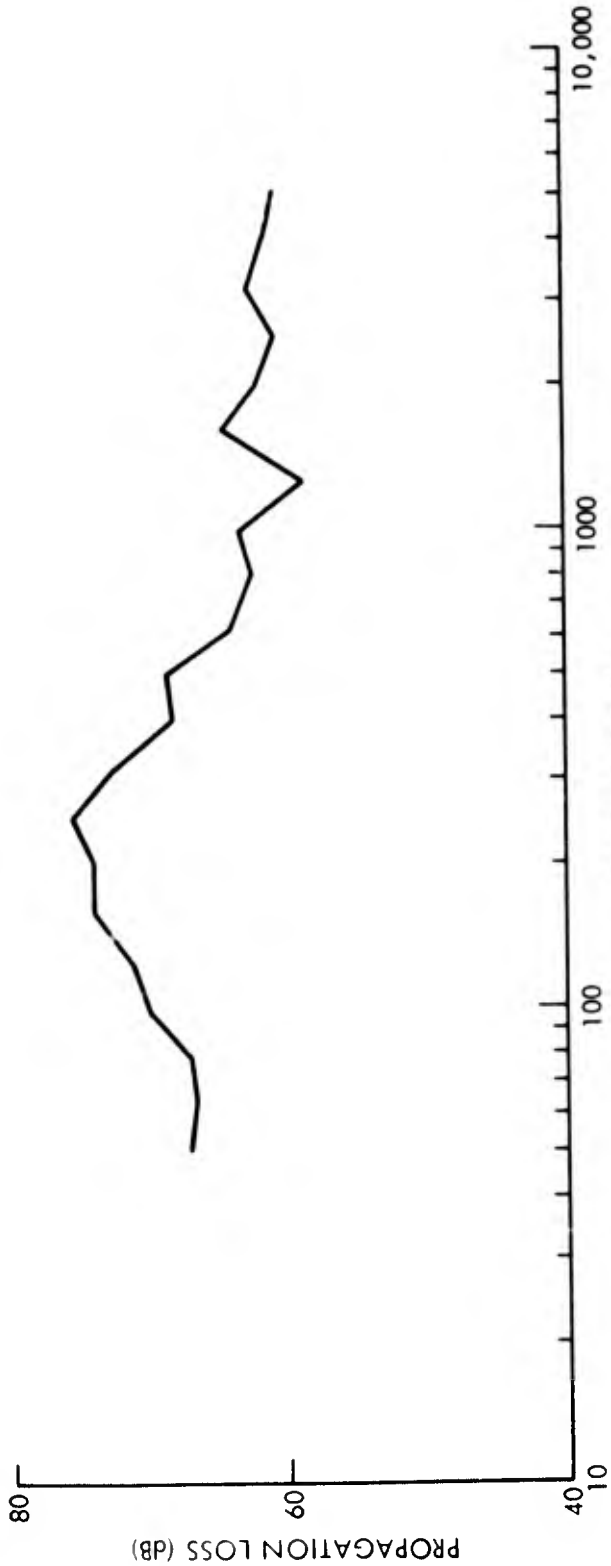

Figure 37. Eckernforde Summer, Propagation Loss Versus Frequency, Range 1.16 nmi, Source Depth 5 m, Receiver Depth 6 m, Water Depth 24 m

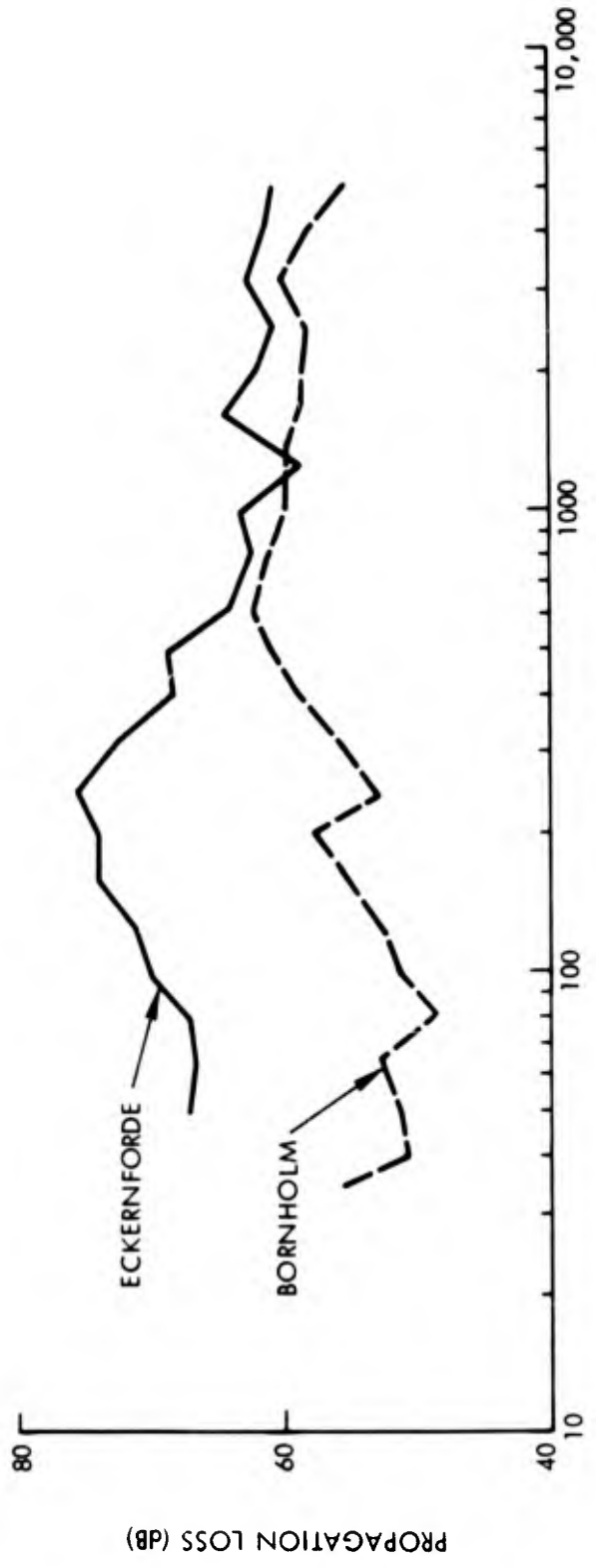

Figure 38. Eckernforde Summer Versus Bornholm Summer, Propagation Loss Versus Frequency, Range 1.1 nmi

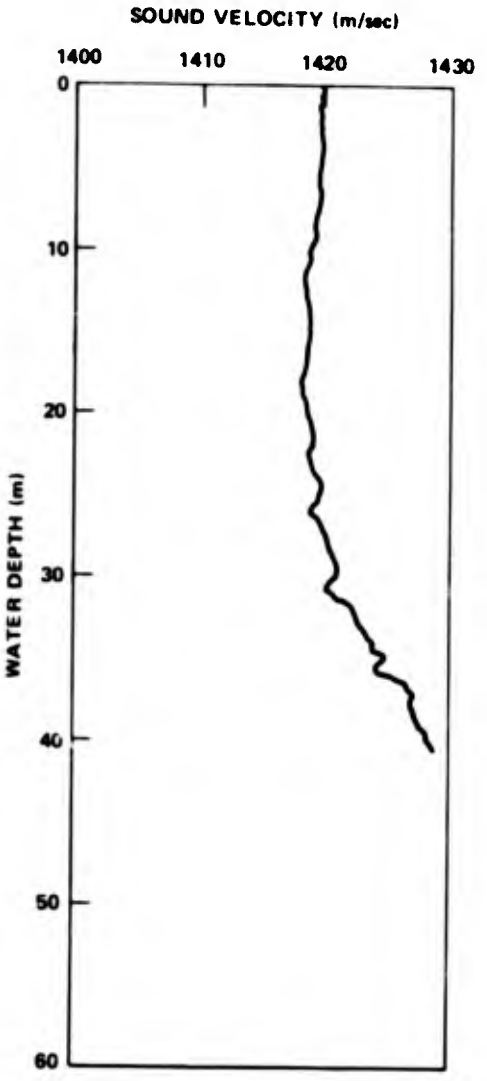

Figure 39. Bornholm Winter, Sound-Velocity Profile

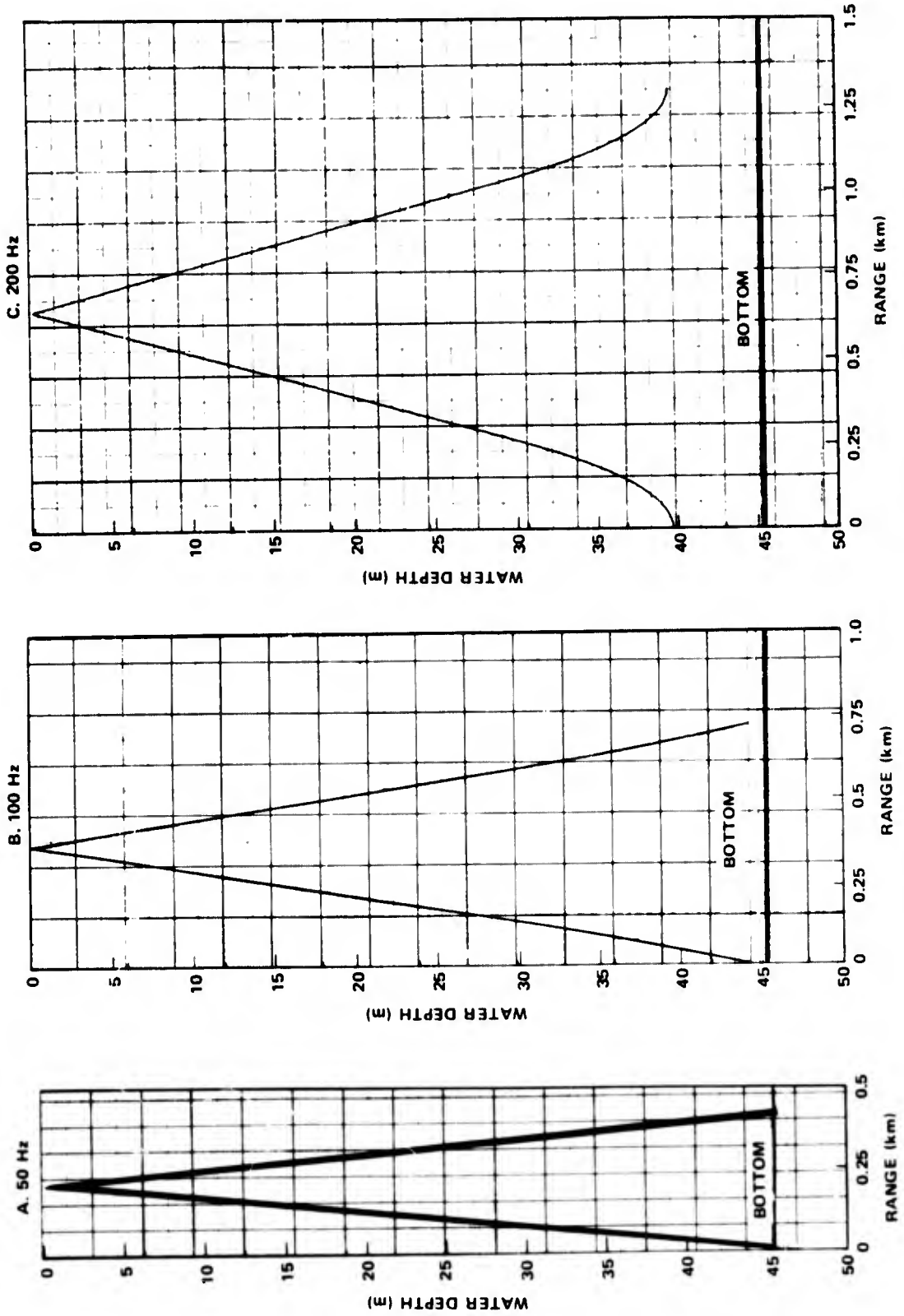

Figure 40. Bornholm Winter, Ray Equivalent, Mode 1, at 50, 100, and 200 Hz

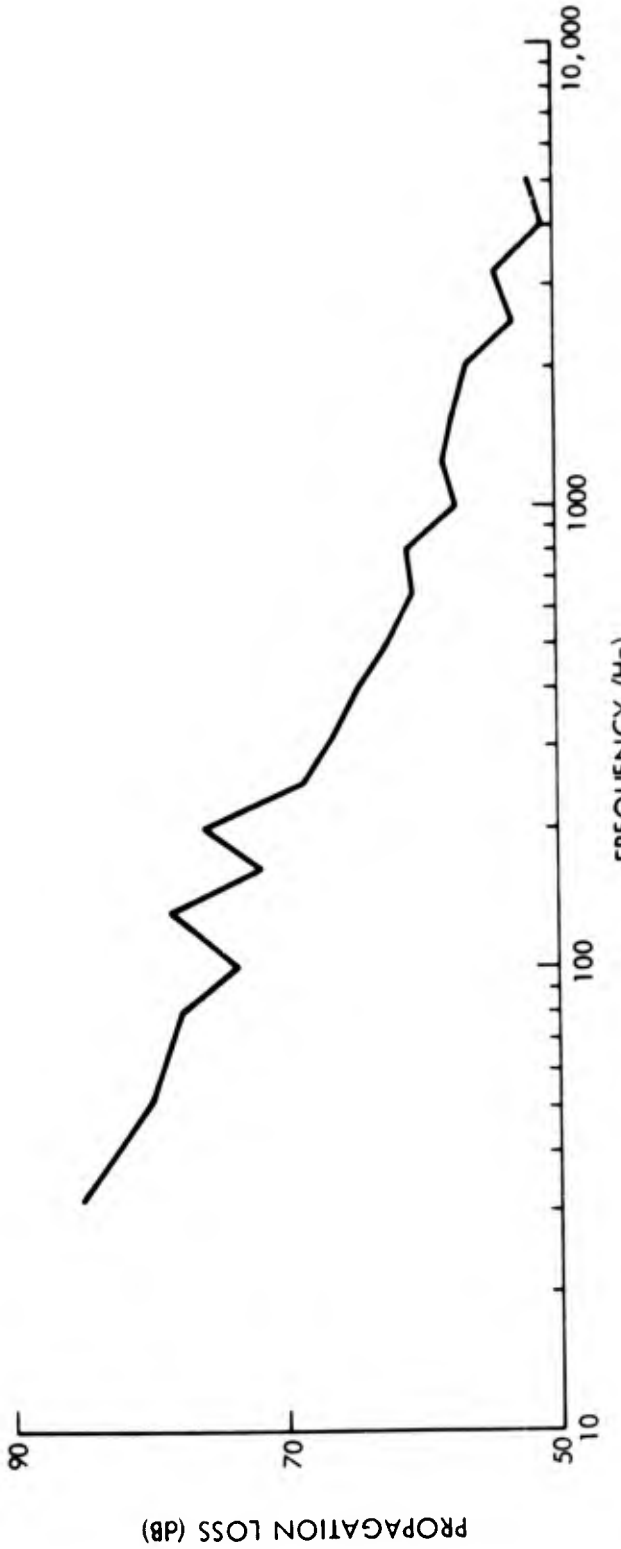

Figure 41. Bornholm Winter, Propagation Loss Versus Frequency, Range 0.60 nmi, Source Depth 12 m, Receiver Depth 10 m, Water Depth 45 m

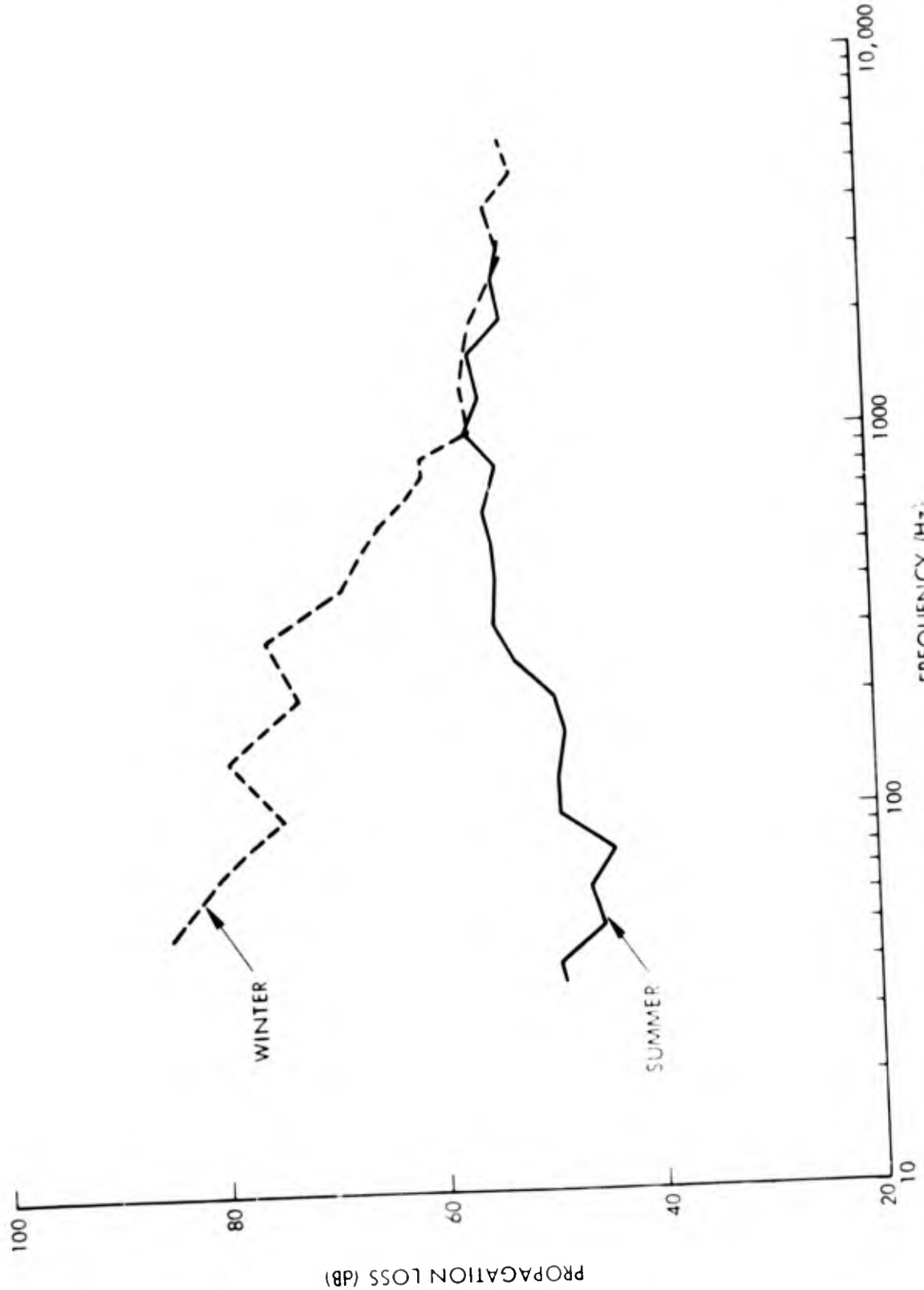

Figure 42. Bornholm Winter Versus Bornholm Summer, Propagation Loss Versus Frequency, Range 3.6 nmi

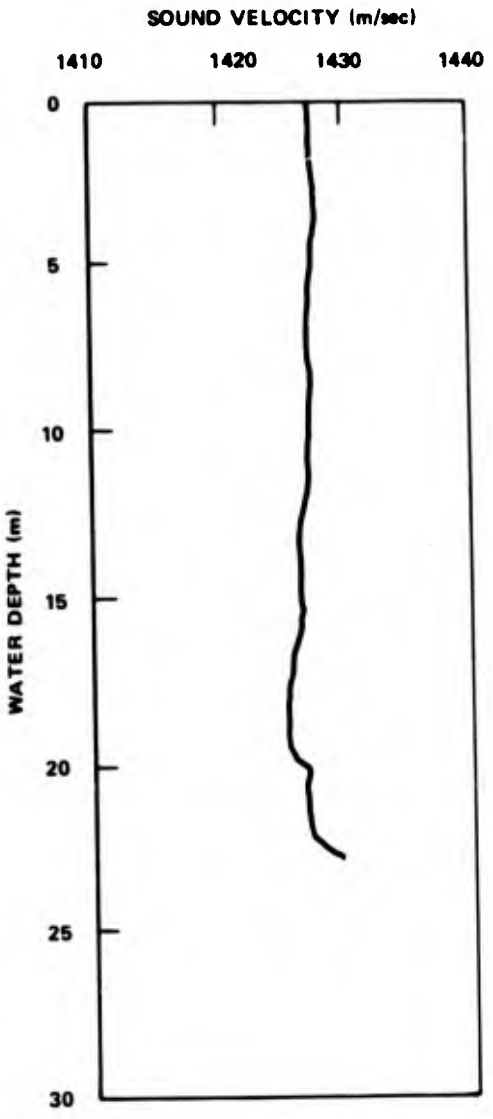

Figure 43. Eckernforde Winter, Sound-Velocity Profile

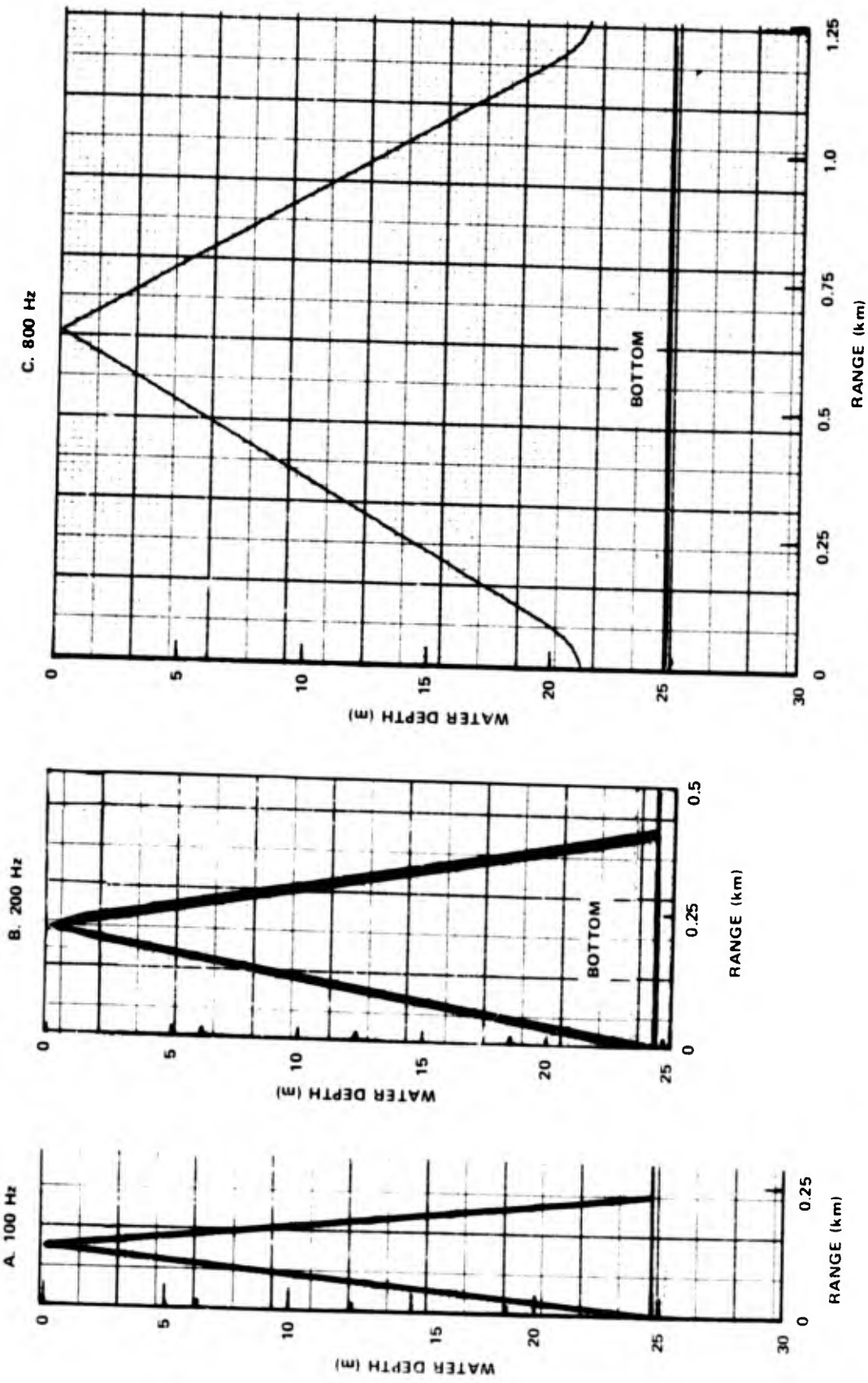

Figure 44. Eckernforde Winter, Ray Equivalent, Mode 1, at 100, 200, and 800 Hz

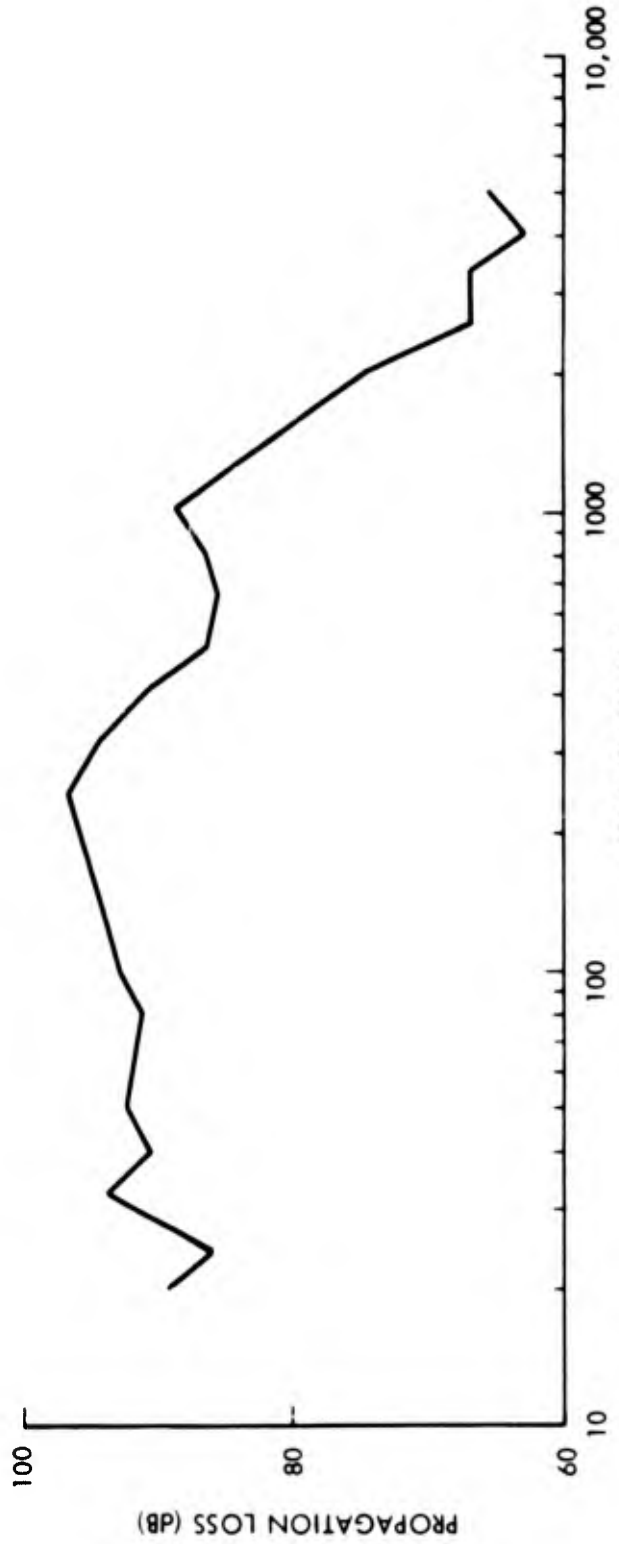

Figure 45. Eckernforde Winter, Propagation Loss Versus Frequency, Range 2.75 nmi, Source Depth 6 m, Receiver Depth 5 m, Water Depth 24 m

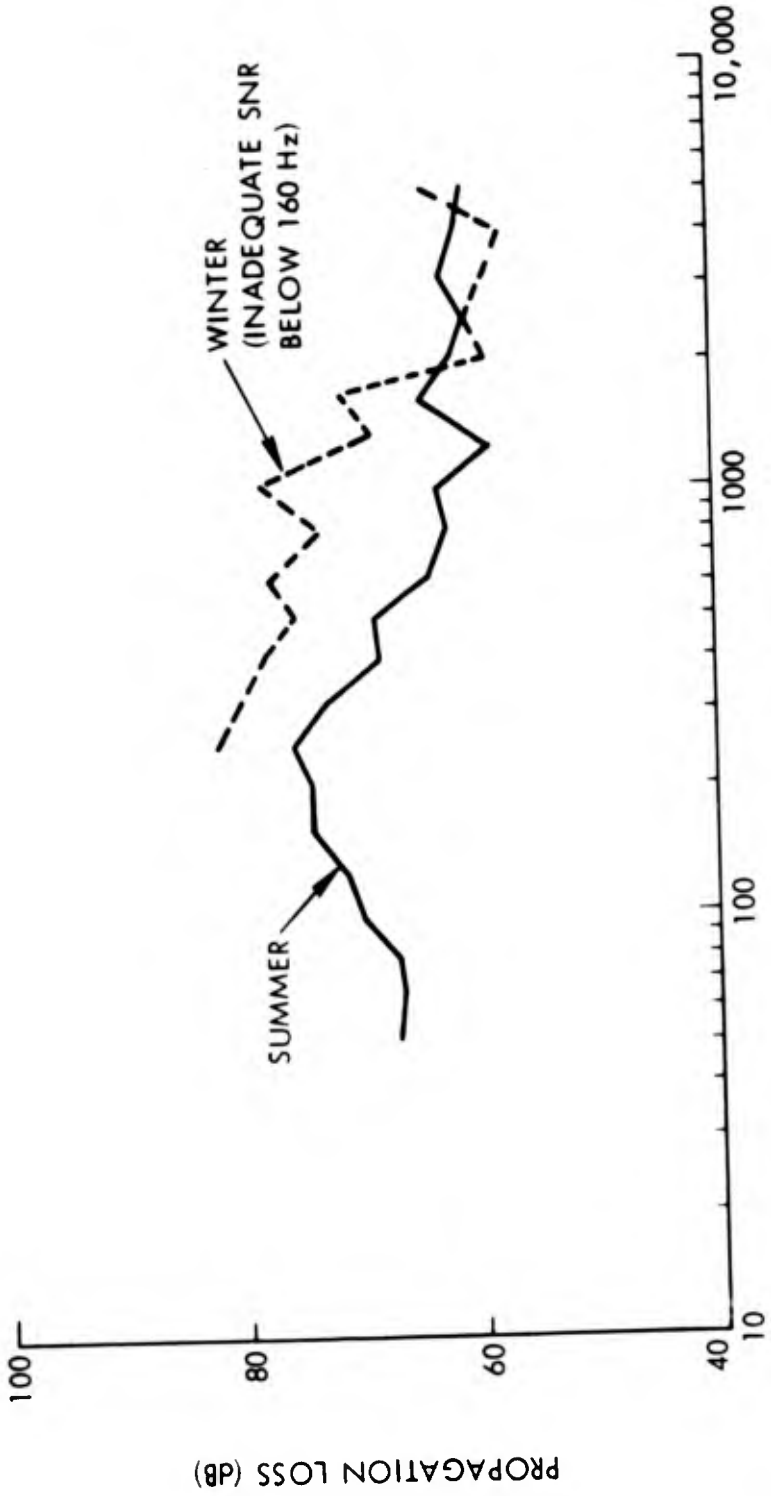

Figure 46. Eckernforde Winter Versus Eckernforde Summer, Propagation Loss Versus Frequency, Range 1.1 nmi

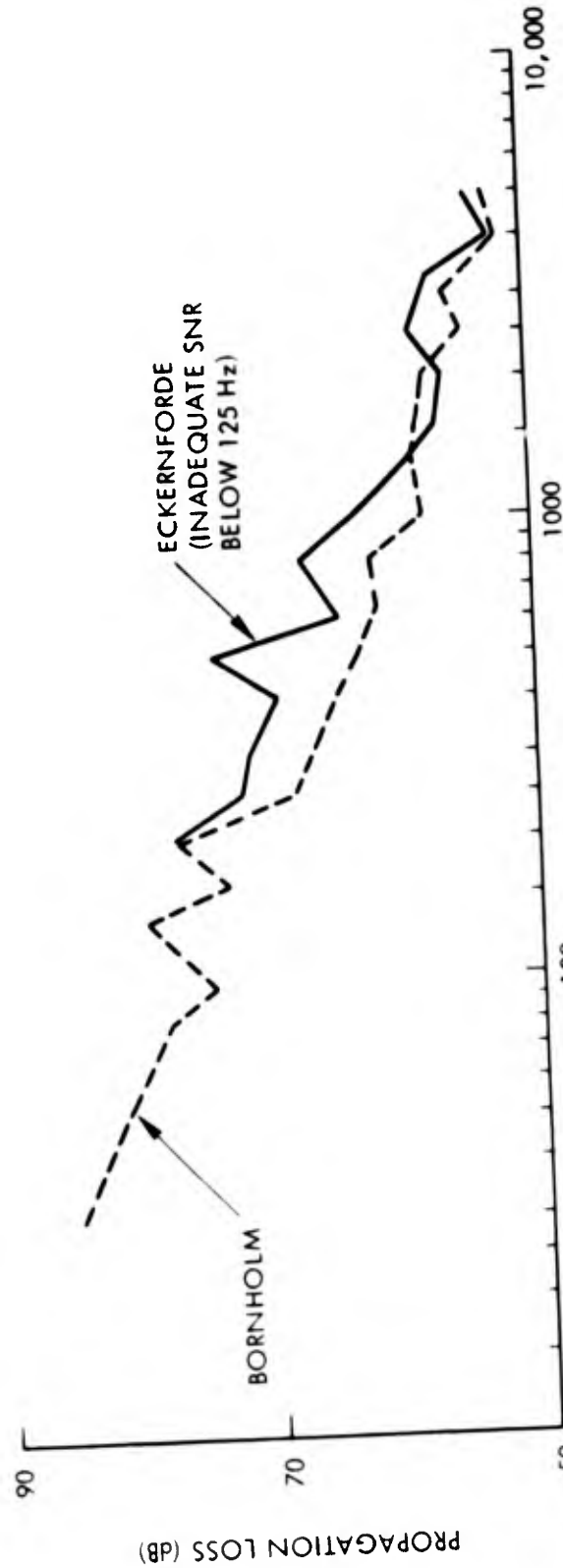

Figure 47. Eckernforde Winter Versus Bornholm Winter, Propagation Loss Versus Frequency, Range 0.6 nmi

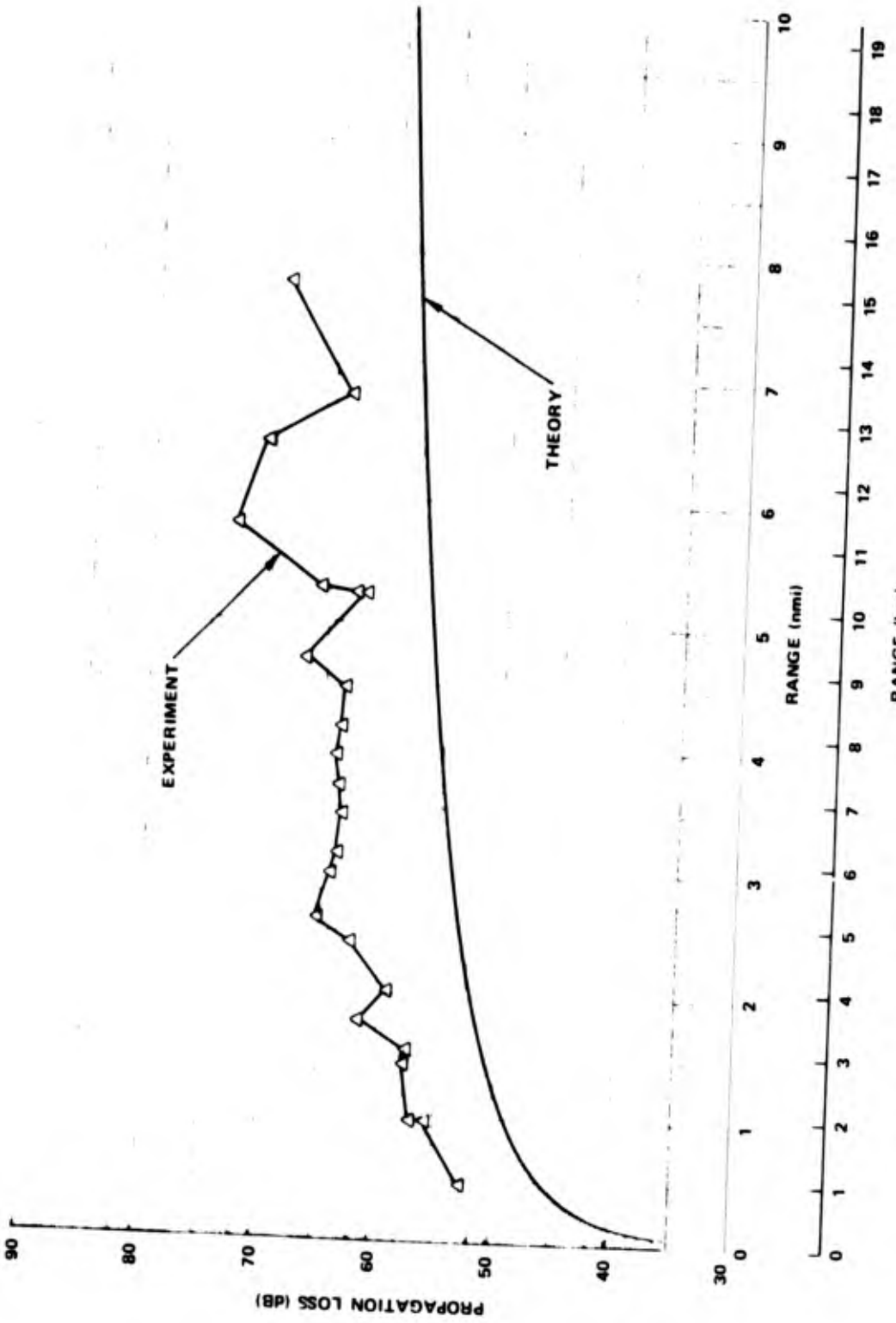

Figure 48. Bornholm Summer, Propagation Loss Versus Range, Theory Versus Experiment, Source Depth 20 m, Receiver Depth 20 m, Frequency 315 Hz, Mode 1

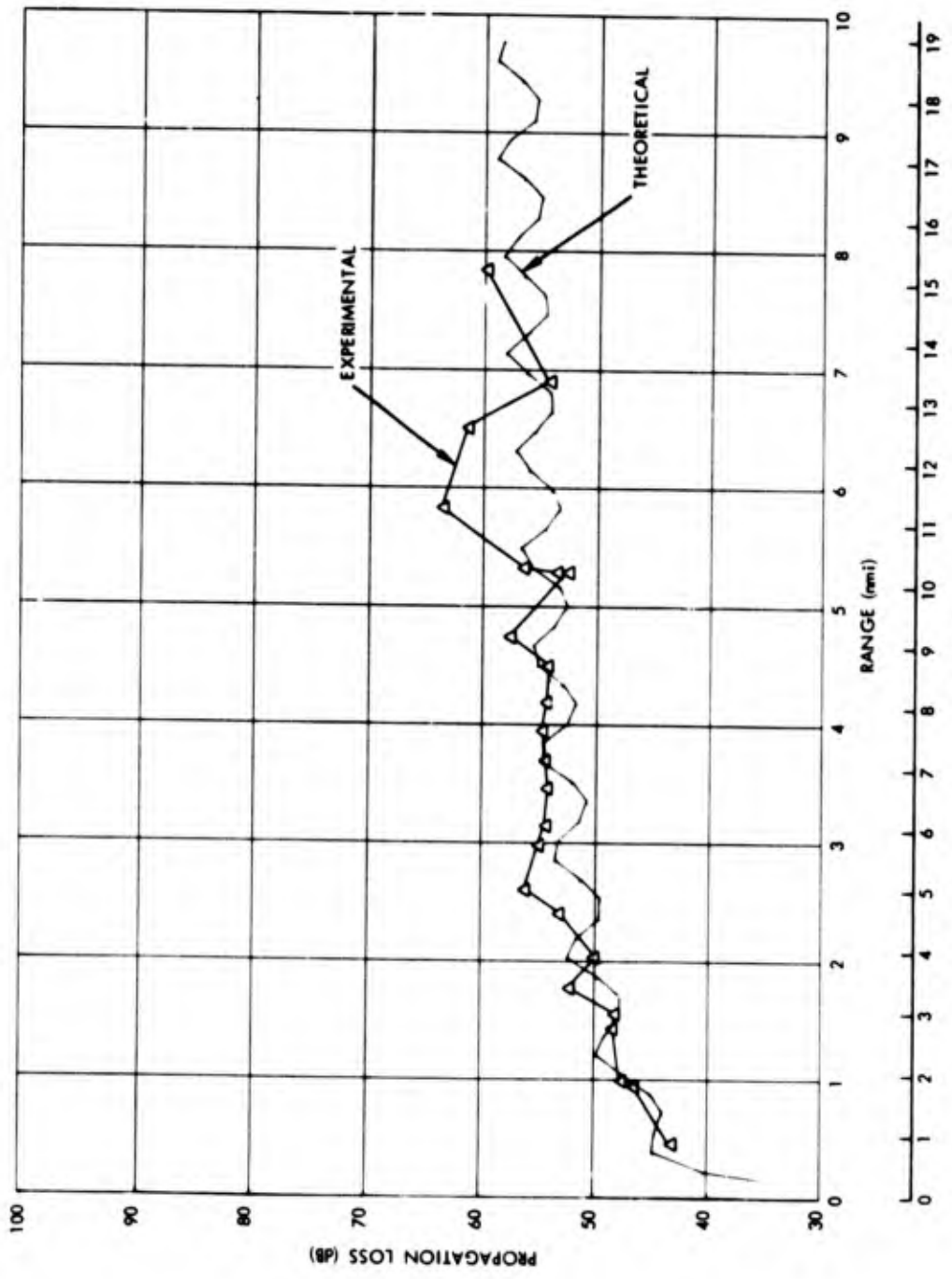

Figure 49. Bornholm Summer, Propagation Loss Versus Range, Theory Versus Experiment, Source Depth 20 m, Receiver Depth 20 m, Frequency 315 Hz, Modes 1-3

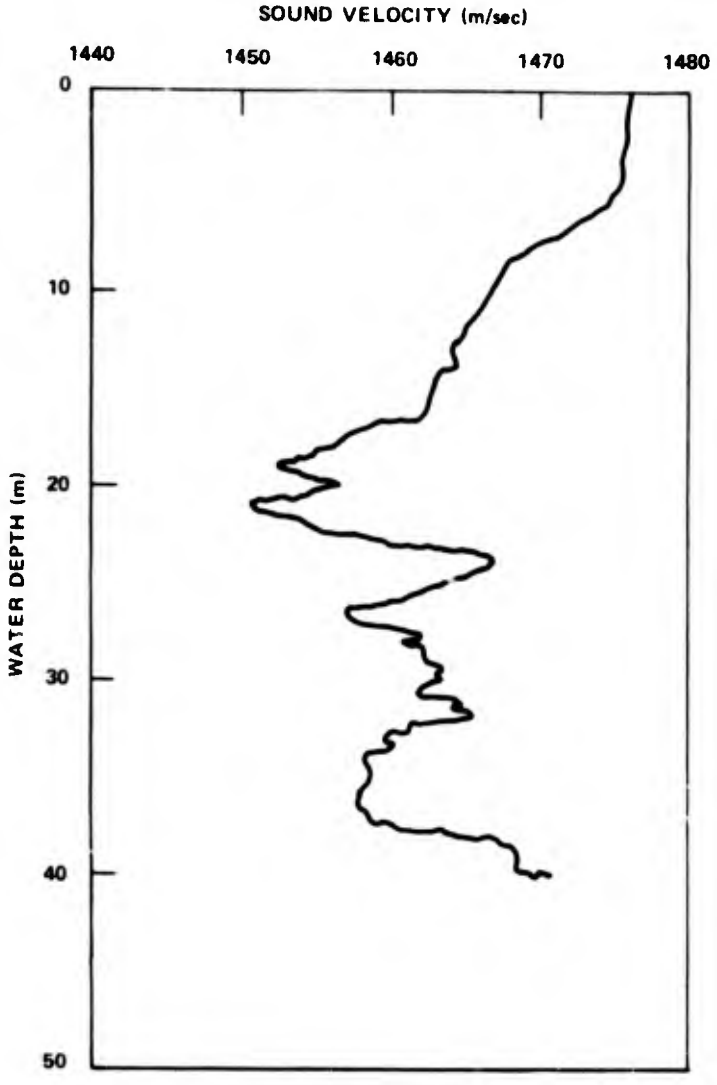

Figure 50. Bornholm Summer, Sound-Velocity Profile Showing Deterioration of the Sound Channel

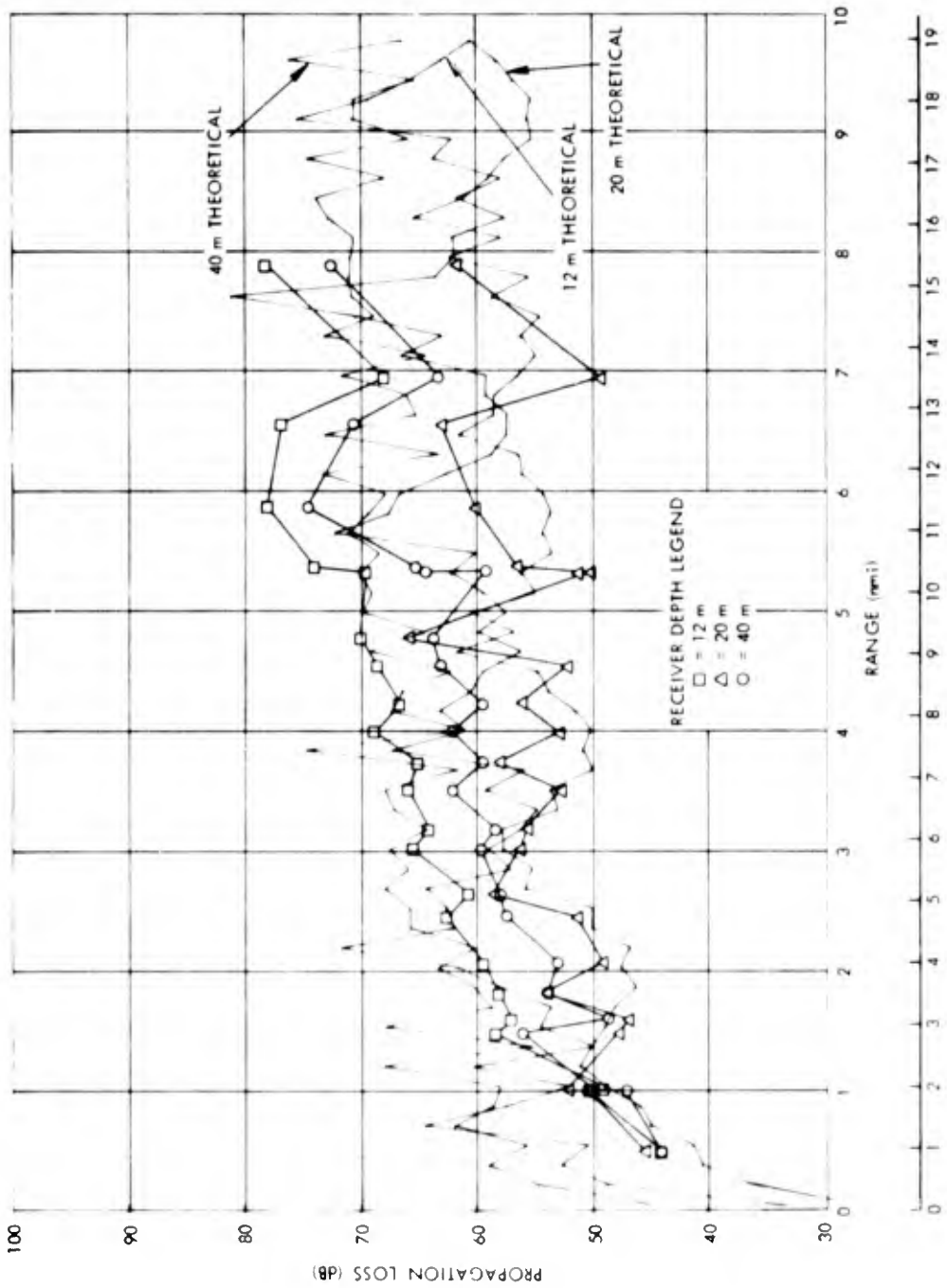

Figure 51. Bornholm Summer, Propagation Loss Versus Range for Three Receiver Depths, Theory Versus Experiment, Source Depth 20 m, Frequency 1000 Hz, Modes 1-8

TESTS USING EXPLOSIVES IN DEEP WATER

Although the model has been used most often in the analysis of shallow water acoustic propagation, it is also applicable to deep water acoustic propagation at low frequencies. The model has also been tested against experimental data taken in deep water in the western part of the North Atlantic Ocean. The data described here are extremely suitable for such an analysis for the following reasons: First, the stratification varied significantly enough with range to clearly influence acoustic propagation, and hence permit the testing of the capability of the model to accommodate changes in stratification with range as well as with depth. Second, the changes with range were slow enough to allow a deterministic description of the medium. Third, the influence of the bottom on acoustic propagation was relatively small, and hence this complicating factor usually present in shallow water tests was diminished considerably.

Such data were obtained over the tract shown in figure 52. The figure gives a rough indication of how the velocity profile was changing with range. The deep sound channel axis did not change very much over the tract but there is appreciable change in the first 1000 m. Figure 53 gives a better comparison of how the upper portion of the profile is changing with range. The profile at the right was taken at the receiver and the one on the left was taken some 200 miles away. It can be seen that a surface duct is formed with increasing range. The strength of the duct increases progressively to a range of 300 miles. Beyond 300 miles, the duct becomes less pronounced. The water depth varies little with range. In order to determine the effect of changing stratification, data taken when explosive sources were detonated at a depth (18 m) where the stratification was changing rapidly are considered. The receiver was at 4300 m, well off the SOFAR axis. The experimental results, shown in figure 54, analyzed in a one-third-octave band are typical for the source-receiver geometry at several low frequencies. It can be seen that out to 300 miles, where a strong surface duct is established, the slope of the propagation loss curve is roughly 10 dB/100 miles. Beyond 300 miles, where the duct becomes less pronounced, the mean loss is roughly constant with range. Propagation loss seems to be controlled near-surface sound-velocity variations which cause a redistribution of energy as a function of range.

Figure 55 compares experimental loss and theoretical predictions when the velocity profile and water depth are assumed to be constant with range. The profile nearest the receiver is used. It can be seen that, although the agreement is good near the receiver, beyond 200 nmi, the mean levels differ by about 5 dB.

Figure 56 is a comparison of theoretical predictions with experimental results when the actual range-dependent stratification was assumed in the calculations. For this purpose, the range was divided into six segments, each with its own characteristic velocity profile. Thirty-five modes were included in the calculation of the sound field. The mean values agree closely and the change in slope at about 300 miles is predicted. However, the interference pattern predicted is not apparent in the data. Calculations have shown that this is due, at least in part, to the assumption of a harmonic source

in the model. The actual sources were explosives. The procedure used in these calculations uses the group velocities of the modes to construct the time history of a received signal in a range-dependent environment. A pulsed CW source which transmitted 100-msec pulses was assumed in the calculations. The resulting time history of the signal is shown in figures 57 through 59 at ranges of 100, 200, and 300 nmi, respectively, from the source. The dominant modes in the sound field, modes 36 through 70, were utilized in obtaining the time histories shown. Each arrival represents one mode. It can be seen that at ranges of 200 nmi and greater, 20 of the 35 modes clearly do not overlap and hence do not contribute to range-dependent interference effects. Only 15 modes overlap to any large extent. (This occurs near the beginning of the received signal.) Hence it can be expected that the fluctuations in propagation loss with range will be considerably less than if an infinite CW source is assumed. This is borne out in figure 60, where the predicted loss for the assumed pulsed CW source is plotted together with the corresponding experimental results. It can be seen that the theoretical predictions agree well with experimental results, not only in mean level but also in the magnitude of the range-dependent fluctuations.

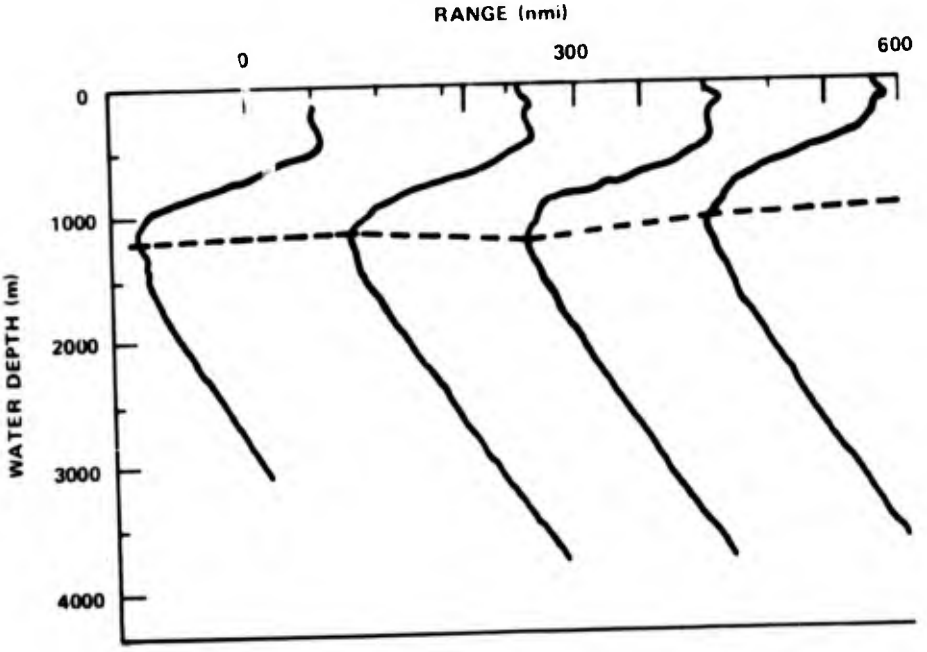

Figure 52. Velocity Profiles Along Deep Water Tract

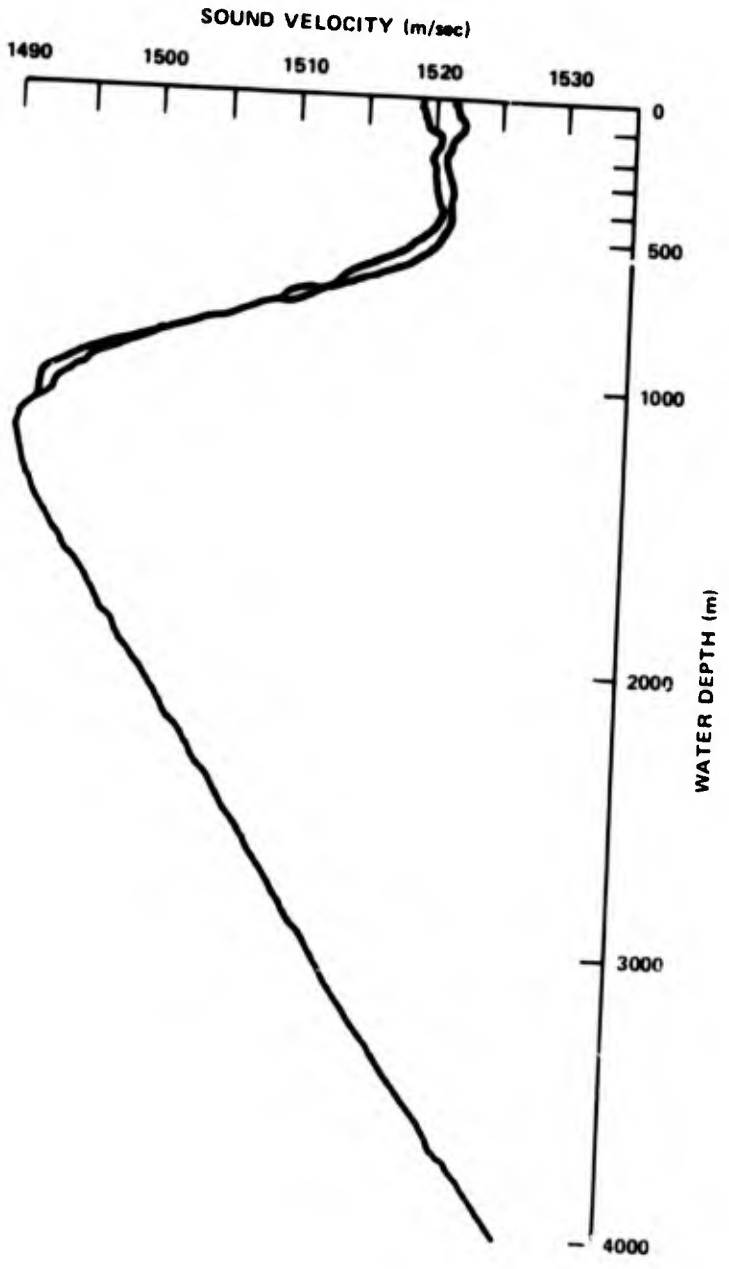

Figure 53. Comparison of Two Velocity Profiles Along Tract

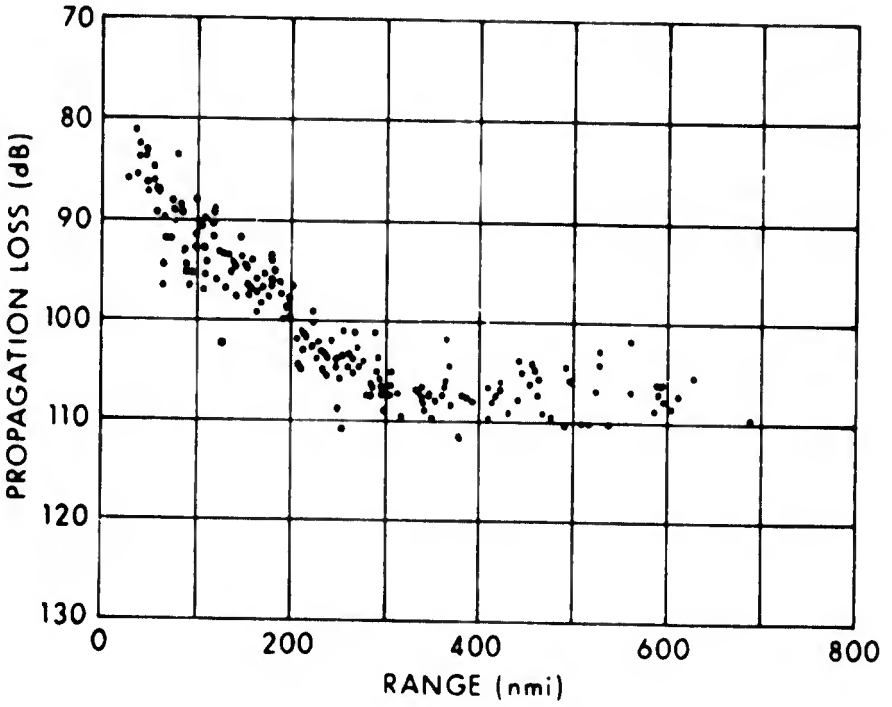

Figure 54. Propagation Loss Versus Range, Source Depth 18 m, Receiver Depth 4300 m, Frequency 50 Hz

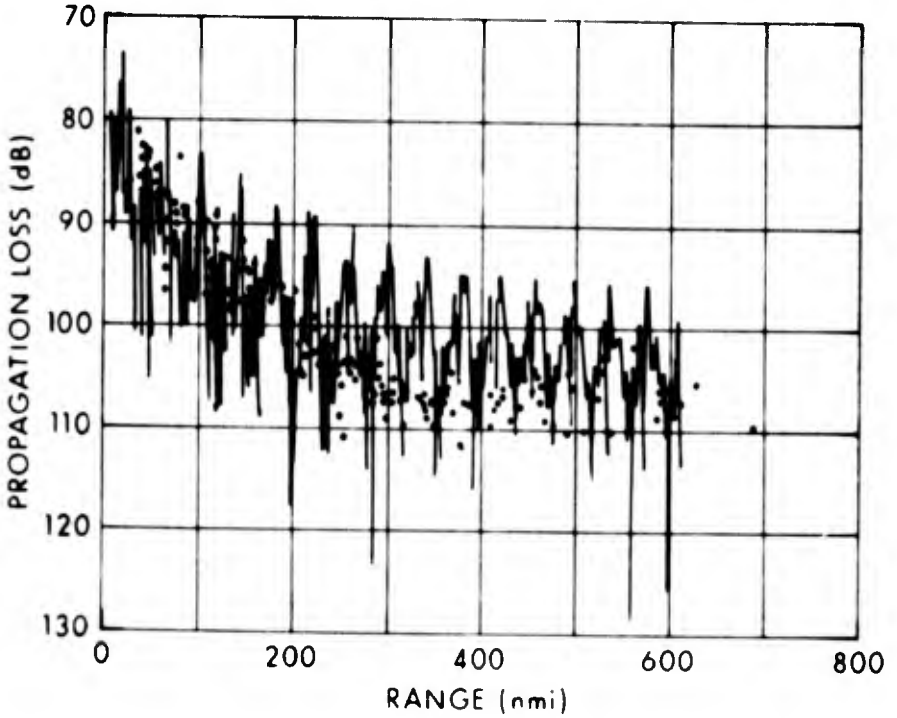

Figure 55. Propagation Loss Versus Range, Theory (Single Profile), and Experiment, Source Depth 18 m, Receiver Depth 4300 m, Frequency 50 Hz

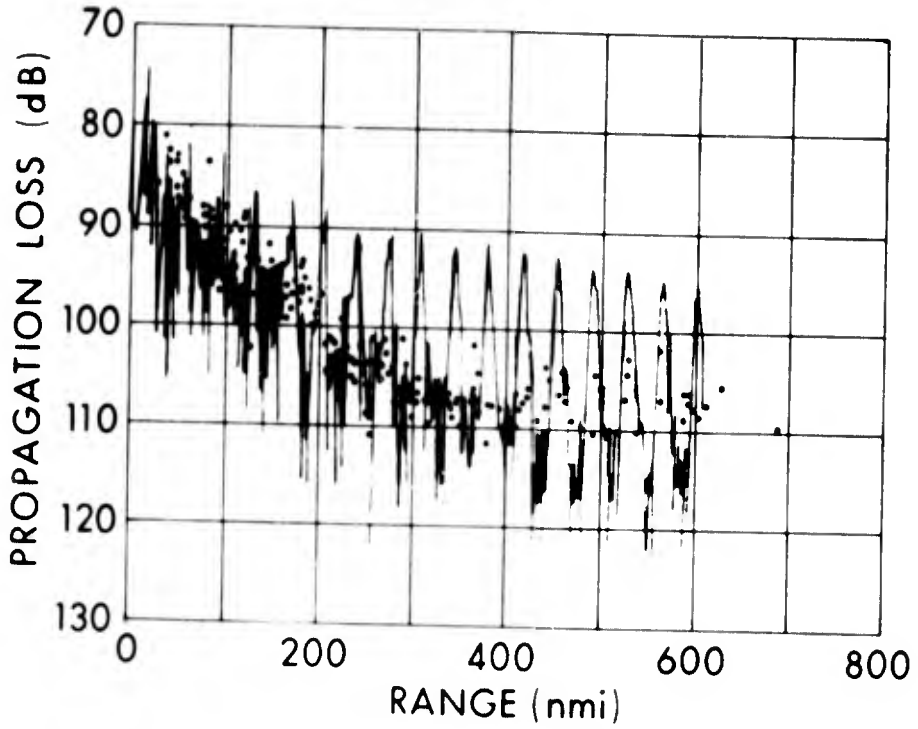

Figure 56. Propagation Loss Versus Range, Theory (Actual Stratification), and Experiment, Source Depth 18 m, Receiver Depth 4300 m, Frequency 50 Hz

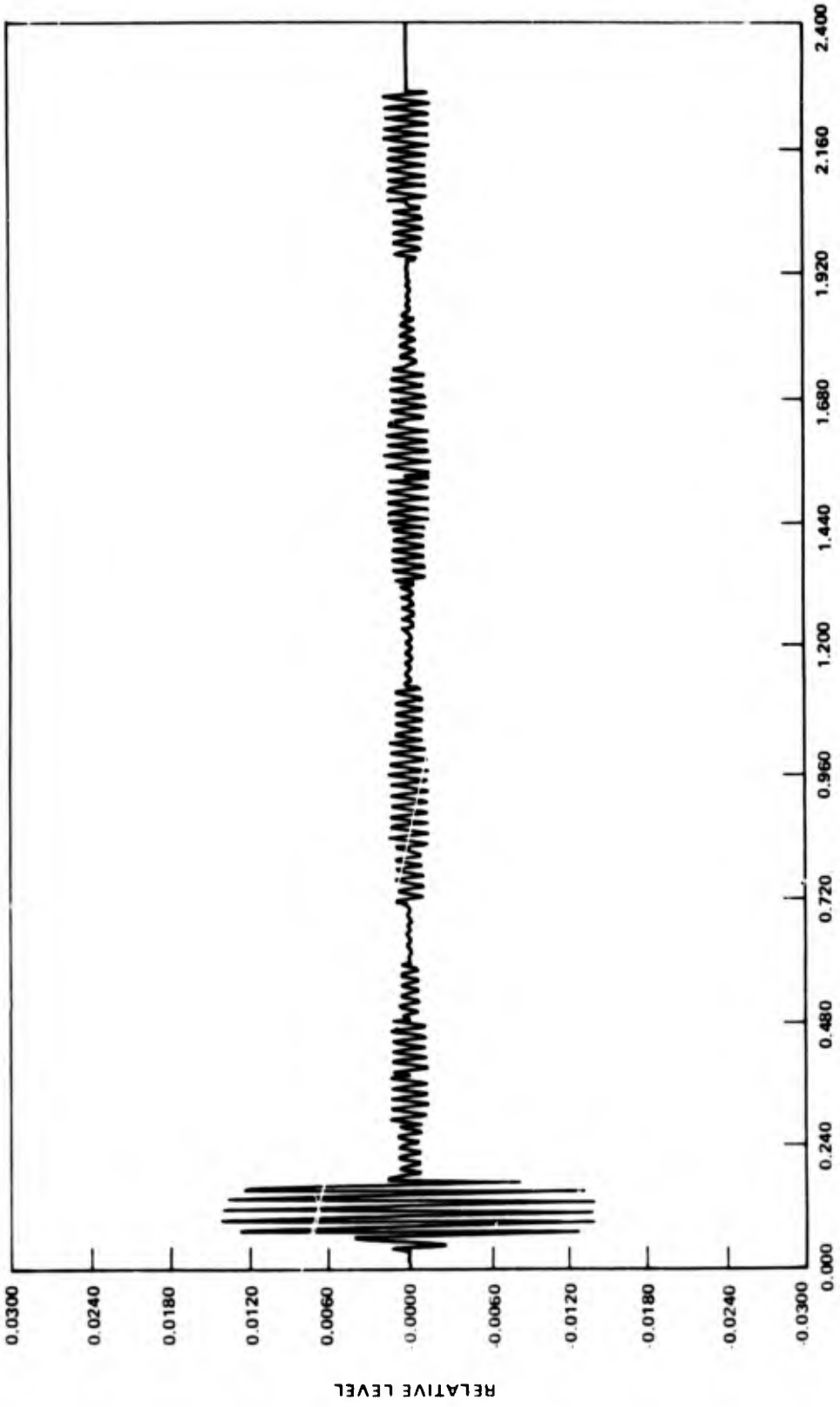

Figure 57. Received Pulse, Predicted at 100 nmi for 100-msec Pulse Transmitted at 50 Hz

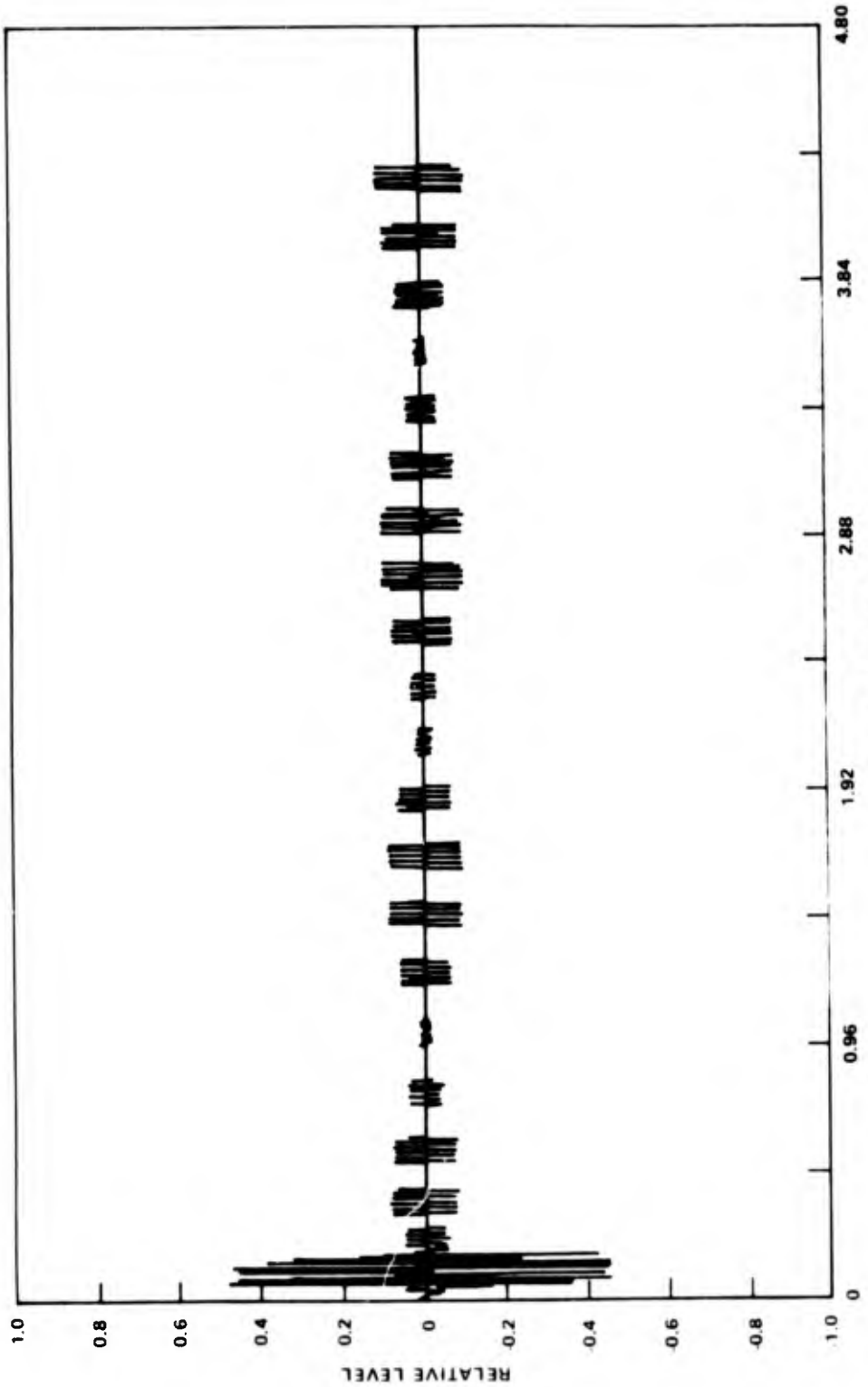

Figure 58. Received Pulse, Predicted at 200 nmi for 100-msec Pulse Transmitted at 50 Hz

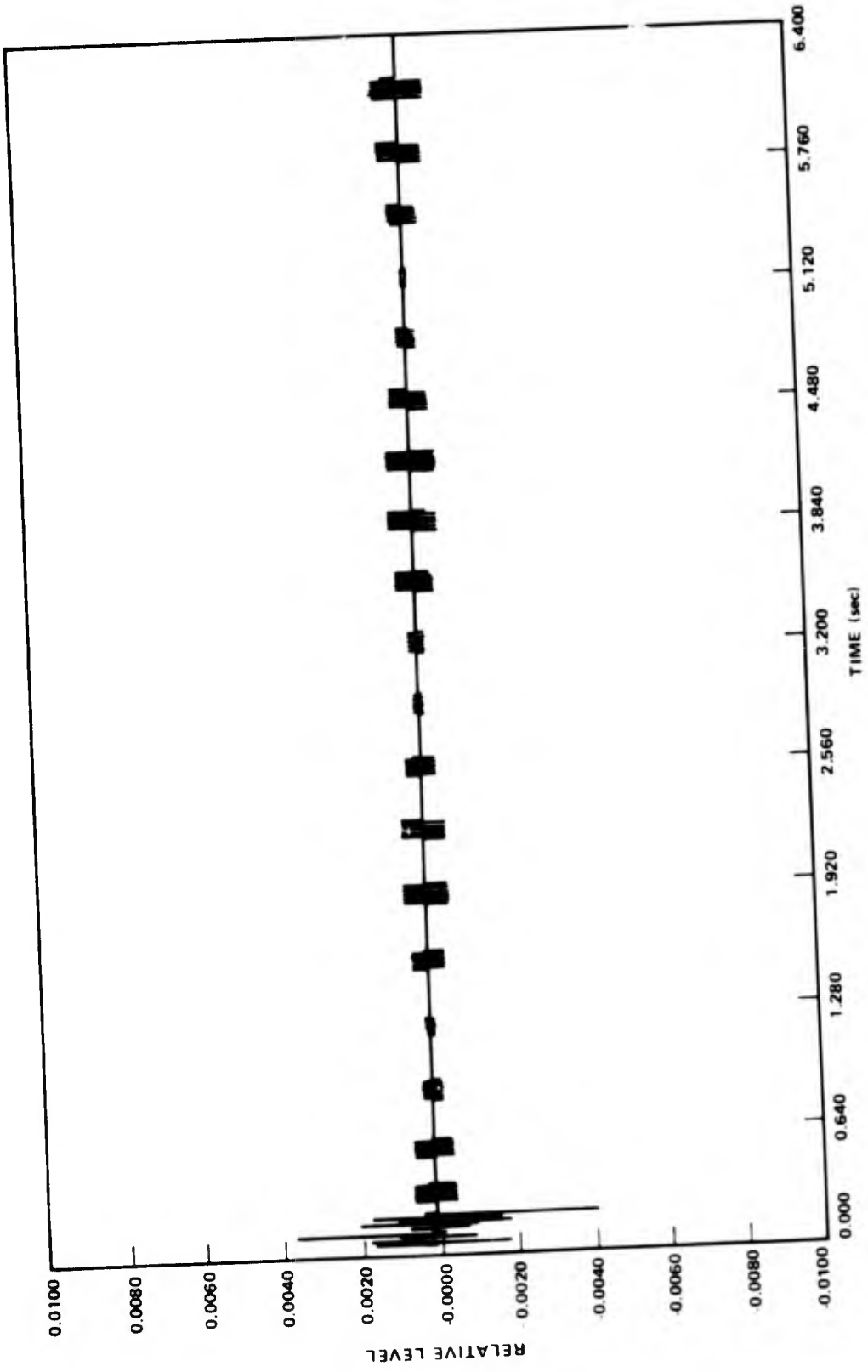

Figure 59. Received Pulse, Predicted at 300 nmi for 100-msec Pulse Transmitted at 50 Hz

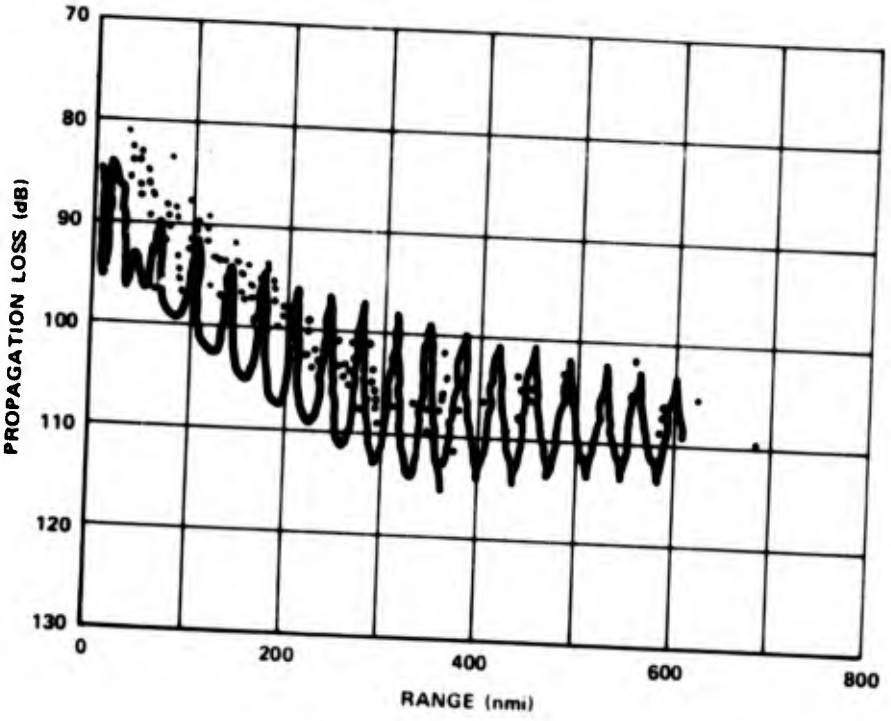

Figure 60. Propagation Loss Versus Range, Theory (Time-Limited Signal and Actual Stratification), and Experiment, Source Depth 18 m, Receiver Depth 4300 m, Frequency 50 Hz

TESTS USING CW SOURCES OVER SLOPING BOTTOM

Experimental data taken in shallow water were used to test the model against experimental data from an environment in which the slope of the bottom influences propagation. Such data, reported by Aubel of the Norwegian Defense Research Establishment (reference 25), are used so that experimental results are compared with theoretical predictions for two tracts in the Norwegian Sea. The first tract considered is shown in figure 61. It can be seen that there is a large variation in the water depth with range. The slope of the bottom, which appears large due to the vertical exaggeration of the scale, is of the order of 0.1 deg. The stratification of the water column varied slowly with range. A typical velocity profile is shown in figure 62. It can be seen that there is a weak surface channel and below the channel the sound velocity progressively decreases with increasing water depth. Data were obtained by towing a CW source at a depth of 15 m and transmitting at a frequency of 116 Hz. Signals were received by a fixed hydrophone suspended at a depth of 15 m. The experimental results, shown in figure 63, were obtained from paper recordings of the received signals. It appears that the variations in the propagation loss with range are tied to the variations in bottom depth with range. For instance, at ranges up to 15 km, the bottom is relatively flat and the propagation loss with range corresponds roughly to that attributable to cylindrical spreading. At ranges from 15 to 25 km, the bottom depth increases abruptly and the propagation loss increases at a rate greater than that attributable to cylindrical spreading. At ranges from 25 to 60 km, the bottom again is relatively flat and the propagation loss again increases at a rate corresponding to cylindrical spreading. Finally, at ranges from 60 to 125 km, a sharp increase in bottom depth is accompanied by a large rate of increase in the propagation loss.

Figure 64 compares theoretical predictions with experimental results when the actual range-dependent stratification is assumed in the calculations. The range was divided into 6 segments, and 12 modes were included in the calculation of the sound field. However, mode conversion is neglected in the calculations. The modes are assumed to be essentially unattenuated with range. It can be seen that the predicted values of propagation loss, which increase at a rate that roughly corresponds to cylindrical spreading, are as much as 30 dB below the measured values. Hence it appears that the vertical redistribution of energy within individual modes caused by changing stratification with range does not produce the excess propagation loss observed.

Figure 65 is a similar comparison of theoretical predictions with experimental results in which the effect of mode conversion (defined in volume 1 of this report) is included in the theoretical calculations. The vertical spacing used in the mode conversion calculations was 10 ft. Again the modes are assumed to be unattenuated with range. The agreement between theory and experiment is very good. Hence it appears that the effect of the variation in bottom depth is a significant redistribution of energy between modes as a function of range, which can account for the excess loss beyond cylindrical spreading observed in the data. This analysis contains the final progressive step which was not included in the corresponding preceding examples. In these examples, the excess loss was attributed to the bottom, but the exact mechanism and

the resulting quantitative predictions of the loss were unspecified. Only an empirical fit to the data was possible. In this case, the mechanism has been specified and quantitative predictions of the resulting loss produce a very good fit to the data.

The second tract considered is shown in figure 66. In the first portion of the tract, from 0 to 40 km, the bottom depth increases at roughly the same rate as in the tract considered previously. The slope is about 0.1 deg. Beyond 40 km, the depth drops off rather abruptly and the slope is roughly 3 deg. It might be of interest to note parenthetically that the vertical exaggeration in the typical bathymetric scale makes it extremely difficult to determine, with a high degree of accuracy, the exact slope of the bottom, and this may be a major problem in predicting propagation when large slopes occur. The stratification of the water column varied slowly with range. A typical profile is shown in figure 67. It can be seen that a rather strong negative gradient occurs.

Data were taken as before by towing a CW source at a depth of 15 m and transmitting at a frequency of 116 Hz. However, signals were received by a deeper, fixed hydrophone suspended at a depth of 90 m. The experimental results are shown in figure 68. It appears again that the variation in propagation loss with range is tied to the variations in the bottom depth with range. At ranges up to 40 km, where the bottom drops off with a slope of about 0.1 deg, propagation loss exceeds that due to cylindrical spreading. At ranges beyond 40 km, where the bottom depth increases much more rapidly, there is a dramatic increase in propagation loss.

Figure 69 compares theoretical predictions with experimental results. The effect of mode conversion is included in the theoretical calculations and the modes are assumed to be essentially unattenuated with range. The range was divided into 11 segments and 48 modes were included in the calculation of the sound field. The vertical spacing used in the mode conversion calculations was 10 ft. The agreement is good out to a range of about 50 km. However, beyond 50 km, it can be seen that the predicted values exceed the measured values of propagation loss, and it appears that the predictions exaggerate the effect of the more rapid increase in bottom depth. It should be noted that since the source level of the projector was about 90 dB, the values of loss determined beyond a range of 70 km are probably not reliable, because the signal level must be very close to that of the noise.

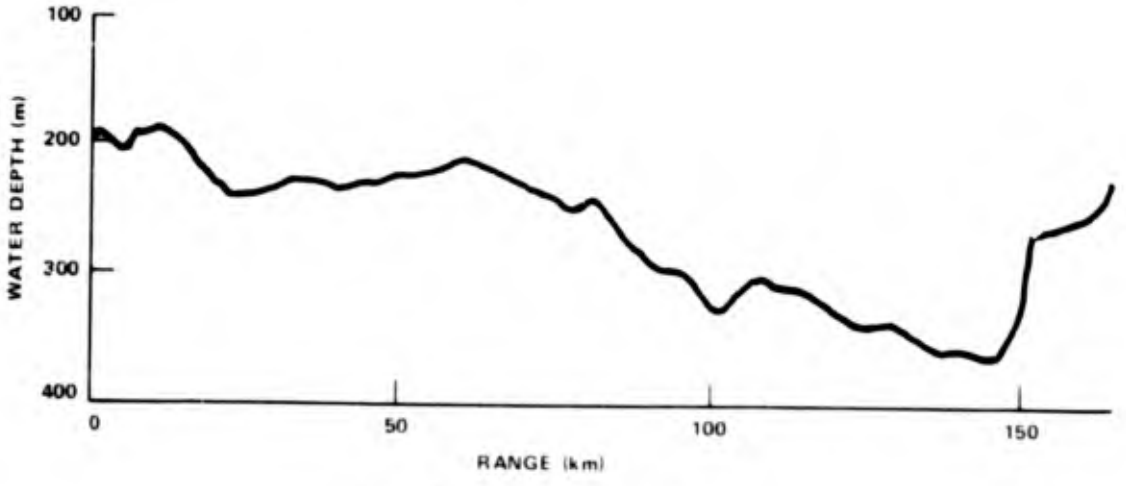

Figure 61. Bottom Profile
(First Tract)

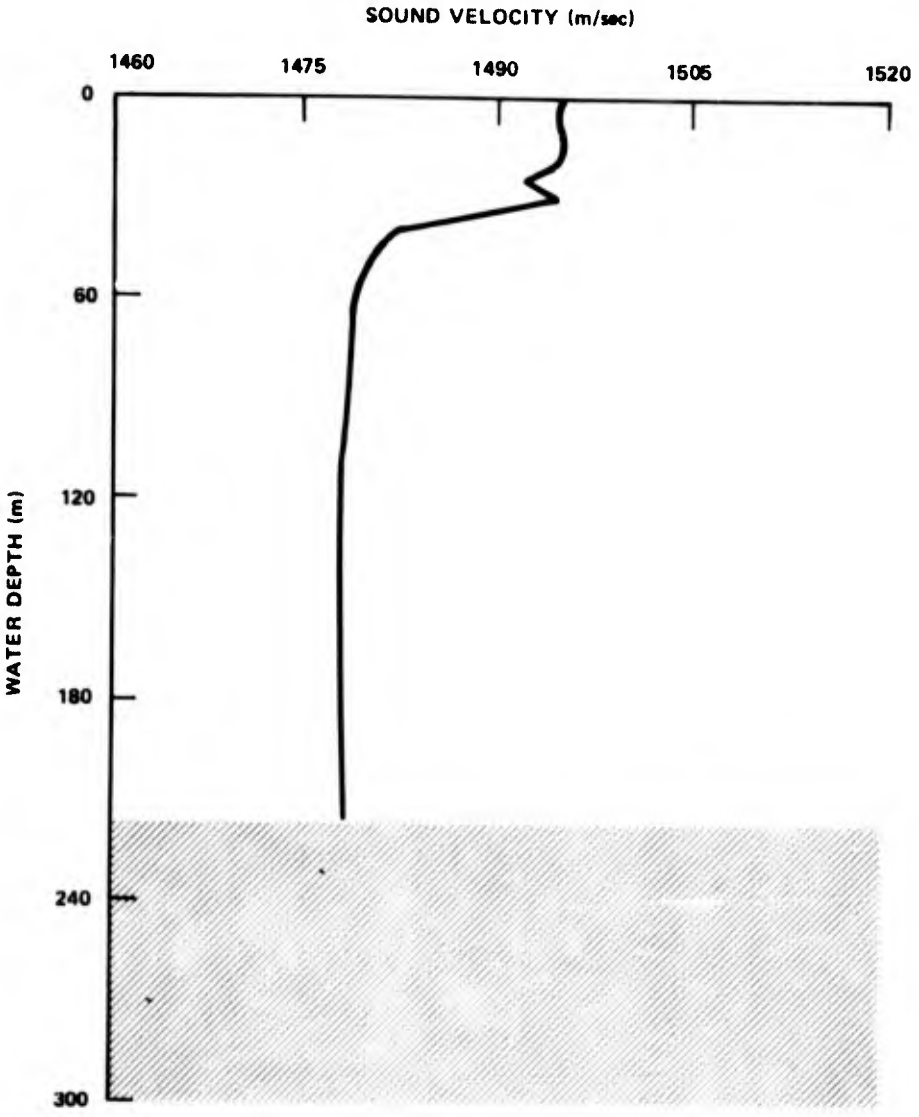

Figure 62. Typical Velocity Profile
(First Tract)

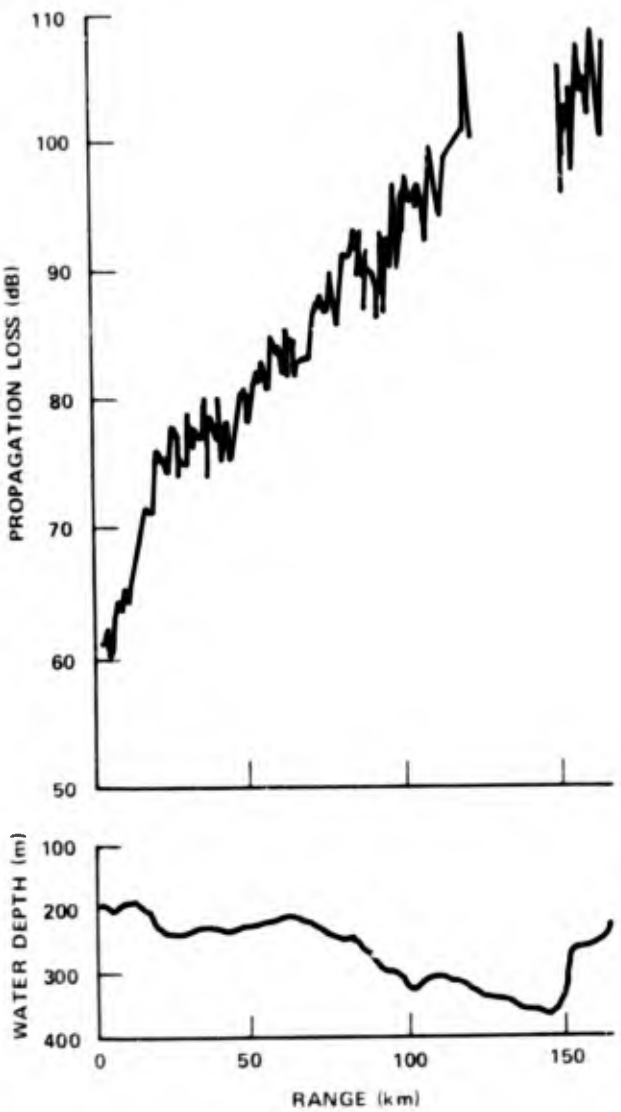

Figure 63. Experimental Results Showing Propagation Loss Versus Range (First Tract)

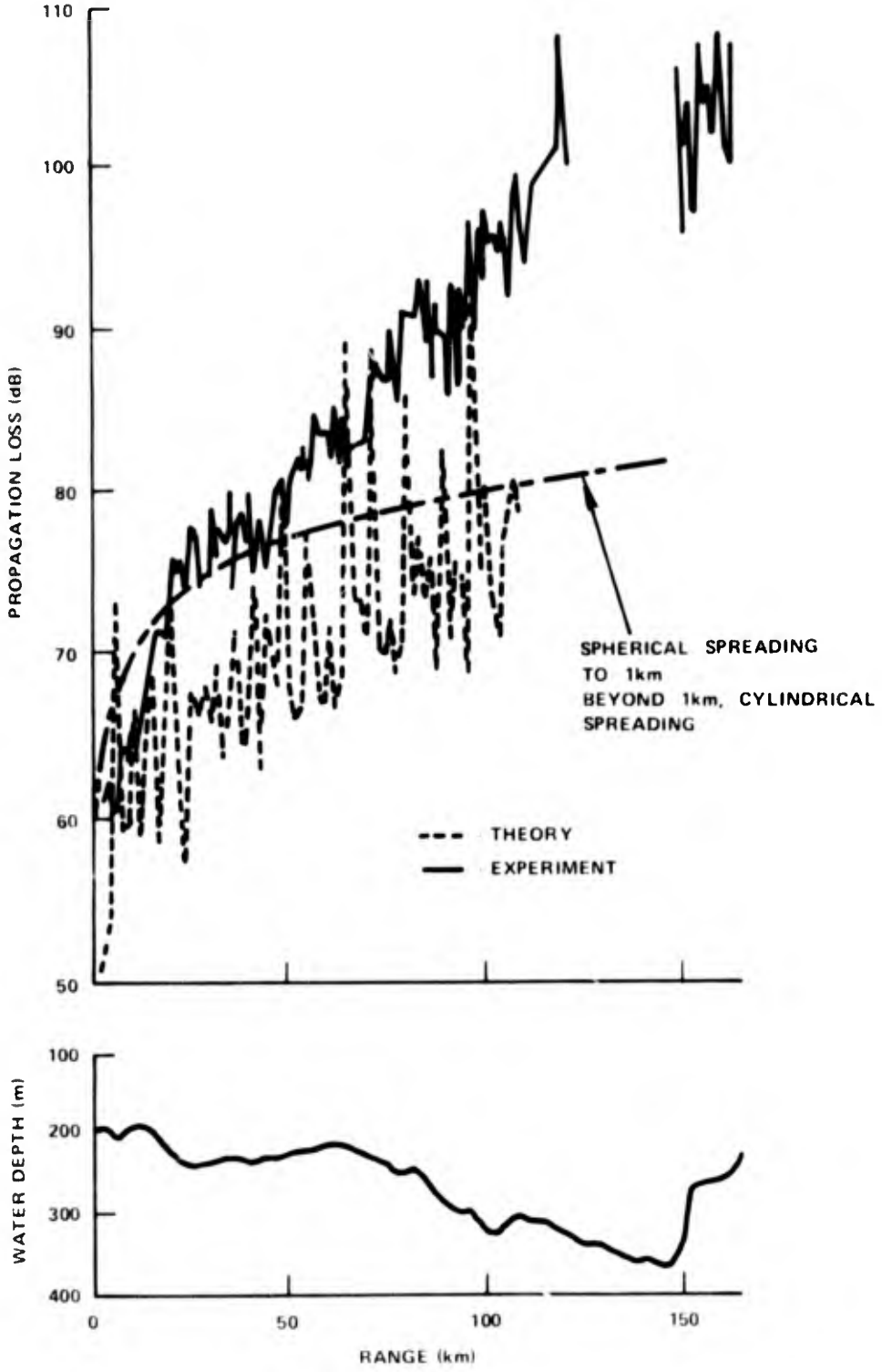

Figure 64. Propagation Loss Versus Range, Comparison Between Experiment and Theory (No Mode Conversion)

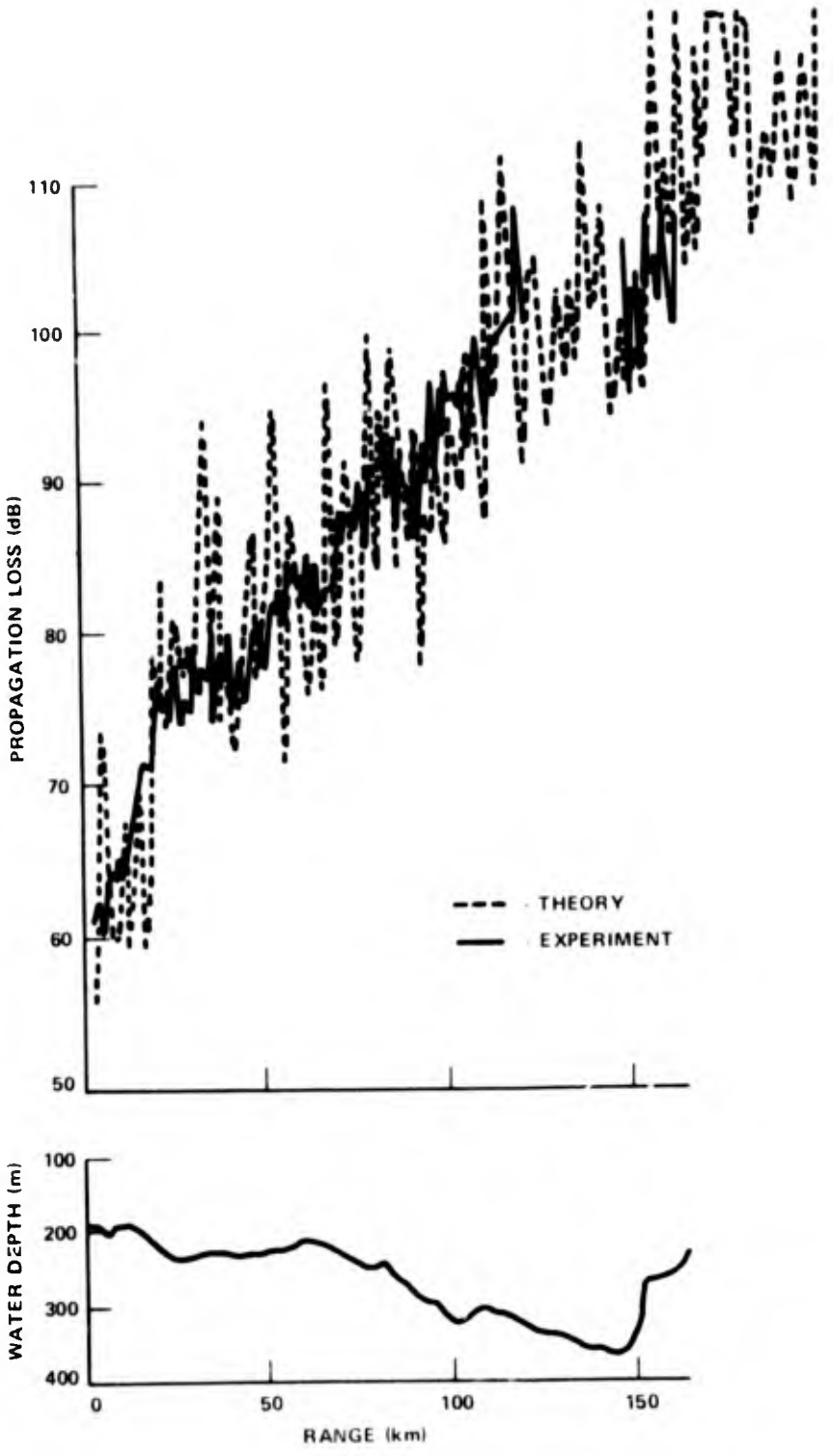

Figure 65. Propagation Loss Versus Range, Comparison Between Experiment and Theory (Considering Mode Conversion)

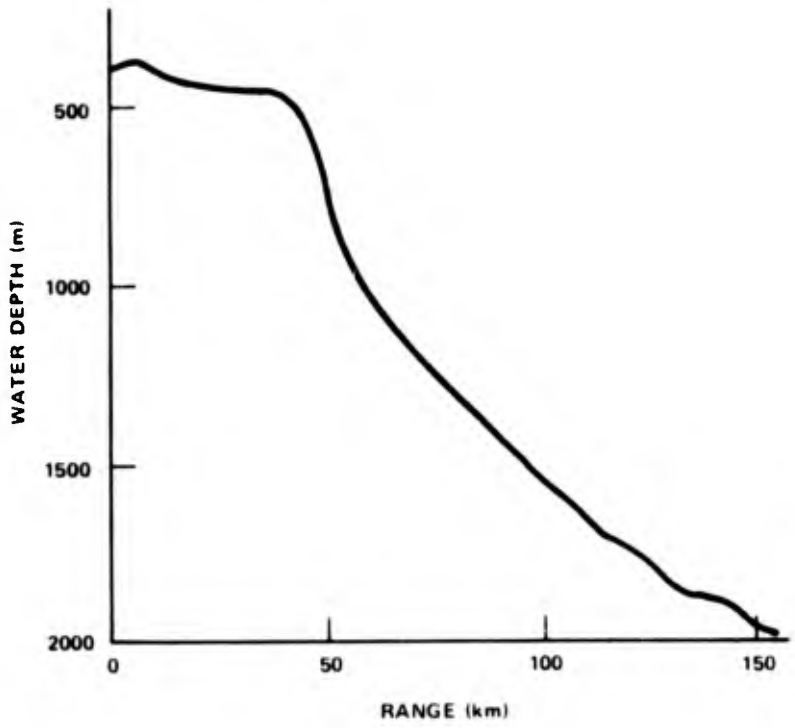

Figure 66. Bottom Profile
(Second Tract)

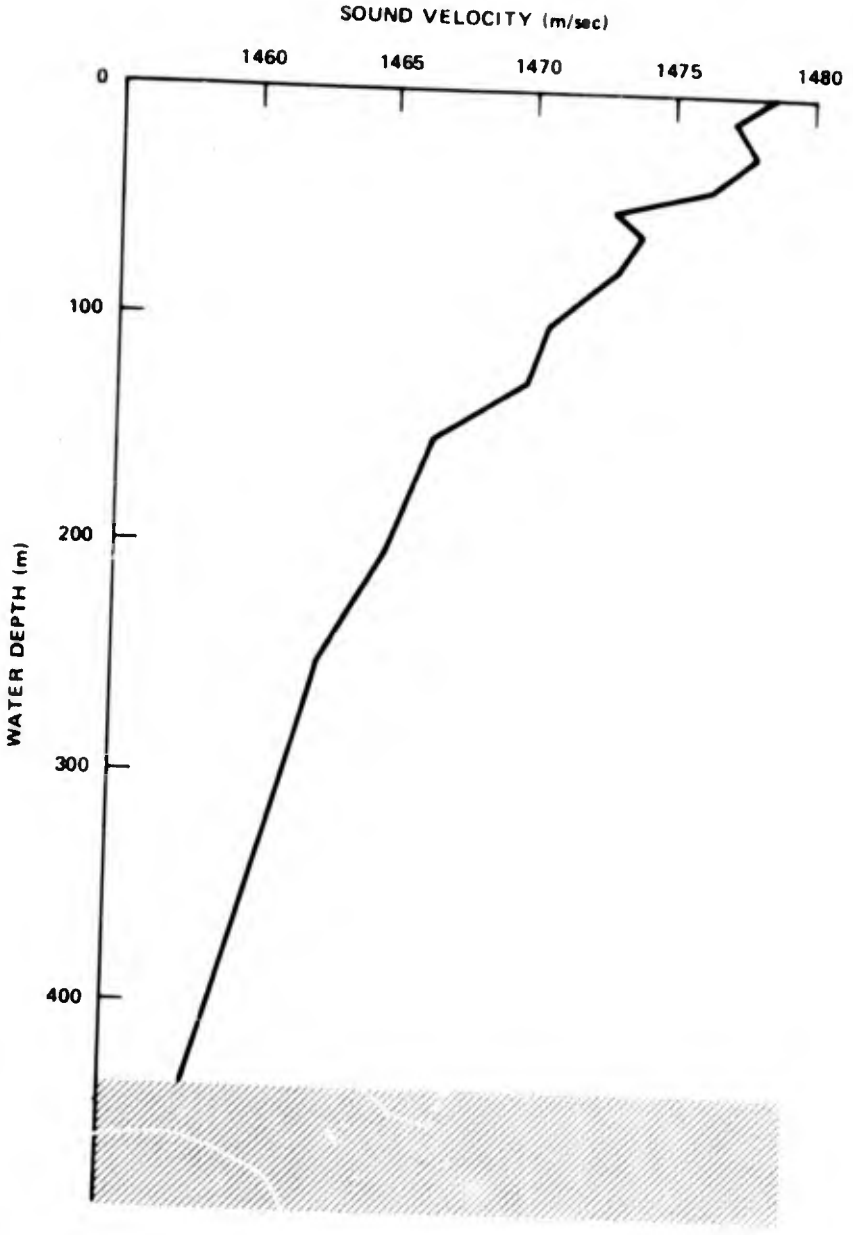

Figure 67. Typical Velocity Profile
(Second Tract)

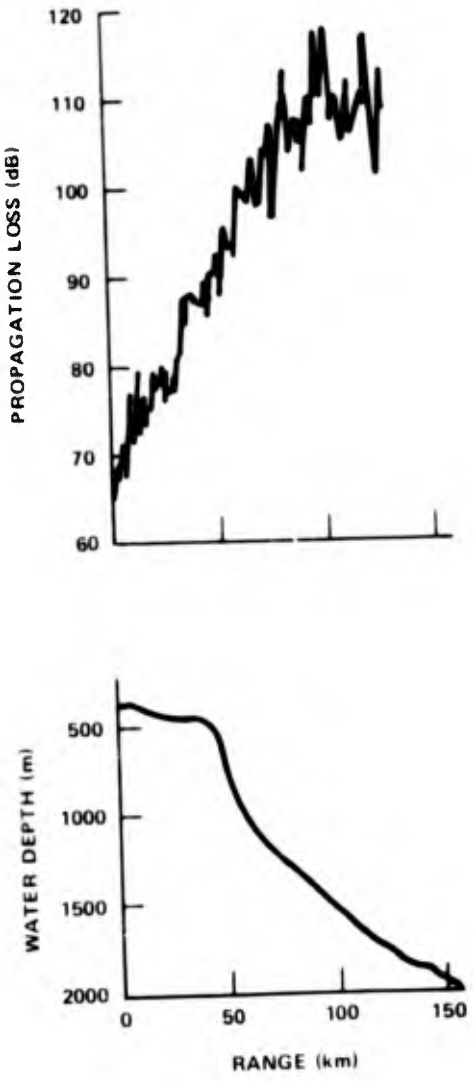

Figure 68. Experimental Results Showing Propagation Loss Versus Range (Second Tract)

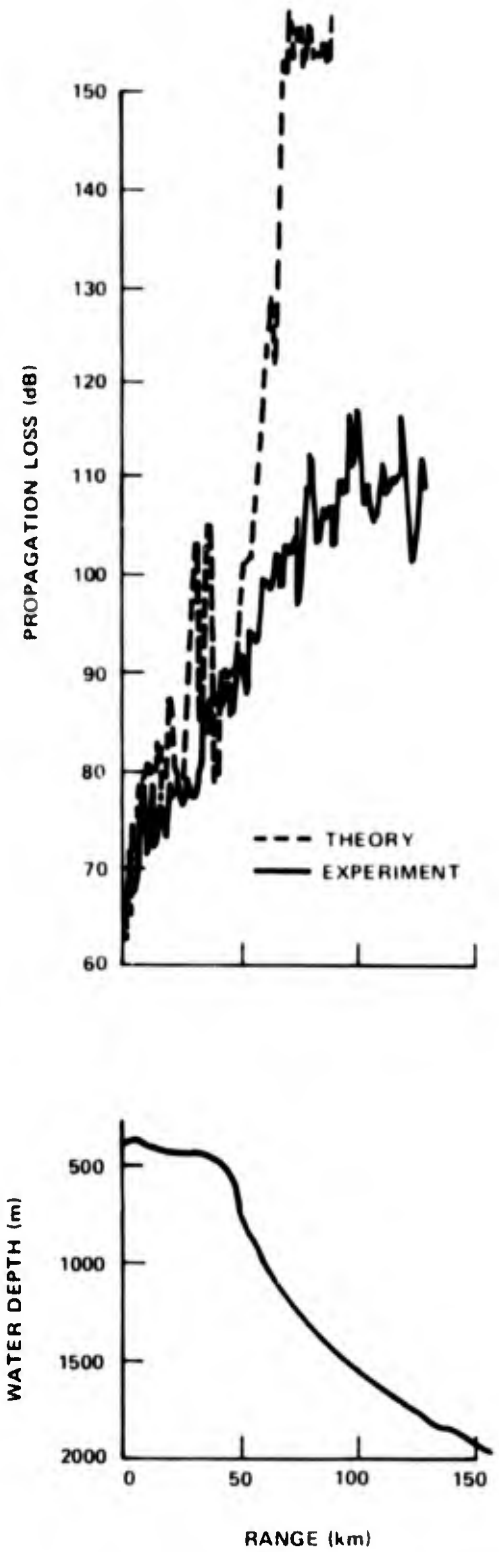

Figure 69. Propagation Loss Versus Range, Comparison Between Experiment and Theory

TESTS USING ARRAY OF CW SOURCES IN BIFI RANGE

We have previously described experiments in which the sound field, produced by a single element source, was measured. Here we describe experiments in which the sound field, produced by a vertical array of elements, was measured. These tests (reference 26), which were conducted by using a vertical array of 25 CW sources (references 27 and 28) in the BIFI range served two purposes. First, they tested the ability of the model to predict propagation loss as a function of range and depth for a vertical array of sources. Second, they served as a test of the possibility of enhancing selected modes in the sound field by weighting the array elements in a manner determined by calculations made with the model. (Mode Enhancement Techniques have been termed METS in reference 26.)

The experiments were conducted in August 1972 and January 1973, along the tract shown in figure 70. The array of sources is located at point N. The vertical sound field was probed at discrete ranges along the tract from point N toward point H. The frequency of transmission was 1700 Hz during all the tests conducted.

Tests were conducted under winter conditions on 8-9 January 1973. A typical sound-velocity profile measured during the tests is listed in table 4, where depth is measured down from the ocean surface. It can be seen that there is a rather strong positive gradient. Because of this gradient, energy in the first mode is concentrated in the upper portion of the water column.

Table 4. Typical Sound-Velocity Profile for January 1973 in the BIFI Range

Depth (ft)	Sound Velocity (ft/sec)
0.0	4801.8
30.0	4803.2
42.0	4804.1
51.0	4805.2
55.0	4806.0
61.0	4809.0
65.0	4810.0
70.0	4812.0
74.0	4814.0
80.0	4818.0
95.0	4819.2
122.0	4820.0

It can be seen in table 5 (derived in a manner described in volume I of this report) that the maximum energy is concentrated at roughly the depth of element 6 at a depth of 25.1 ft. Since the pressure amplitude of mode 1 exceeds 0.5 at the depths of the first 11 elements of the array, matching roughly to the first mode dictates that the elements should transmit energy in phase and equal amplitude. This should provide a good match to the first mode. In addition, the other modes should be suppressed because, as shown in table 5, arrivals corresponding to other modes should, to some extent, interfere destructively. For instance, in the case of mode 2, the arrivals from elements 1-7 will interfere destructively with the arrivals from 8-11. For mode 3, the arrivals from elements 1-4 will interfere destructively with those from elements 5-11. In the cases of modes 4-6, the arrivals from five elements will interfere destructively with those from six other elements.

While transmitting energy in this manner, matched to mode 1, the vertical sound field was determined at 7 stations at ranges from about 1 to 8.7 nmi from the array. The measured values of propagation loss as a function of depth at a range of 0.968 nmi are plotted as points in figure 71. The corresponding predicted values of loss are plotted as connected lines in the figures. Modes 1-6 are included in the theoretical calculations. It can be seen that agreement between theory and experiment is good in the upper water column. However, in the lower portion of the water column, the sound field is much stronger than predicted. It might be reasonable to think that the extra energy in the lower column could be due to the presence of higher order modes in the sound field, since their energy is concentrated lower in the water column. However, when modes 7-12 are added to the sound field, as shown in figure 72, in the theoretical predictions, the predicted field varies little from that of modes 1-6 alone. Thus, as anticipated, the higher order modes effectively cancel out. It is more likely that this excess energy represents energy transferred by means of mode conversion from lower to higher order modes, and hence to deeper parts of the water column. Such a transfer of energy could occur if only a small fraction of the energy in the upper column were transferred and added to the much smaller energy contained in the lower column. The theoretical predictions were made without taking into account the effects of mode conversion. This was done because changing velocity profiles with range would, owing to the positive gradient in the profile, be the prime cause of mode conversion, but only one profile was measured during the time corresponding to the calculations. Hence the additional expenditure of computer time was not justified.

Figures 73 through 78 show similar comparisons between theory and experiment when the sound field was determined at stations at six other ranges out to a maximum of about 8.7 nmi. Generally, at all ranges agreement between theory and experiment is very good in the upper part of the water column where the energy of mode 1 is concentrated. At deeper depths, there is generally more energy than predicted. At all ranges, the loss does not exceed that due to cylindrical spreading, and hence the values of propagation loss are very low (generally less than 60 dB in the upper water column). The vertical sound field is extremely stable with range so that the vertical distribution of energy varies little as a function of range. (It is more stable in the upper column where the first mode is concentrated than in the deeper levels where the higher modes are concentrated.) This is remarkable in view of the high frequency (1700 Hz) and previous studies (reference 19) which showed large signal fluctuations

Table 5. Element Amplitudes and Phases for Modes 1-6

	Element No.	Depth (ft)	Amplitude	Phase (deg)
Mode 1				
Amplitude Matching	1	8.0	0.511	0.0
	2	11.4	0.686	0.0
	3	14.8	0.826	0.0
	4	18.3	0.927	0.0
	5	21.7	0.983	0.0
	6	25.1	1.000	0.0
	7	28.5	0.981	0.0
	8	31.9	0.931	0.0
	9	35.3	0.857	0.0
	10	38.8	0.764	0.0
	11	42.2	0.662	0.0
Phase Matching	1	8.0	0.261	30.7
	2	11.4	0.471	43.3
	3	14.8	0.682	55.7
	4	18.3	0.858	67.9
	5	21.7	0.966	79.4
	6	25.1	1.000	91.1
	7	28.5	0.962	101.3
	8	31.9	0.867	111.4
	9	35.3	0.735	121.0
	10	38.8	0.583	130.2
	11	42.2	0.439	138.5
Mode 2				
Amplitude Matching	1	8.0	0.686	180.0
	2	11.4	0.843	180.0
	3	14.8	0.886	180.0
	4	18.3	0.809	180.0
	5	21.7	0.631	180.0
	6	25.1	0.375	180.0
	7	28.5	0.075	180.0
	8	31.9	0.234	0.0
	9	35.3	0.518	0.0
	10	38.8	0.756	0.0
	11	42.2	0.914	0.0
Phase Matching	1	8.0	0.531	50.7
	2	11.4	0.800	71.7
	3	14.8	0.885	93.1
	4	18.3	0.738	114.2
	5	21.7	0.448	134.7
	6	25.1	0.159	155.0
	7	28.5	0.006	175.2
	8	31.9	0.055	193.6
	9	35.3	0.269	211.2
	10	38.8	0.571	229.1
	11	42.2	0.835	246.0

Table 5. (Cont'd) Element Amplitudes and Phases for Modes 1-6

	Element No.	Depth (ft)	Amplitude	Phase (deg)
Mode 3				
Amplitude Matching	1	8.0	0.801	0.0
	2	11.4	0.864	0.0
	3	14.8	0.725	0.0
	4	18.3	0.405	0.0
	5	21.7	0.000	180.0
	6	25.1	0.406	180.0
	7	28.5	0.722	180.0
	8	31.9	0.885	180.0
	9	35.3	0.860	180.0
	10	38.8	0.652	180.0
	11	42.2	0.319	180.0
Phase Matching	1	8.0	0.732	67.2
	2	11.4	0.859	96.4
	3	14.8	0.604	123.5
	4	18.3	0.189	152.2
	5	21.7	0.000	180.0
	6	25.1	0.183	206.9
	7	28.5	0.580	233.5
	8	31.9	0.871	260.0
	9	35.3	0.823	286.8
	10	38.8	0.474	313.4
	11	42.2	0.113	339.2
Mode 4				
Amplitude Matching	1	8.0	0.756	180.0
	2	11.4	0.694	180.0
	3	14.8	0.398	180.0
	4	18.3	0.046	0.0
	5	21.7	0.463	0.0
	6	25.1	0.730	0.0
	7	28.5	0.759	0.0
	8	31.9	0.547	0.0
	9	35.3	0.162	0.0
	10	38.8	0.286	180.0
	11	42.2	0.635	180.0
Phase Matching	1	8.0	0.746	80.7
	2	11.4	0.628	115.1
	3	14.8	0.207	148.7
	4	18.3	0.003	183.4
	5	21.7	0.275	216.5
	6	25.1	0.684	249.5
	7	28.5	0.738	283.3
	8	31.9	0.384	315.4
	9	35.3	0.034	348.0
	10	38.8	0.102	380.9
	11	42.2	0.502	412.3

Table 5. (Cont'd) Element Amplitudes and Phases for Modes 1-6

	Element No.	Depth (ft)	Amplitude	Phase (deg)
Mode 5				
Amplitude Matching	1	8.0	0.693	0.0
	2	11.4	0.528	0.0
	3	14.8	0.137	0.0
	4	18.3	0.326	180.0
	5	21.7	0.637	180.0
	6	25.1	0.681	180.0
	7	28.5	0.436	180.0
	8	31.9	0.013	180.0
	9	35.3	0.417	0.0
	10	38.8	0.683	0.0
	11	42.2	0.667	0.0
Phase Matching	1	8.0	0.693	90.0
	2	11.4	0.403	130.3
	3	14.8	0.027	168.6
	4	18.3	0.152	207.7
	5	21.7	0.579	245.3
	6	25.1	0.660	283.9
	7	28.5	0.271	321.5
	8	31.9	0.000	358.9
	9	35.3	0.244	395.8
	10	38.8	0.655	433.5
	11	42.2	0.624	470.6
Mode 6				
Amplitude Matching	1	8.0	0.662	180.0
	2	11.4	0.404	180.0
	3	14.8	0.062	0.0
	4	18.3	0.506	0.0
	5	21.7	0.676	0.0
	6	25.1	0.503	0.0
	7	28.5	0.073	0.0
	8	31.9	0.394	180.0
	9	35.3	0.663	180.0
	10	38.8	0.602	180.0
	11	42.2	0.245	180.0
Phase Matching	1	8.0	0.652	100.2
	2	11.4	0.243	143.1
	3	14.8	0.006	185.2
	4	18.3	0.378	228.3
	5	21.7	0.674	266.1
	6	25.1	0.373	312.1
	7	28.5	0.008	353.8
	8	31.9	0.227	395.2
	9	35.3	0.644	436.1
	10	38.8	0.531	478.2
	11	42.2	0.088	519.0

in the BIFI range. Thus it appears that mode matching can be used to produce a sound field which is stable with range, and also to produce a high level sound field. Further, modeling techniques, it appears, can be used to determine the proper matching and the resulting sound field. However, it should be noted that the medium effectively filters out higher order modes and that not all the success in mode enhancement is due to the matching procedure. This suggests that future tests should include attempts at enhancement of higher order modes. Thus one could separate effects of the medium and effects produced by the array.

During the same tests, a form of cosine weighting was also used for elements 1-11 of the array. All elements transmitted in phase and with the relative pressure amplitudes given in table 6. By comparing these amplitudes with those corresponding to mode 1 in table 5, it can be seen that this weighting provided a fairly good match to mode 1. The predicted vertical sound field is, as a result, fairly stable with range and the agreement between theory and experiment, shown at 3 ranges in figures 79 through 81, is fairly good.

Table 6. Cosine Weighting of Array Elements

Element No.	Relative Pressure Amplitude
1	0.0
2	0.282
3	0.562
4	0.794
5	0.891
6	1.000
7	0.891
8	0.794
9	0.562
10	0.282
11	0.0

In addition, during the same tests, an attempt at steering energy was made, using elements 1-11 of the array. All elements transmitted with the same amplitude and with the relative phases given in table 7. Comparison with the phases corresponding to the progressive wave associated with mode 1 and the recommended amplitude shading shows a fairly large divergence. The comparison between theory and experiment at three ranges in figures 82 through 84 show the least stable vertical sound field and the least satisfactory comparisons between theory and experiment.

Table 7. Phases of Array Elements in Steering

Element No.	Relative Phases (deg)
1	0.0
2	-9.2
3	-18.5
4	-27.7
5	-37.0
6	-46.2
7	-55.4
8	-64.7
9	-73.9
10	-83.2
11	-92.4

Tests were conducted under summer conditions on 14, 16, and 17 August 1972. A typical sound-velocity profile measured during the tests is listed in table 8 where depth is measured down from the ocean surface. It can be seen that there is a very strong gradient. Because of this gradient, energy tends to concentrate in the lower portion of the water column. Unfortunately for this analysis, array elements 1-11 in the upper portion were used to transmit energy, hence the array was not matched to mode one, nor to any particular higher order mode. Theoretical calculations showed that the vertical field would be expected to vary considerably within small increments in range. Thus the best that one could hope for, in the comparison of theory with experment, would be a rough agreement in mean level over the water column. All elements

of the array transmitted in phase, and with the relative pressure amplitudes given in table 6. Figure 85 compares theoretical and experimental values of loss as a function of depth at a range of 1 nmi. The mean predicted and measured levels are close. One additional complicating factor is the strong interaction of the sound field with the bottom, and the resulting large loss with range due to this interaction. In figures 86 through 90, similar comparisons are made at longer ranges. In each case, there is an excess loss observed, generally increasing with range, that may be attributed to bottom loss. It is interesting to note that at ranges of around 2 nmi (about 3 miles from point S in figure 5 where single CW sources are located), where anomalous propagation was previously observed, the largest excess was measured.

Table 8. Typical Sound-Velocity Profile for August 1972 in the BIFI Range

Depth (ft)	Sound Velocity (ft/sec)
0.0	4956.5
10.5	4956.5
20.5	4956.5
28.0	4954.0
34.0	4954.0
37.8	4952.2
42.0	4950.3
49.0	4949.5
55.5	4946.8
62.0	4944.8
68.0	4939.8
80.0	4938.2
84.0	4935.4
94.5	4931.4
100.0	4920.0
115.0	4915.0

One might infer from the preceding discussion that, had the proper mode matching been utilized in the summer tests, a strong and stable sound field could have been produced. However, oceanographic measurements of the variation of the stratification of the water column with time and calculations by means of the model of the effect of such variations on mode matching cast doubt on such an inference. These calculations indicate that the sound field at 1700 Hz is so unstable during the summer that mode enhancement would be much more difficult in practice in the summer than in the winter.

Such oceanographic data (reference 29) were taken by using temperature sensors, attached to the tower containing the array near Block Island, at the four depths shown in figure 91. (Sensor T2 was not operative during the measurements.) The output of these sensors was recorded on tape digitally at a rate of two samples per minute on each sensor. Later, historical salinity data were used to obtain sound velocity as a function of time, and these values were plotted with a Calcomp plotter.

Oceanographic data taken between 30 August and 14 September 1972 are shown in figure 92. (To avoid congestion, the plotted values are separated by an increment of 15 minutes; hence, only 1 of every 30 measured values is shown.) Looking from the bottom to the top of the ordinate, it can be seen that the sound velocity at sensors T1, T3, T4, and T5 are plotted as a function of time. Next, the difference in sound velocity, D, between T1 and T5 is plotted. Finally, wind speed and atmospheric temperature are plotted as a function of time. Determination of the temporal stability of a sound field and its effect on mode matching was accomplished in the following manner. First, for the initial velocity profile determined from the oceanographic data, the necessary weighting of the array elements was determined by means of the model in order to enhance mode 1 at 127, 400, and 1700 Hz, respectively. Then the field at an arbitrary range produced by an array so weighted was calculated for individual modes 1-4 at 1700 Hz, modes 1 and 2 at 400 Hz, and mode 1 at 127 Hz (since only one mode was possible at 127 Hz). Later, as the velocity profile changed, the same sound field components were calculated by assuming the same array weighting, and the differences in the levels for the matched mode (mode 1) and the unmatched modes were observed. The effect of the receiver depth on the levels of the modes in the sound field was removed by setting the function $u_m(z)$, which determines the pressure level for mode m as a function of depth, taken at the receiver equal to unity in all calculations. This was necessary because, as $u_m(z)$ changes with changing velocity profile, the location of a fixed receiver could easily correspond to different extreme values of $u_m(z)$, as for example changing from the position of a node to that of an antinode of $u_m(z)$. The level calculated after this modification would be similar to that obtained by determining the total energy in the water column at a given range and for a given mode. Mode enhancement is designed to maximize the energy in the matched mode for a given velocity profile. The levels of other modes tend to be depressed. However, for different profiles the resultant sound field is dependent upon functions, such as the excitation function (defined in volume I of this report), which vary with the velocity profile. As a result, the degree to which the matched mode can be enhanced and the other modes depressed depends upon the given velocity profile. Thus, in order to determine the decrease in mode enhancement resulting from a profile change, the most

meaningful comparison would be between the sound fields for the matched and unmatched state for that given profile. However, such calculations would have resulted in two sets of calculations for each succeeding profile considered. To reduce the computation time, the comparisons here are between the initial matched sound field and the subsequent unmatched fields resulting from a change in velocity profile, but with the initial array weighting. The appropriateness of such comparisons can be justified, since for any given profile the levels of the unmatched modes are at least 10 to 20 dB below that of the matched mode. By using this as a reference, one can easily detect extreme deterioration in mode matching. Such calculations were made for about thirty profiles taken during the tests. The results of four sets of calculations, shown in table 9, are chosen to show the extremes of the deterioration in mode enhancement at 1700 Hz. The corresponding calculations at 400 Hz are shown for the purpose of comparison. It was determined from such calculations that the normal fluctuations in the velocity of sound, such as those observed on the first day, were enough to cause a significant deterioration in the effectiveness of mode enhancement at 1700 Hz (at times, as shown in table 9, the level of mode 2 exceeded that of mode 1) in periods of time of less than 1 hour. The sound fields at 127 and 400 Hz were not sensitive to this type of environmental fluctuation. It can be seen in the table that during the time in which there was deterioration in mode enhancement at 1700 Hz, the relative level of mode 2 at 400 Hz remained well below that of mode 1. The relative level of mode 2 actually declined from -12.0 to -15.3 dB at this time due to the effect of the changing profile on the ability to enhance a given mode. It should be noted that the relative level of mode 2 (not shown in table) varied between -10.0 to -15.3 dB at 400 Hz as the profile changed during the first day. After nearly 4 days there was a storm (note wind speed in plot) and as a result of the water's churning, there was at times a small positive gradient in the velocity profile (note the plot of D). The effect of the storm persisted for several days. The effect on mode enhancement is shown in the table. Again at 1700 Hz, the mode enhancement deteriorated, but at 127 and 400 Hz, there was no noticeable effect. Finally on about the thirteenth day, an unusual oceanographic phenomenon was observed as cold water entered the lower portion of the water column, as seen in the plot of the sound velocity at the depth of sensors T5. As a result, the characteristics of the sound velocity profile changed tremendously. In this case, as expected, there was great deterioration of mode enhancement at 1700 Hz. This can be seen in the table where the levels of both mode 2 and 3 exceed that of mode 1. Even at 400 Hz, there was some deterioration. The -8.0 dB level of mode 2 probably represents a real deterioration in mode enhancement, since the calculations corresponding to several adjacent profiles yielded approximately the same result. Only at 127 Hz was there no visible effect.

Even in late November and early December, the same sort of measurements led to similar conclusions. The previously measured parameters are again plotted for the time period between 27 November and 1 December 1972 in figure 93. It can be seen in the plot of D that the sound-velocity profile oscillates from possessing a small positive gradient to a small negative gradient. Calculations have shown that this small variation disrupts mode enhancement at 1700 Hz, as the concentration of energy in the first mode oscillates from the upper to the lower portion of the water column. This can be seen in table 10 where the relative levels of modes are listed at the start of the tests, when

Table 9. Relative Levels of Modes During August-September Test

	Relative Levels of Modes During the Tests (dB)				
Modes	Start	Later During 1st Day	After Storm	13th Day	
1	0.0	-2.5	-3.5	-5.4	1700 Hz
2	-13.7	0.0	0.0	0.0	
3	-14.9	-20.3	-28.1	-1.8	
4	-28.4	-11.5	-9.0	-14.4	
1	0.0	0.0	0.0	0.0	400 Hz
2	-12.0	-15.3	-16.3	-8.0	

Table 10. Relative Levels of Modes During November-December Test

	Relative Levels of Modes During the Tests (dB)		
Modes	Start (negative gradient)	Later (positive gradient)	
1	0.0	-4.0	1700 Hz
2	-19.1	0.0	
3	-17.5	-0.6	
4	-30.6	-7.4	
1	0.0	0.0	400 Hz
2	-16.6	-22.8	

mode 1 is matched and the profile possesses a negative gradient. Later, when the gradient is positive, the levels are again listed. It can be seen that the deterioration in mode enhancement is such that the levels of modes 2 and 3 exceed that of mode 1. As before, at 127 and 400 Hz, little effect is expected.

Thus it appears that it is only in winter, when a positive gradient is firmly established in the velocity profile, that the stratification is stable enough to ensure a relatively stable sound field at 1700 Hz.

It is probably appropriate to end this section with a discussion concerning the selection of the transmitting frequency when it is desired to enhance individual modes. There are two divergent factors which must be considered in such a selection. First, with increasing frequency, energy in a mode tends to become trapped, and hence concentrated at certain depths in the water column. This situation lends itself to exploitation by mode matching, when array elements are situated at depths corresponding to the energy maxima. By contrast, at low frequencies, energy in a mode is spread more over the water column and placement of the elements becomes less important. Further, at low frequencies fewer modes are excited and hence enhancement of a single mode at low frequencies will improve the sound field less in terms of stability. In addition, it may be desired to separate the elements of the transmitting array by greater than one-half wavelength in order to avoid mutual coupling effects between the elements (reference 30). Thus in shallow water, the array gain decreases at lower frequencies, if the half-wavelength criterion is maintained. For instance, in the BIFI range at 100 Hz, elements of the transmitting array should be separated by a half wavelength, or about 25 ft. In 100 ft of water, this limits the array to a maximum of five elements. The second factor, divergent from the first, is the decrease in coherence (reducing the ability to predict the phase of a given signal) at higher frequencies, which makes it increasingly difficult to add coherently, and hence to enhance a mode with increasing frequency. A related property is the decrease in angular separation of modes with increasing frequency, and hence a greater possibility of instability in mode enhancement techniques at higher frequencies. To summarize, in a perfectly stable environment more can be gained by mode enhancement at high frequencies, but in practice it is more difficult to achieve these gains due to greater instability at these frequencies. Hence the best results in mode enhancement are attained in practice at the highest frequency for which the environment is stable. Such an optimum frequency can be determined by using a procedure similar to that used in this section. The parameters of the environment should be determined as a function of time. (An additional factor, which wasn't considered here, should be included: environmental changes as a function of range.) Then, using the acoustic model, the stability of the sound field at frequencies of interest should be compared, and hence the optimum frequency can be selected.

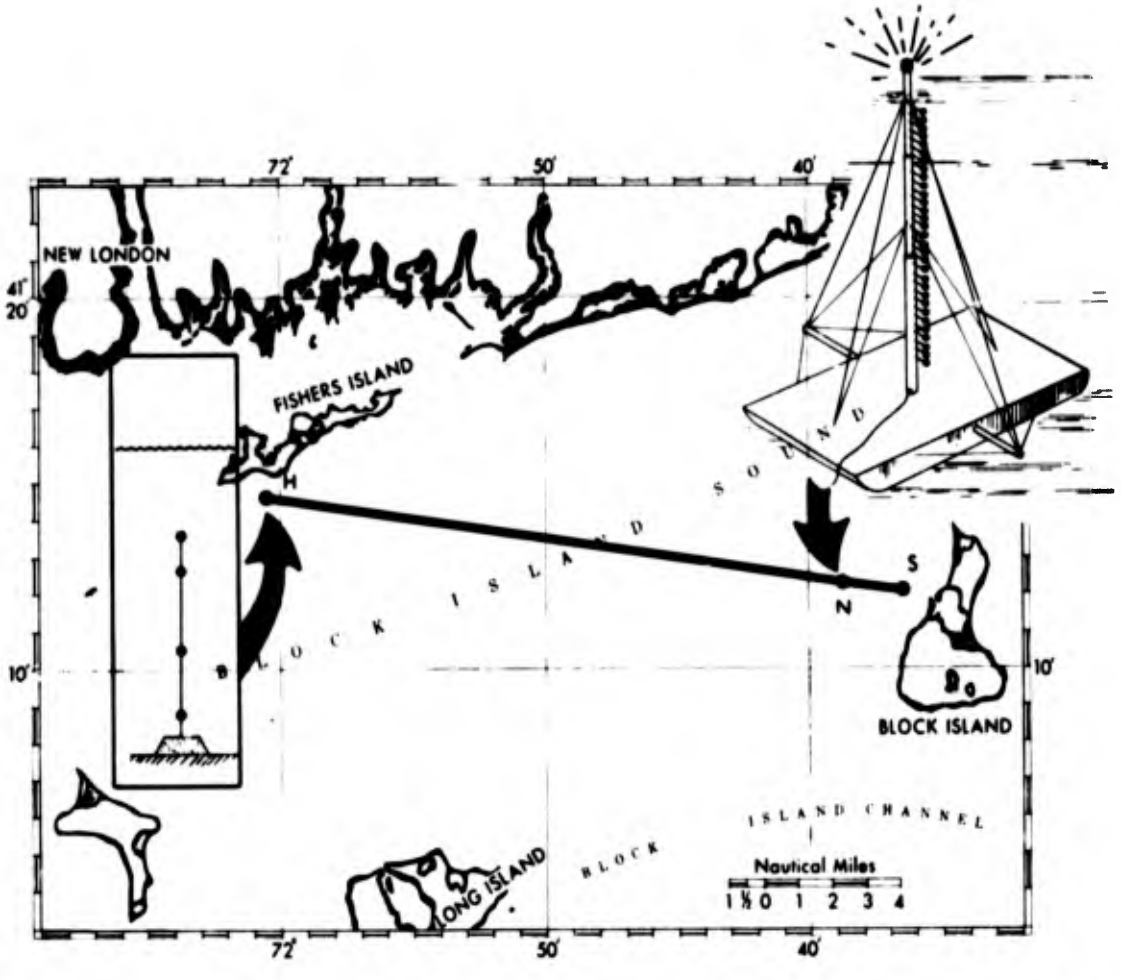

Figure 70. BIFI Range Showing Array of Projectors

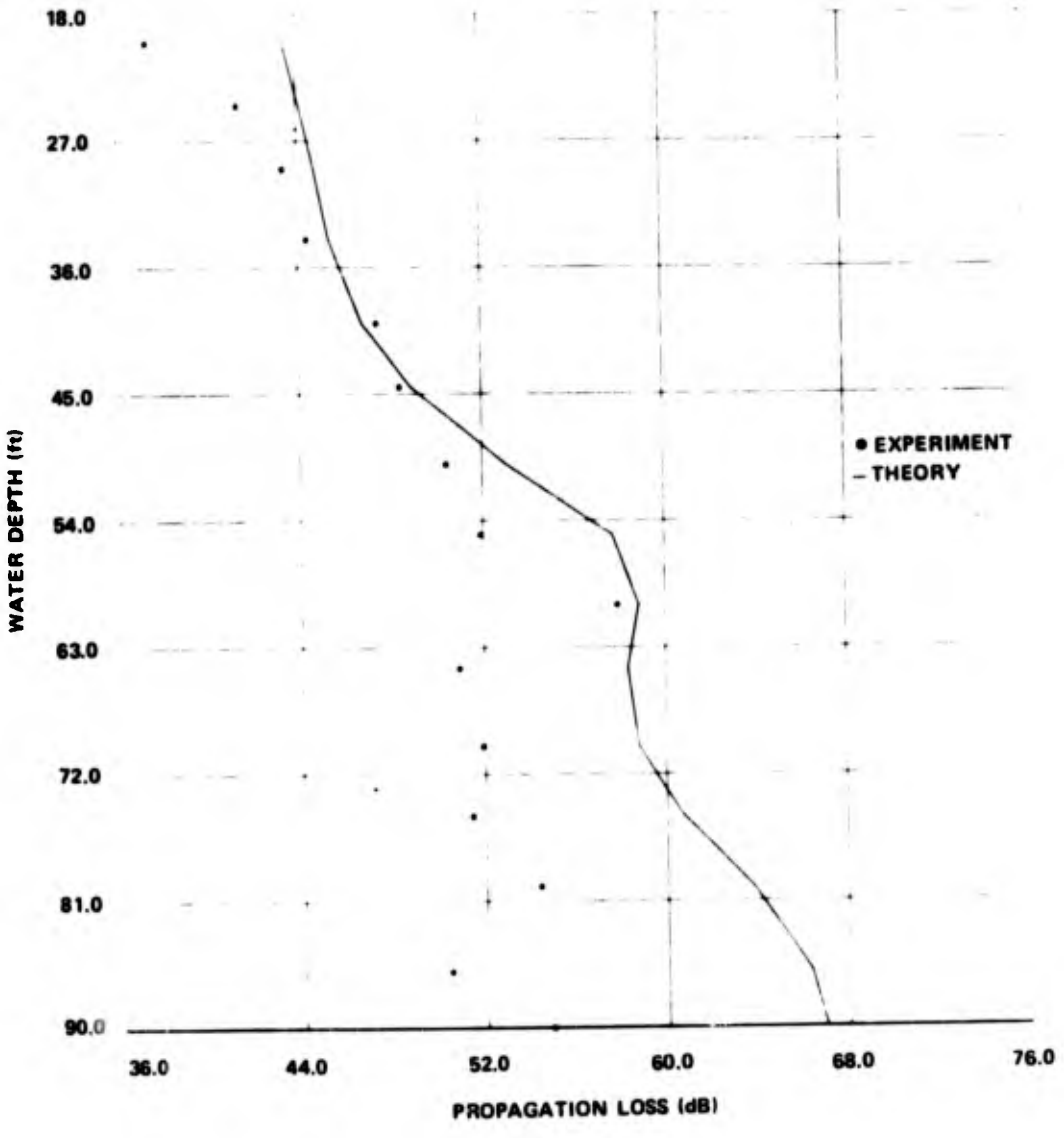

Figure 71. Loss Profile, Comparison Between Experiment and Theory, Range 0.968 nmi, Winter, Modes 1-6

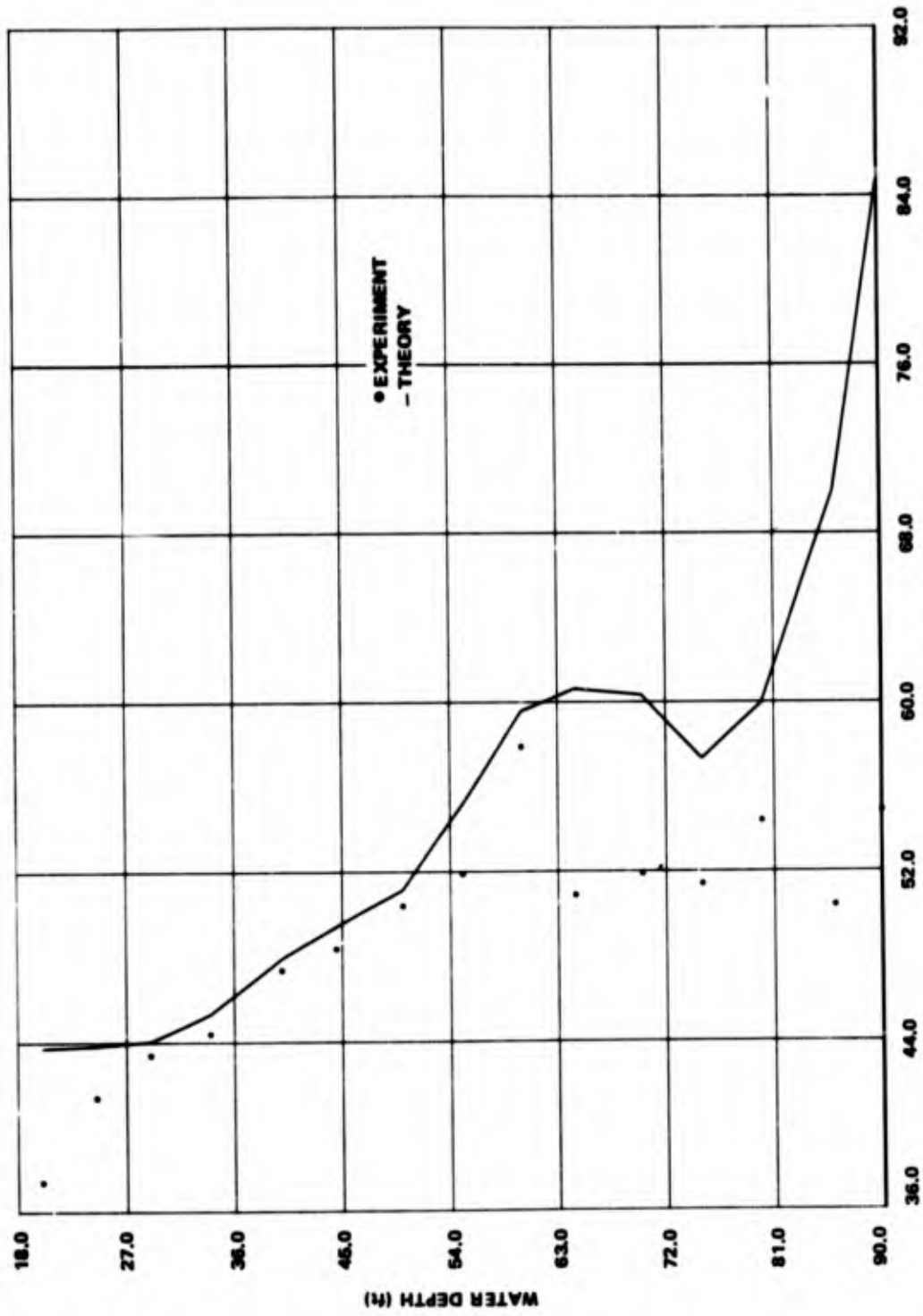

Figure 72. Loss Profile, Comparison Between Experiment and Theory, Range 0.968 nmi, Winter, Modes 1-12

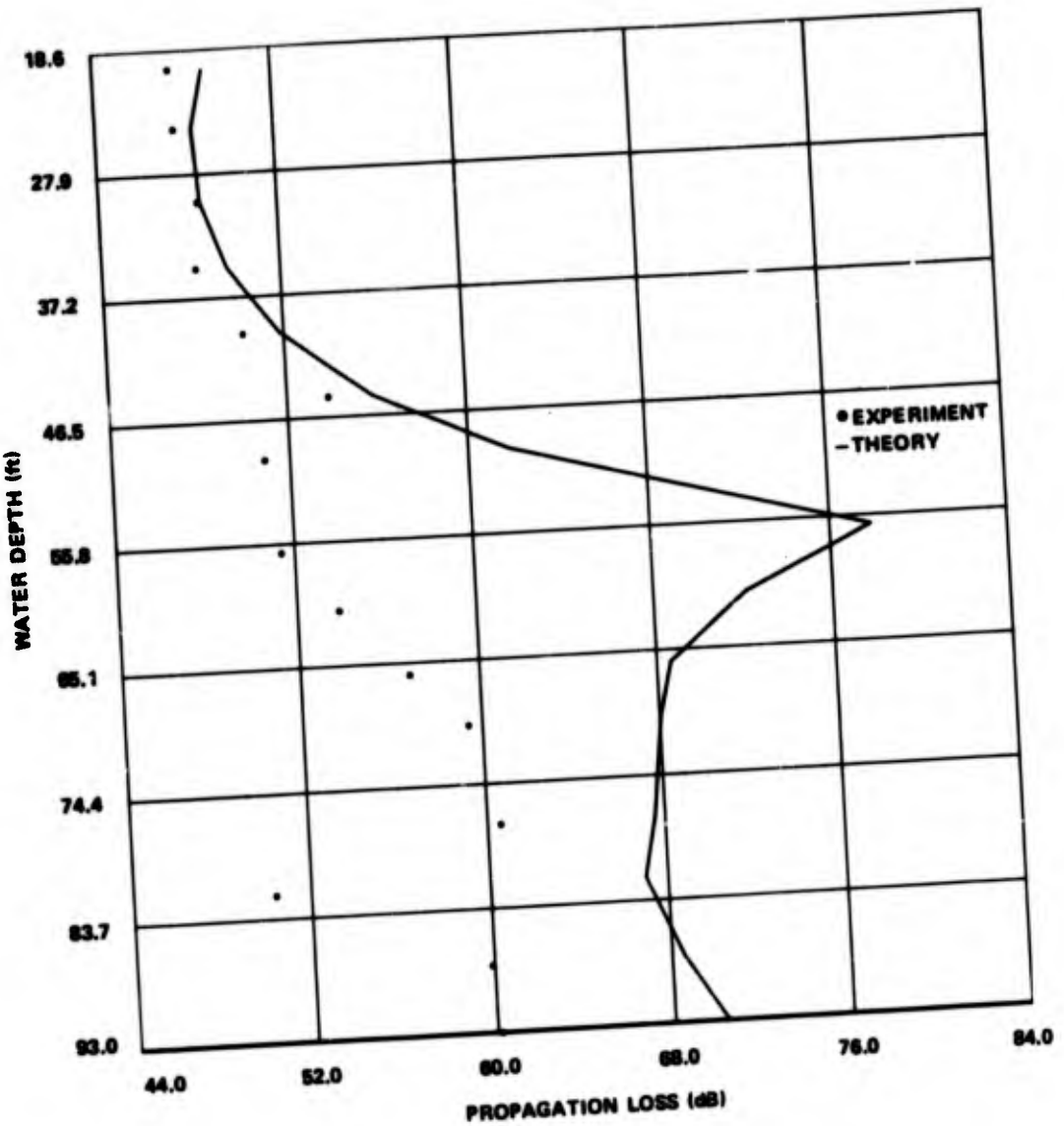

Figure 73. Loss Profile, Comparison Between Experiment and Theory, Range 3.14 nmi, Winter

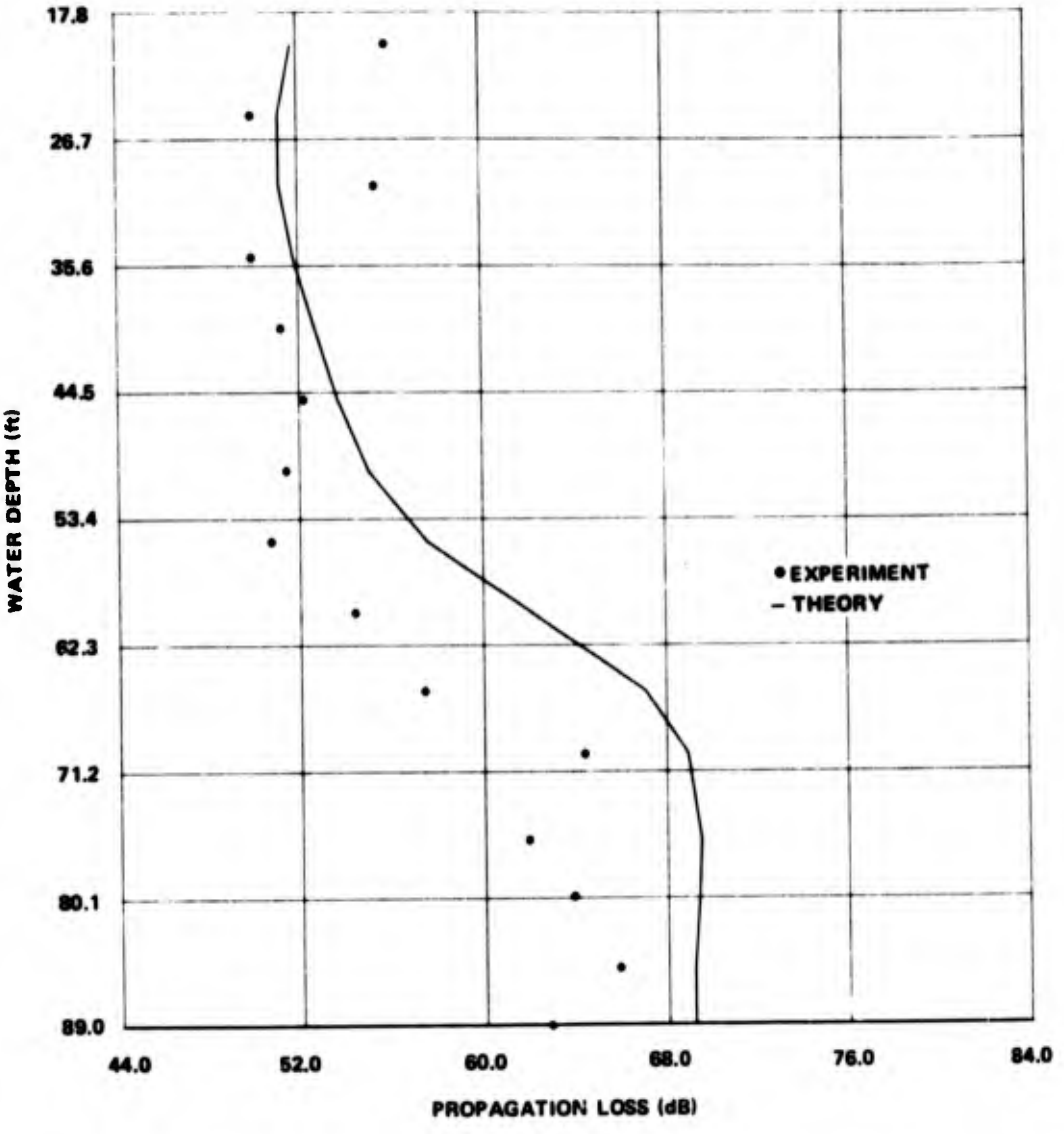

Figure 74. Loss Profile, Comparison Between Experiment and Theory, Range 4.42 nmi, Winter

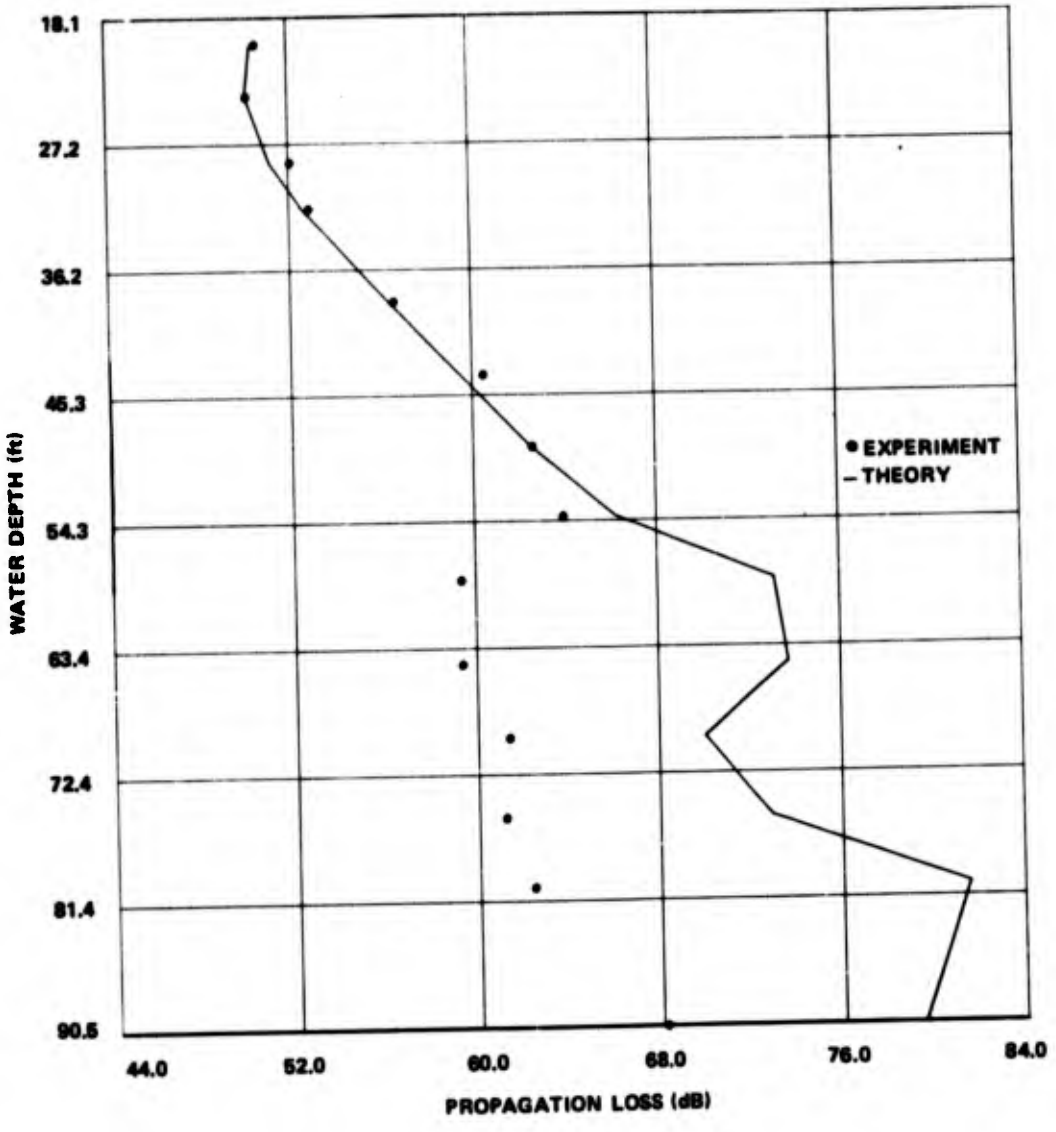

Figure 75. Loss Profile, Comparison Between Experiment and Theory, Range 5.46 nmi, Winter

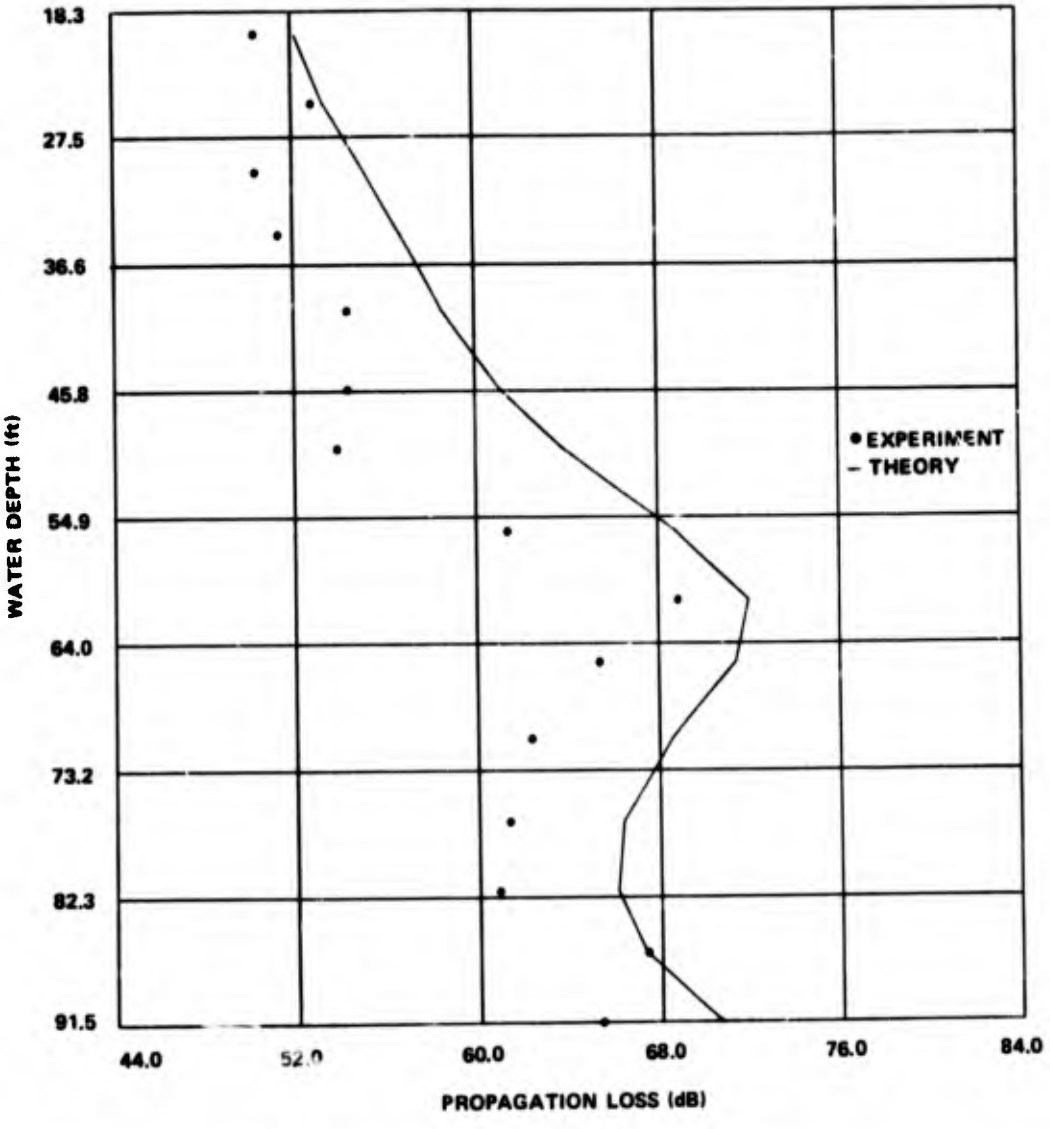

Figure 76. Loss Profile, Comparison Between Experiment and Theory, Range 6.57 nmi, Winter

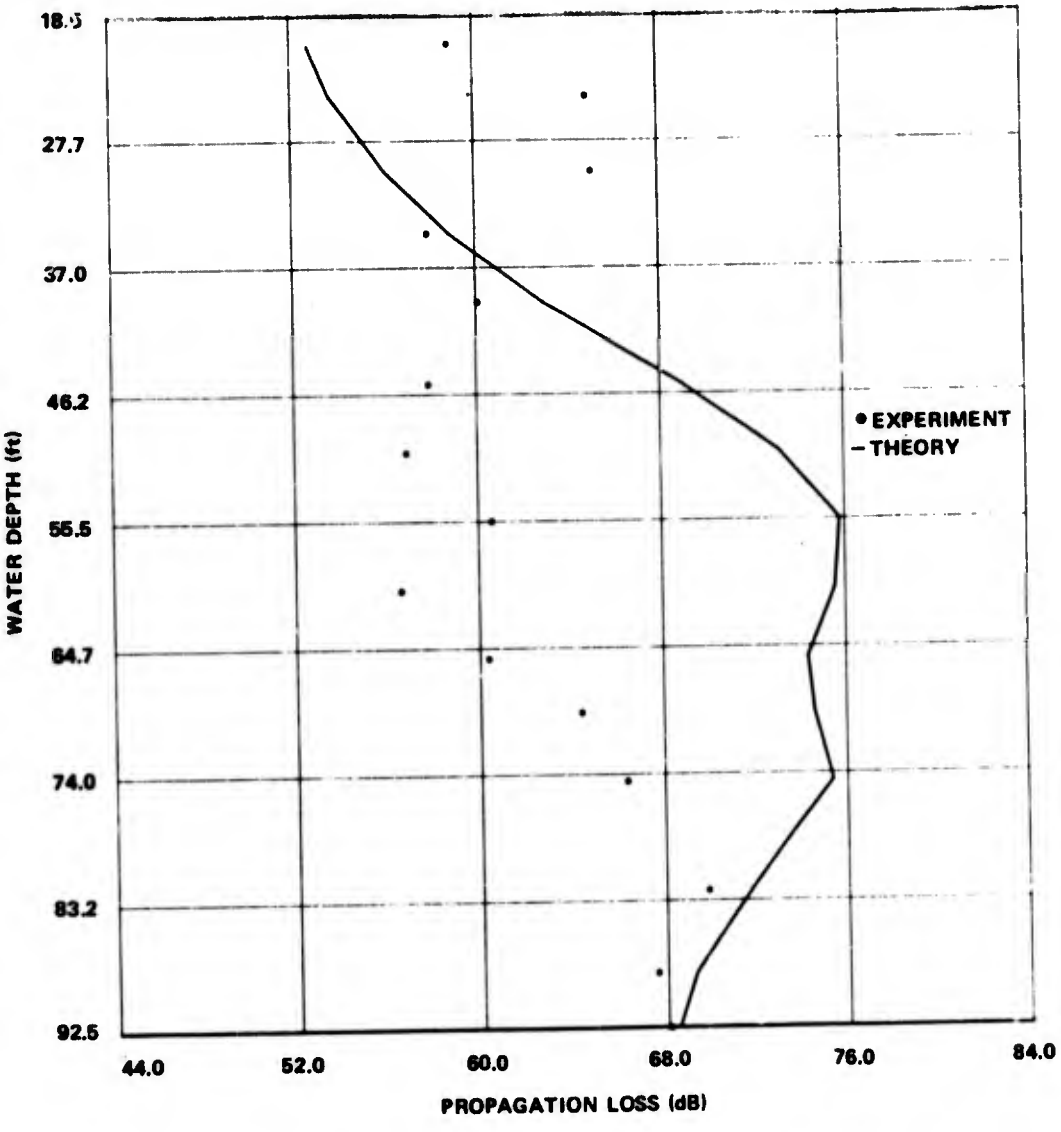

Figure 77. Loss Profile, Comparison Between Experiment and Theory, Range 7.84 nmi, Winter

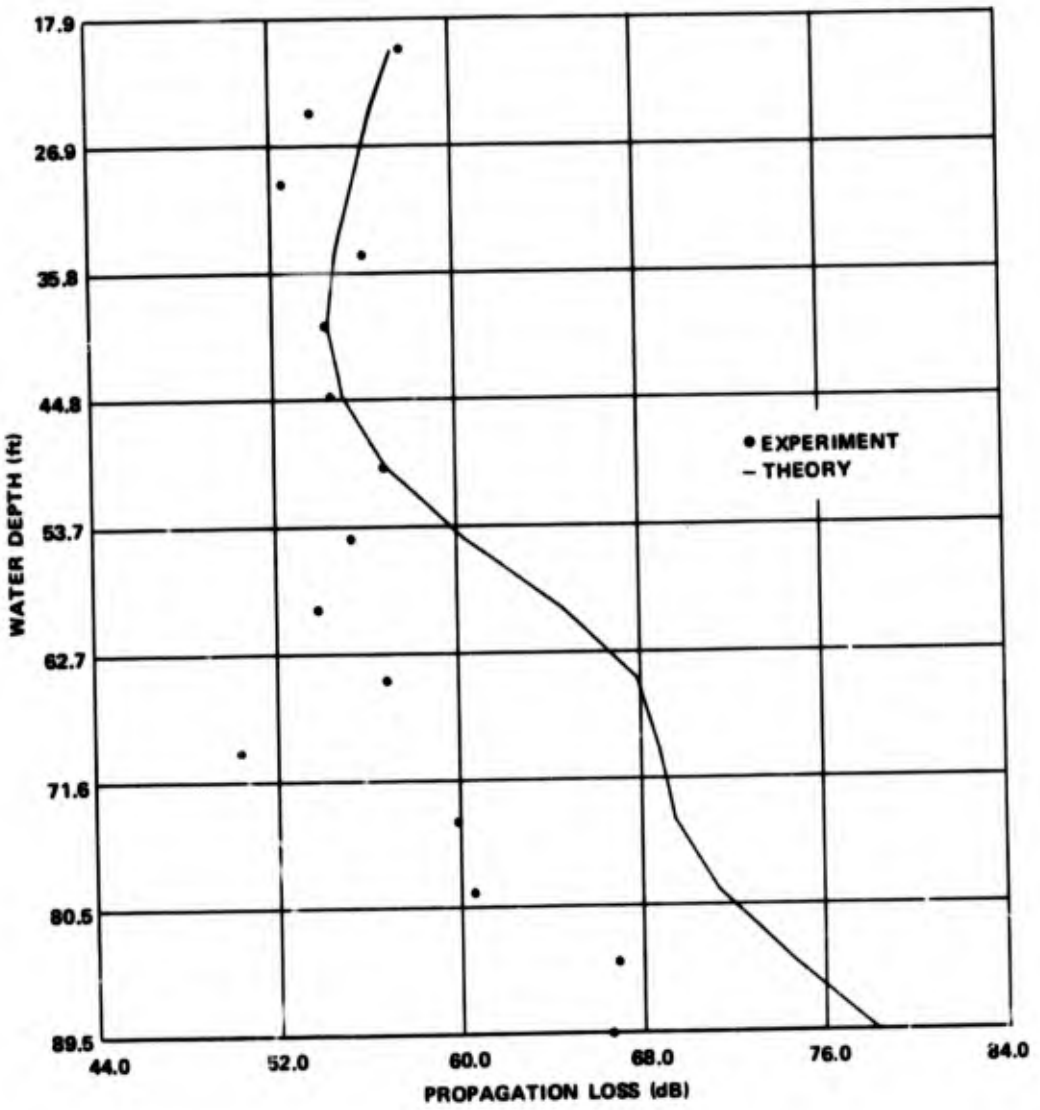

Figure 78. Loss Profile, Comparison Between Experiment and Theory, Range 8.66 nmi, Winter

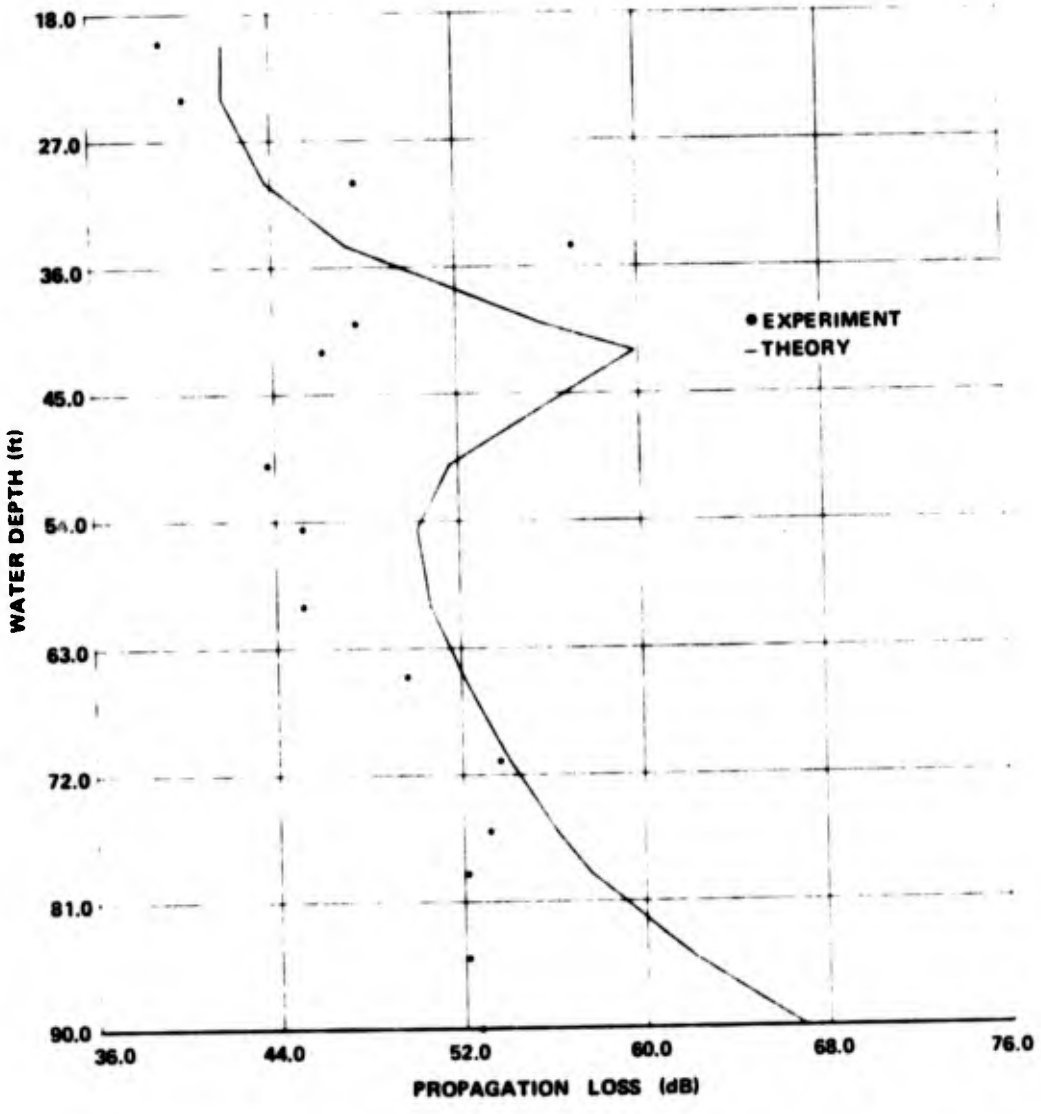

Figure 79. Loss Profile, Cosine Weighting, Comparison Between Experiment and Theory, Range 0.97 nmi, Winter

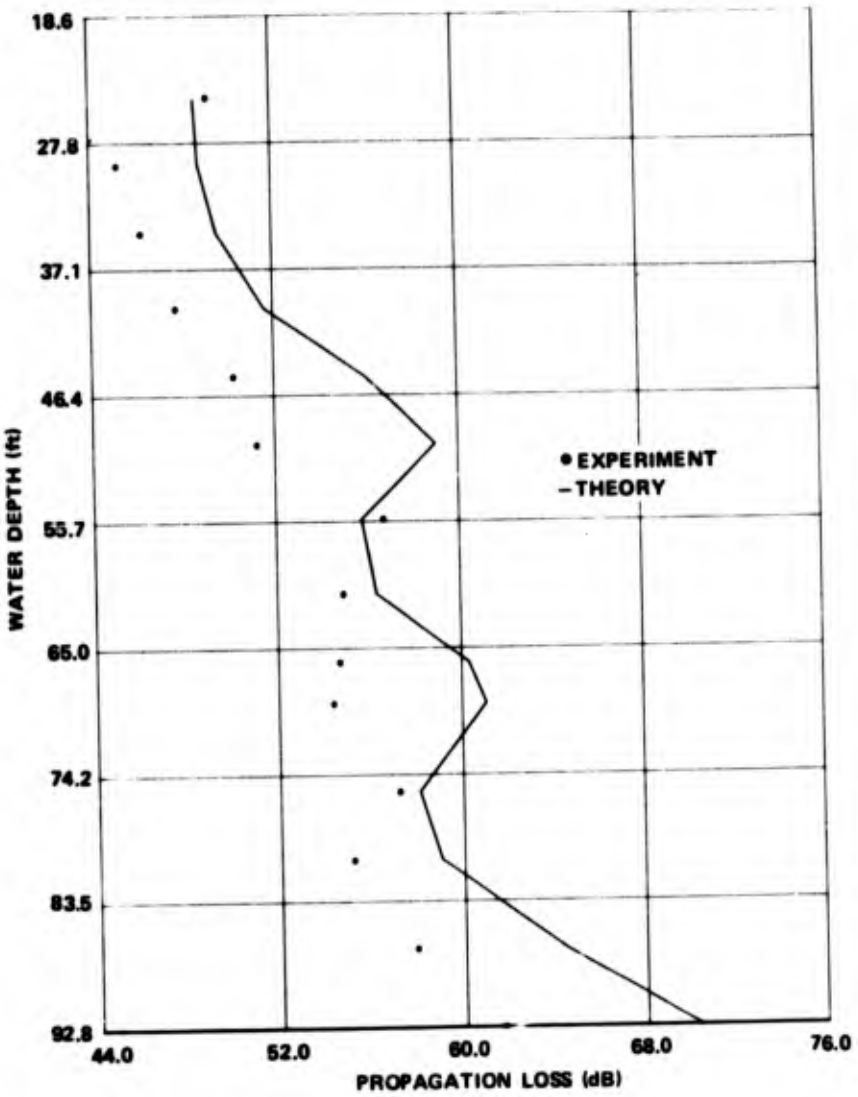

Figure 80. Loss Profile, Cosine Weighting, Comparison Between Experiment and Theory, Range 3.14 nmi, Winter

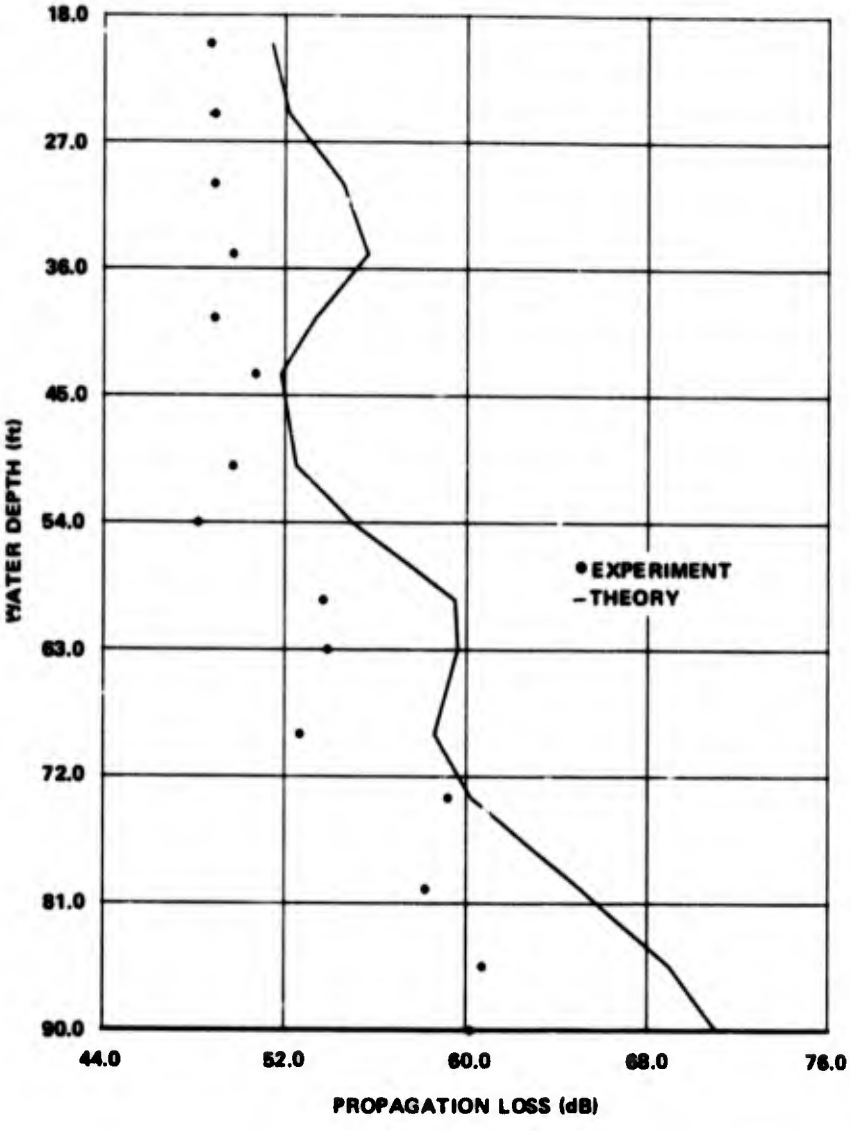

Figure 81. Loss Profile, Cosine Weighting, Comparison Between Experiment and Theory, Range 4.42 nmi, Winter

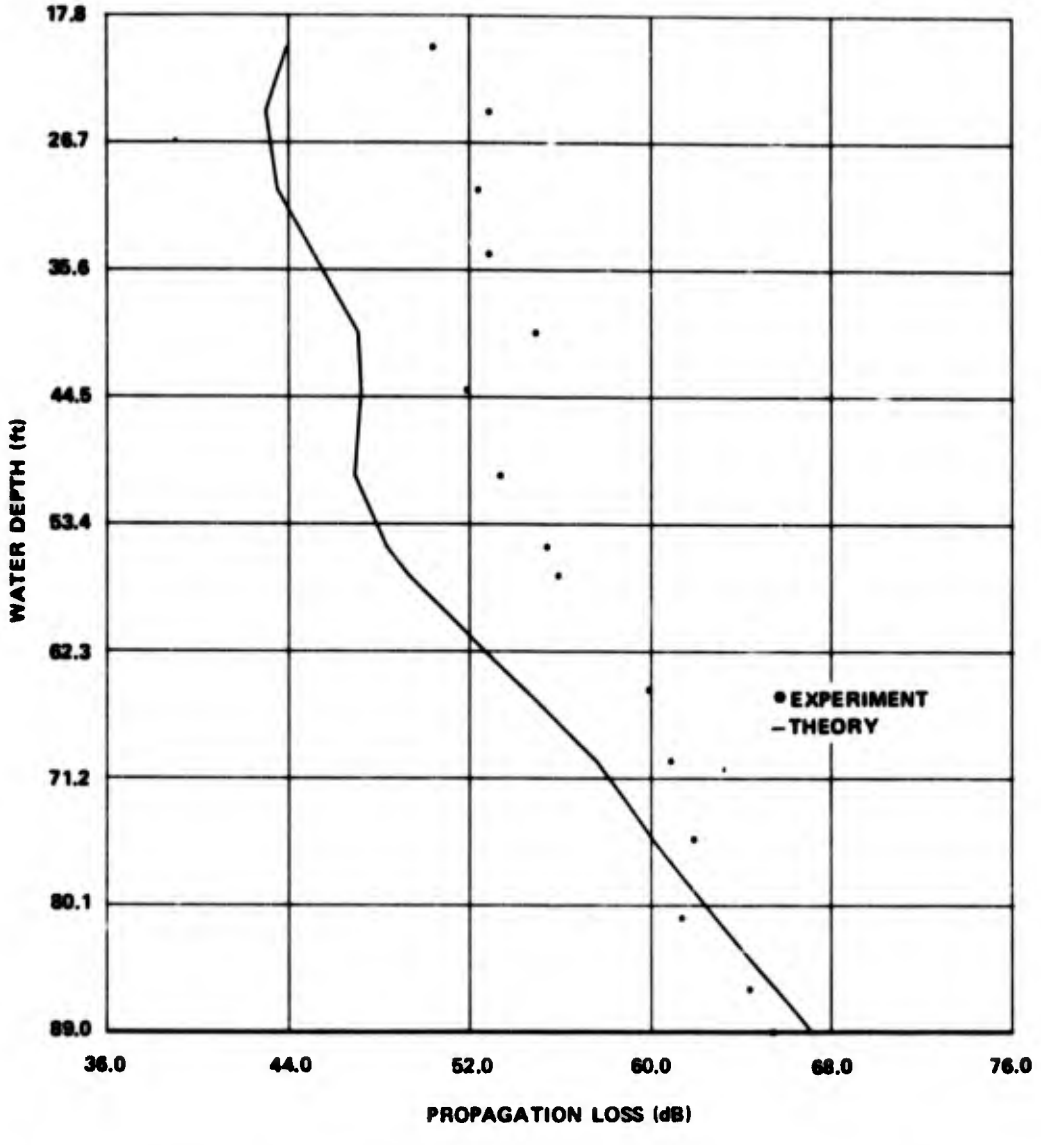

Figure 82. Loss Profile, Steering, Comparison Between Experiment and Theory, Range 0.97 nmi, Winter

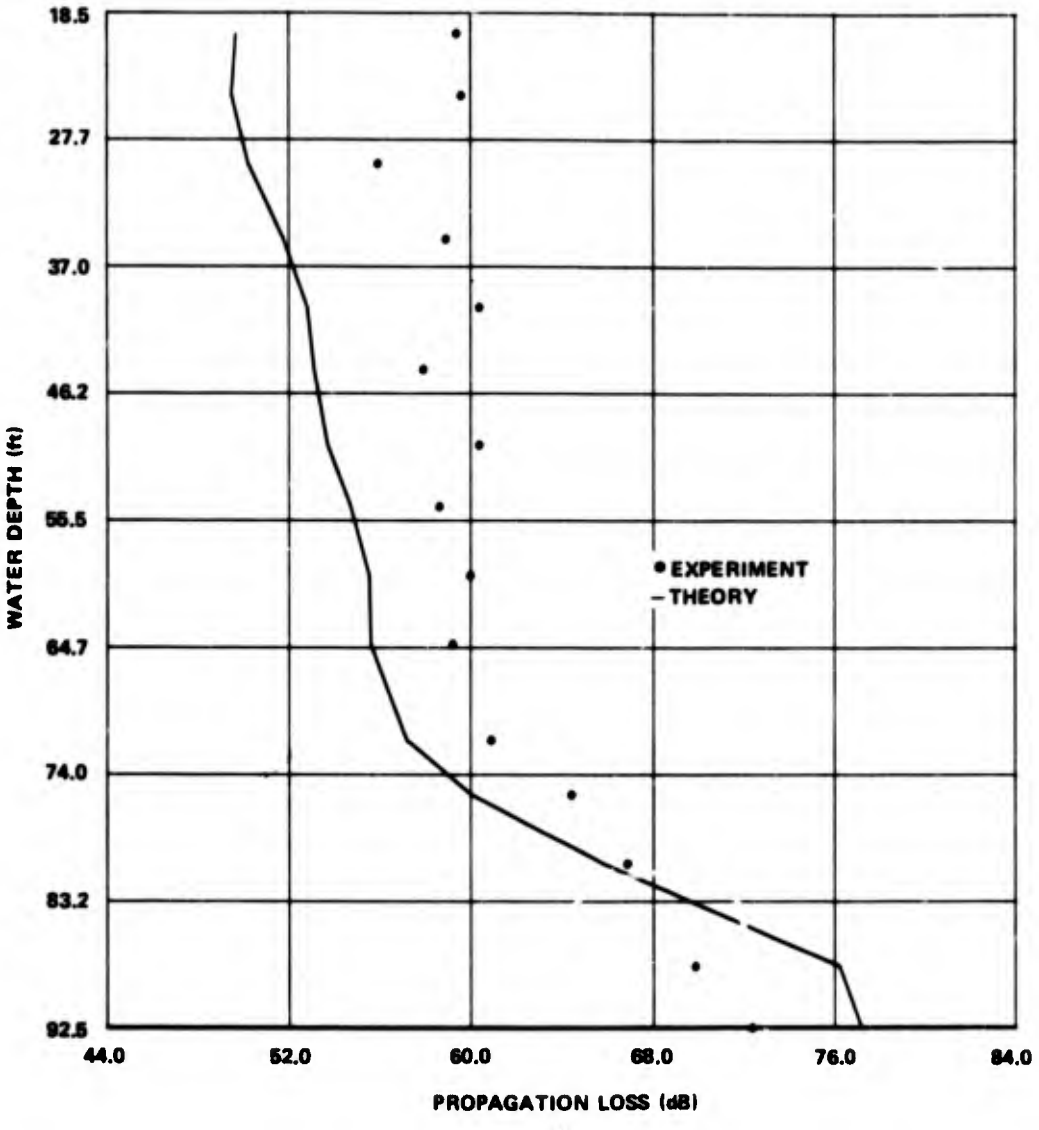

Figure 83. Loss Profile, Steering, Comparison Between Experiment and Theory, Range 3.14 nmi, Winter

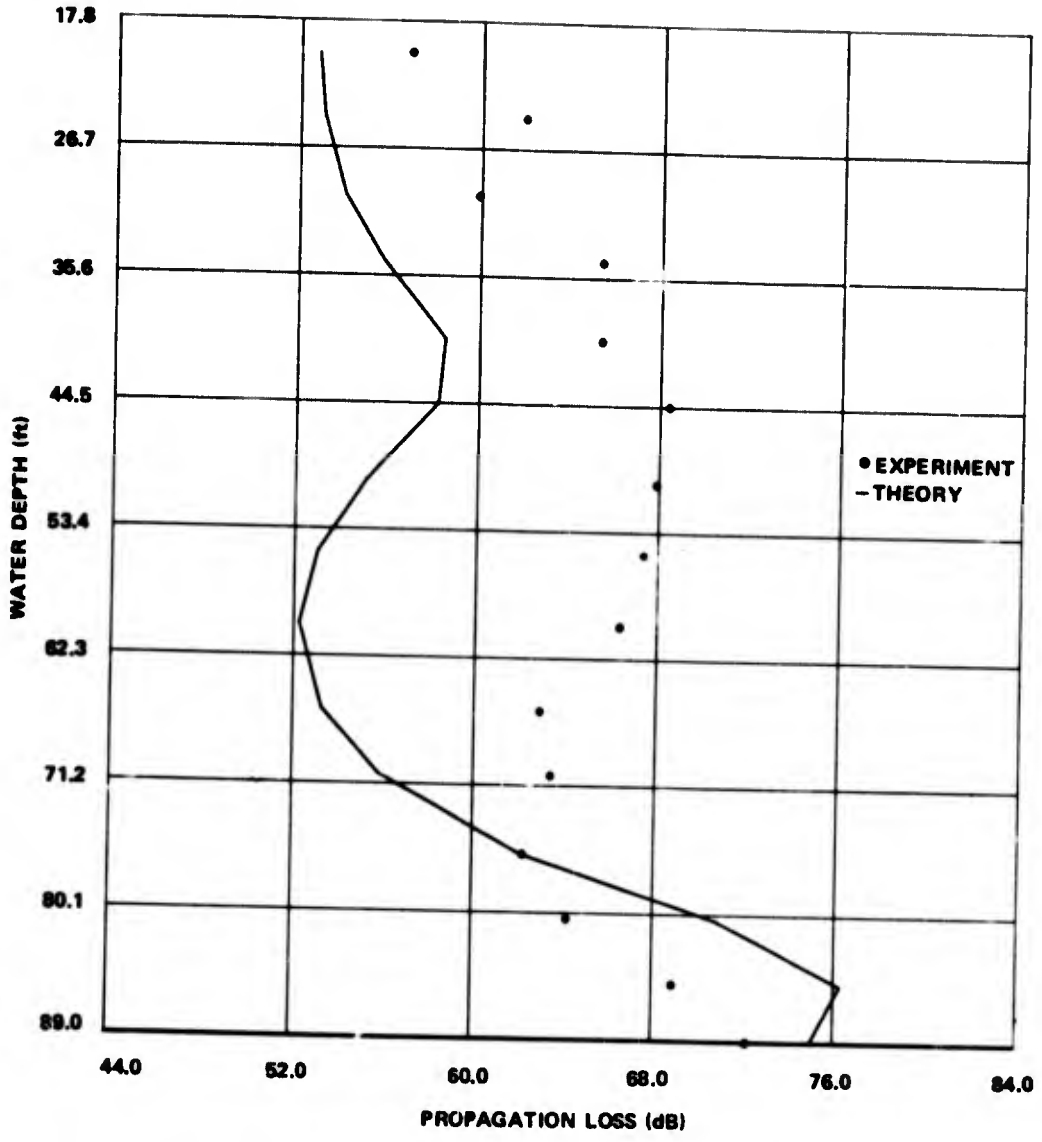

Figure 84. Loss Profile, Steering, Comparison Between Experiment and Theory, Range 4.42 nmi, Winter

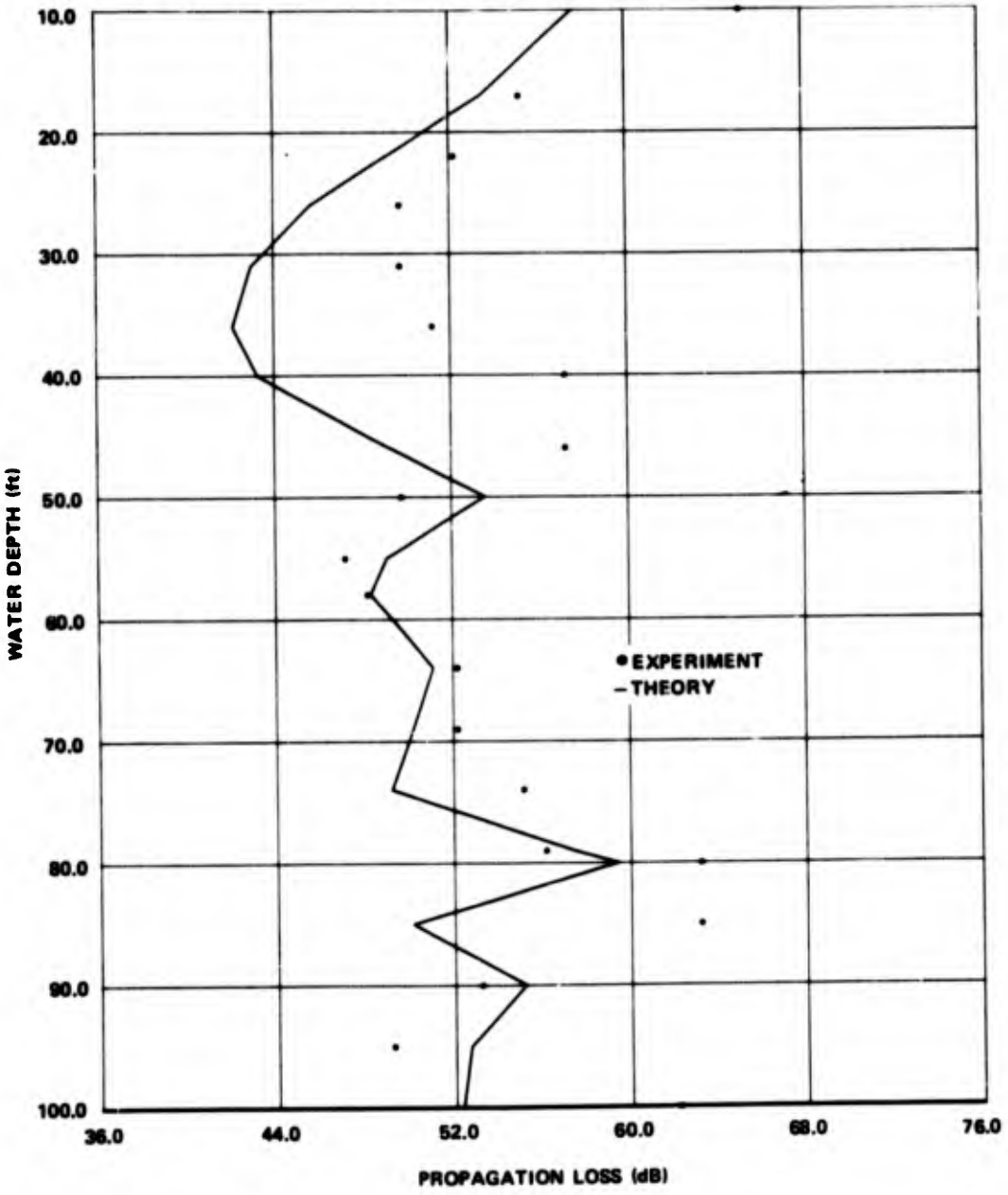

Figure 85. Loss Profile, Comparison Between Experiment and Theory, Range 1.0 nmi, Summer

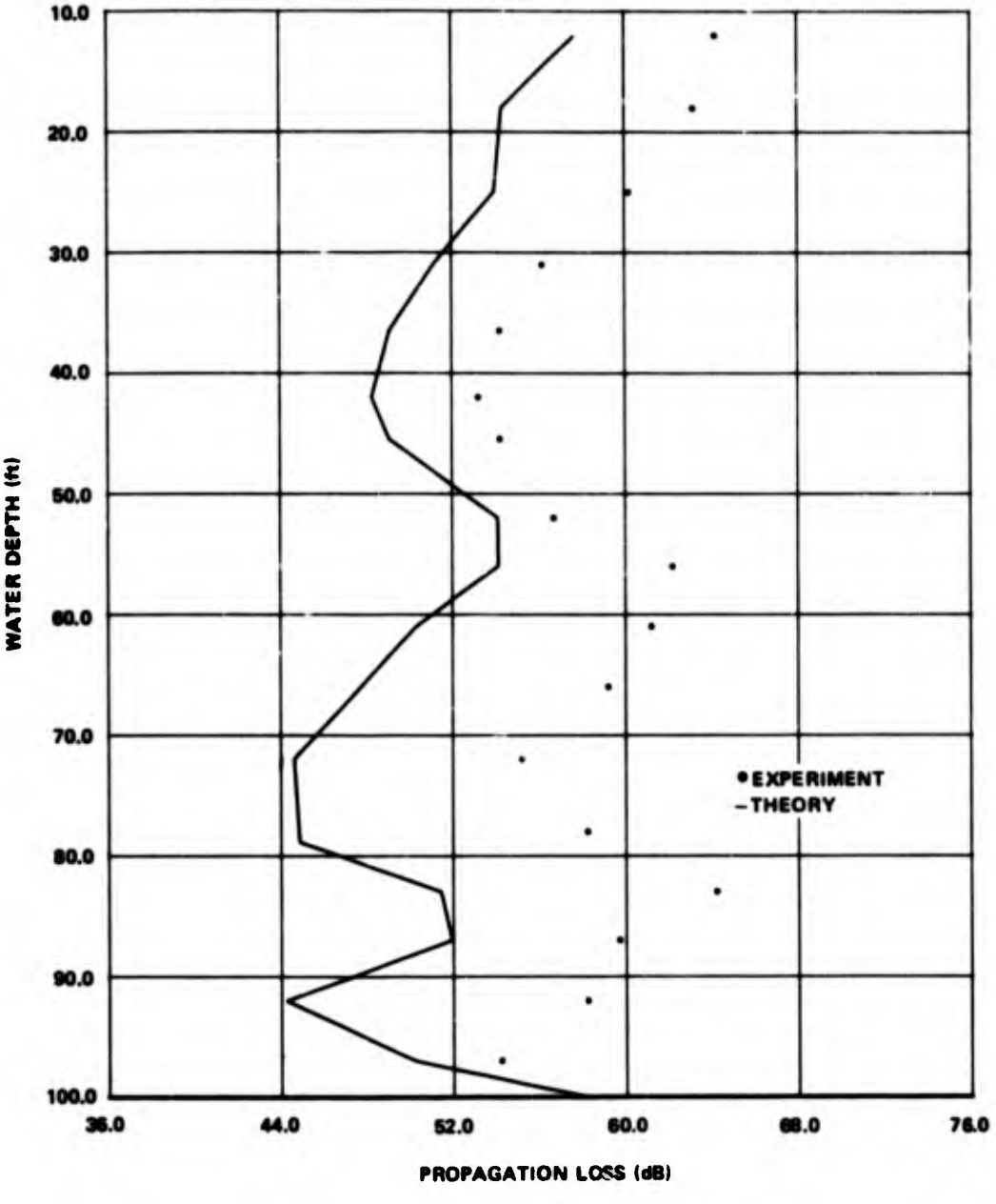

Figure 86. Loss Profile, Comparison Between Experiment and Theory, Range 1.08 nmi, Summer

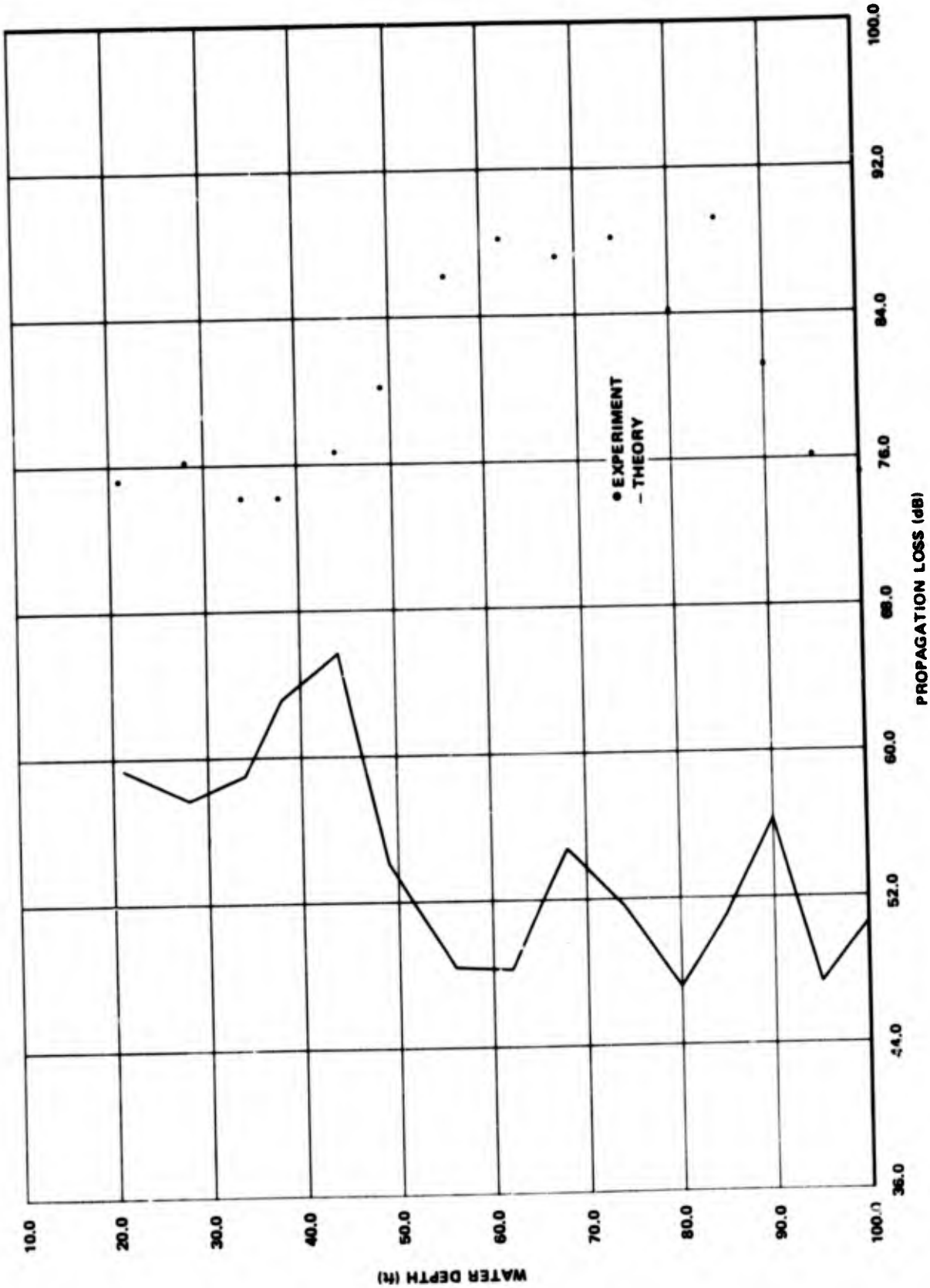

Figure 87. Loss Profile, Comparison Between Experiment and Theory, Range 1.98 nmi, Summer

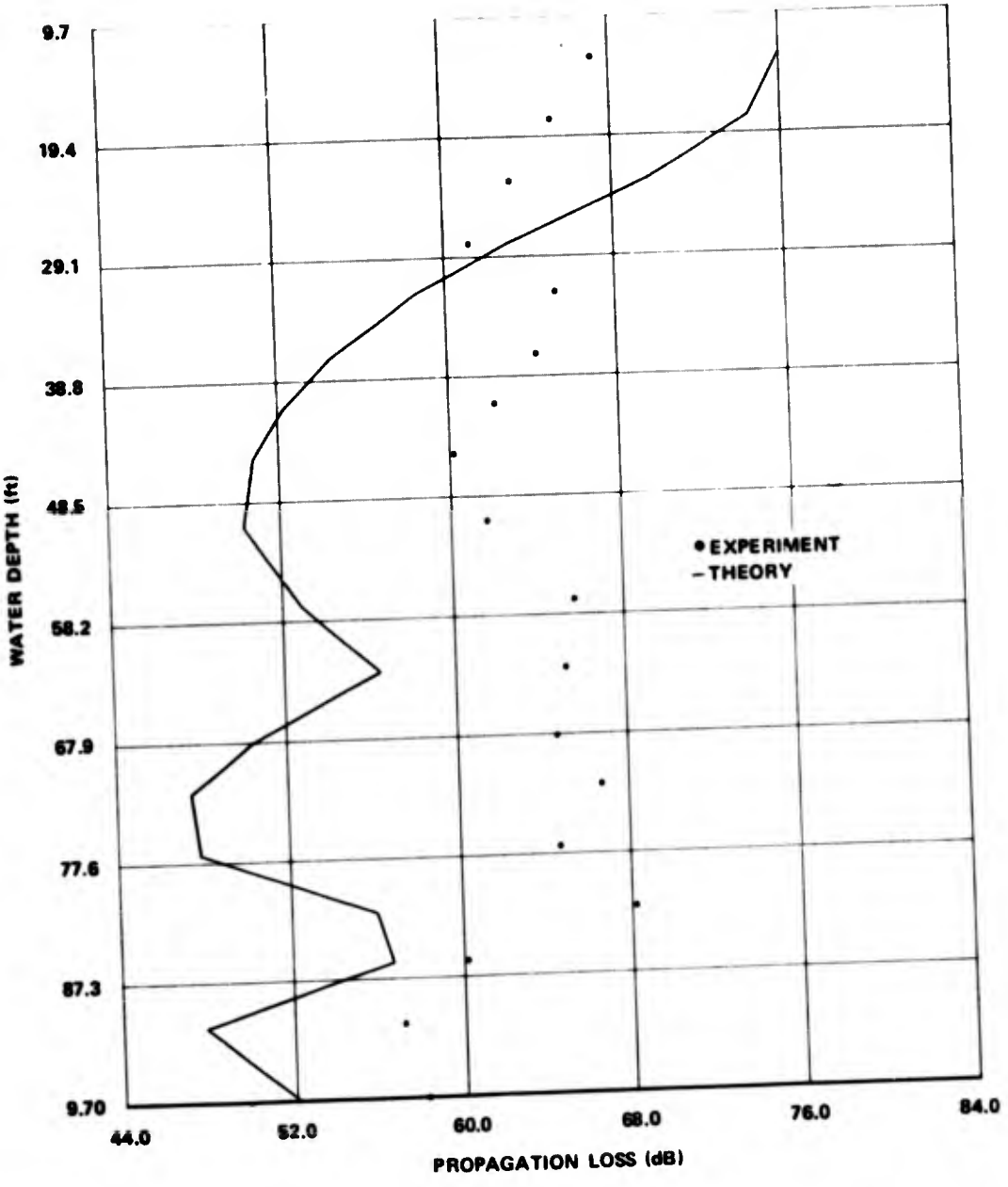

Figure 88. Loss Profile, Comparison Between Experiment and Theory, Range 2.18 nmi, Summer

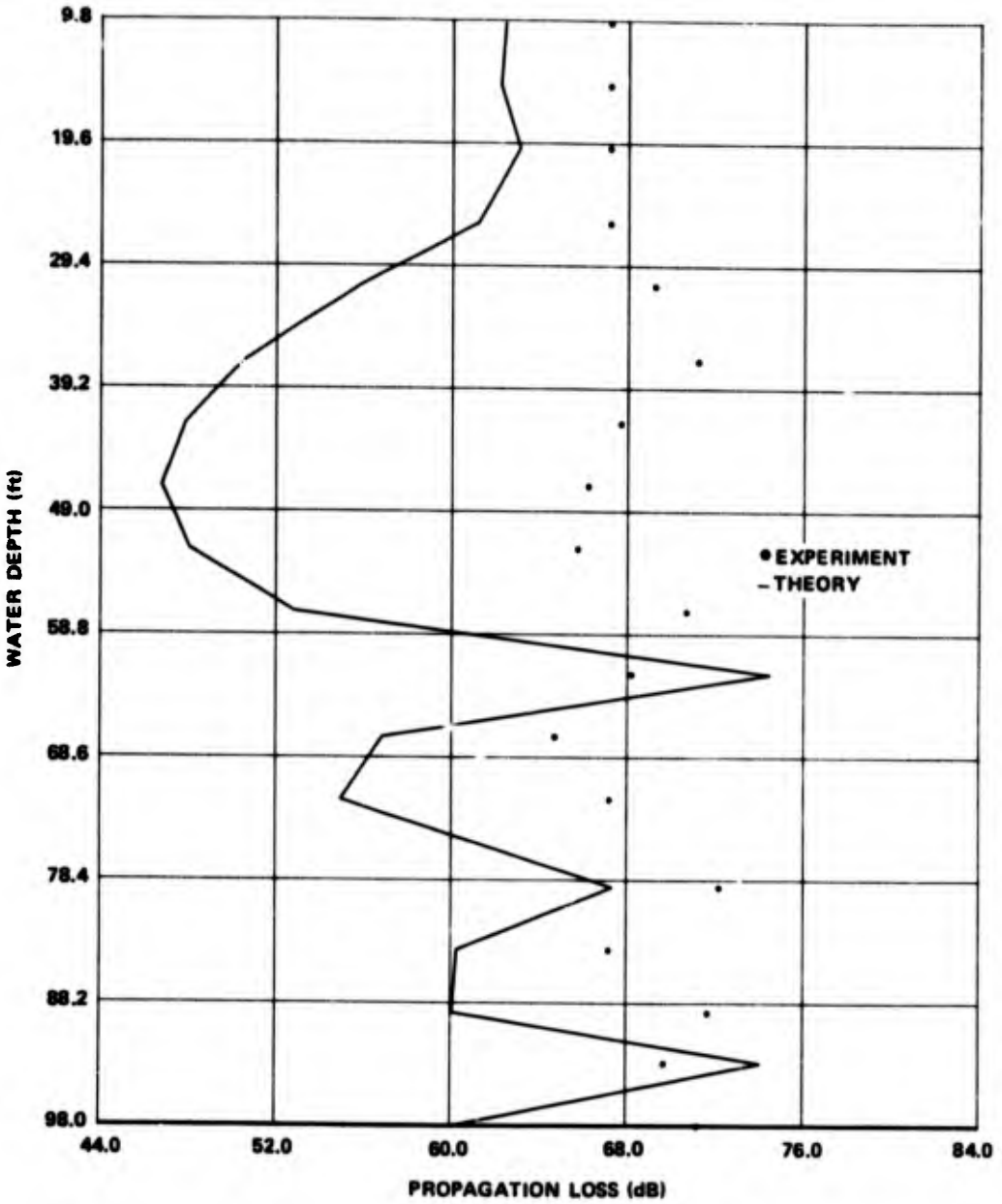

Figure 89. Loss Profile, Comparison Between Experiment and Theory, Range 3.10 nmi, Summer

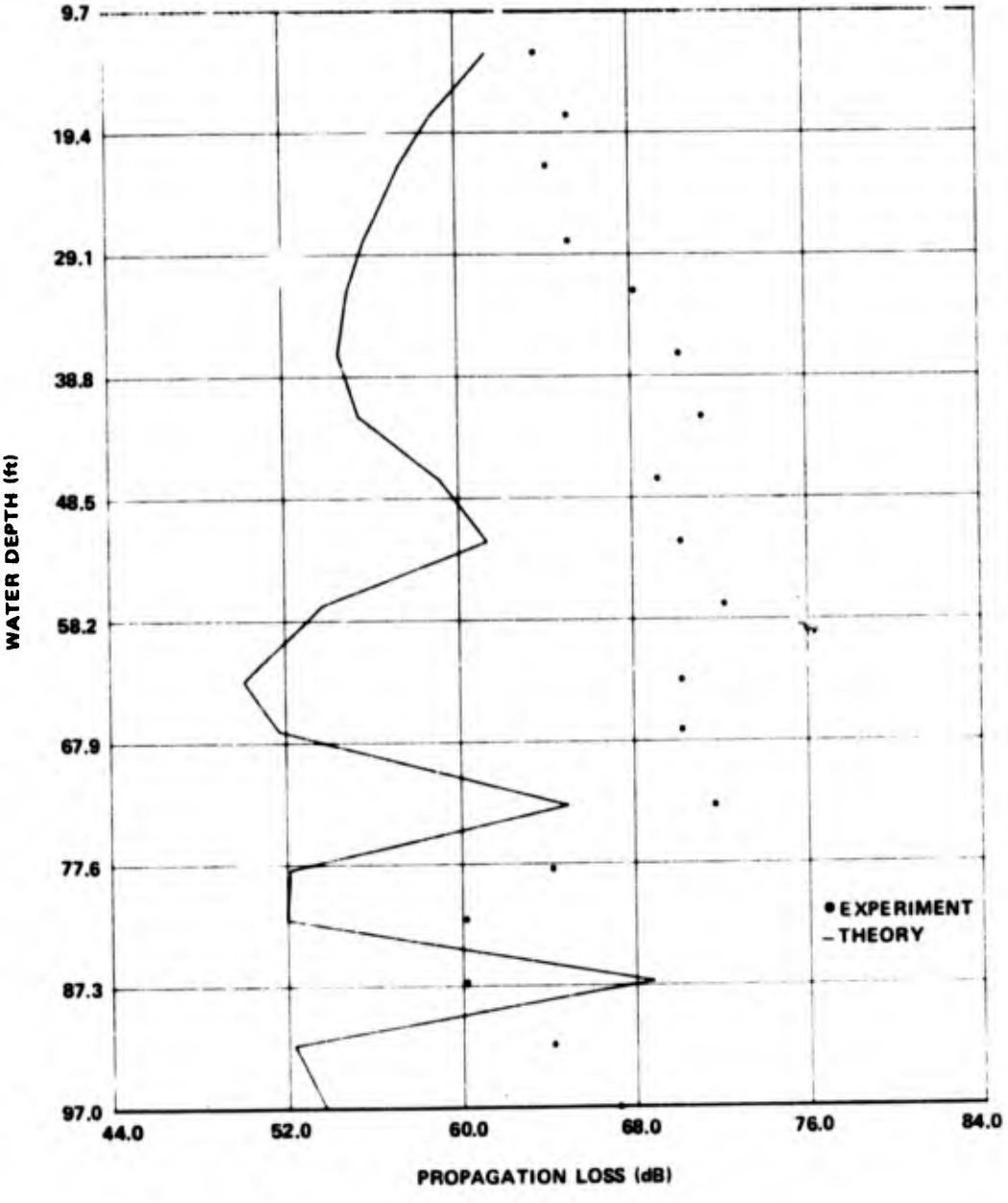

Figure 90. Loss Profile, Comparison Between Experiment and Theory, Range 3.23 nmi, Summer

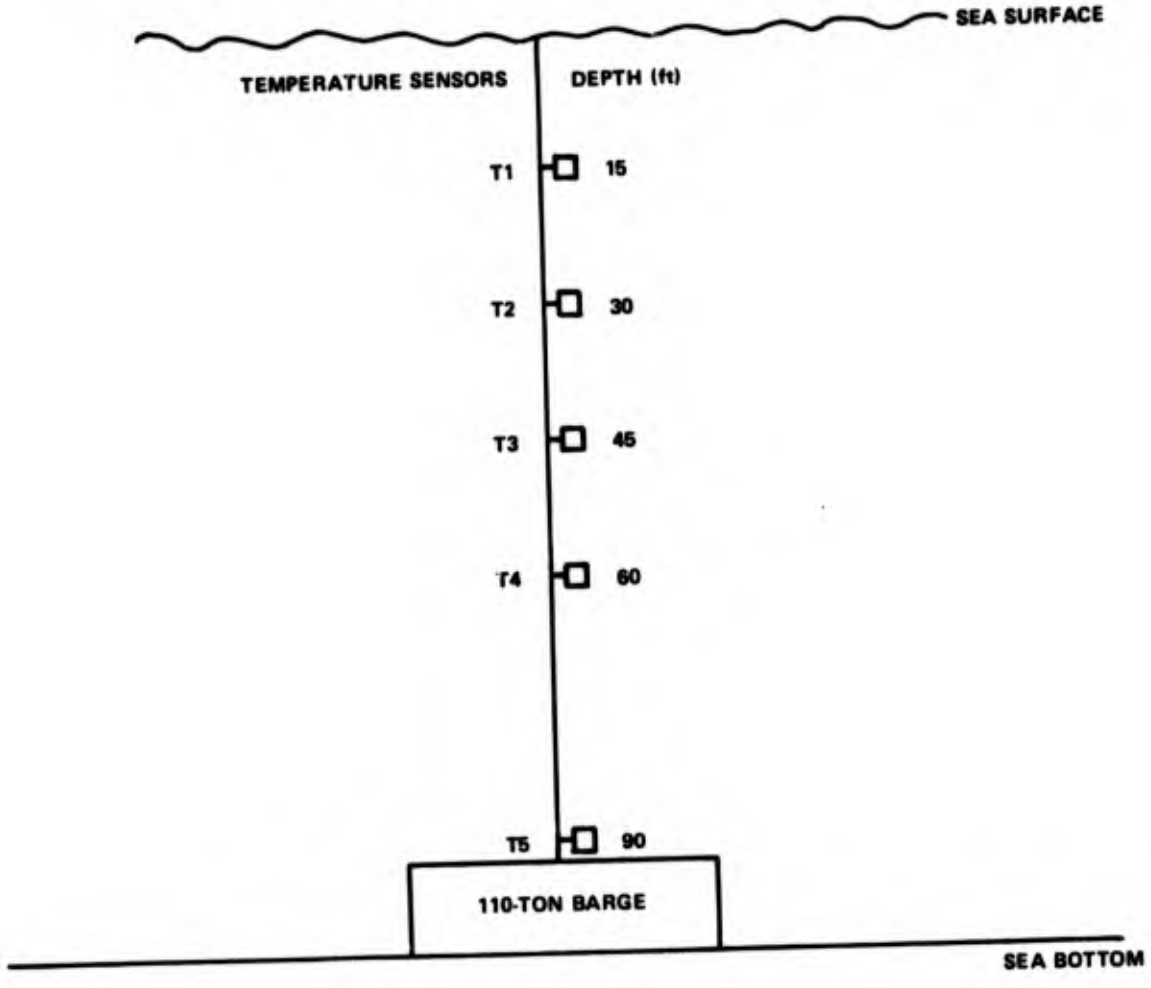

Figure 91. Temperature Sensors on Tower Near Block Island

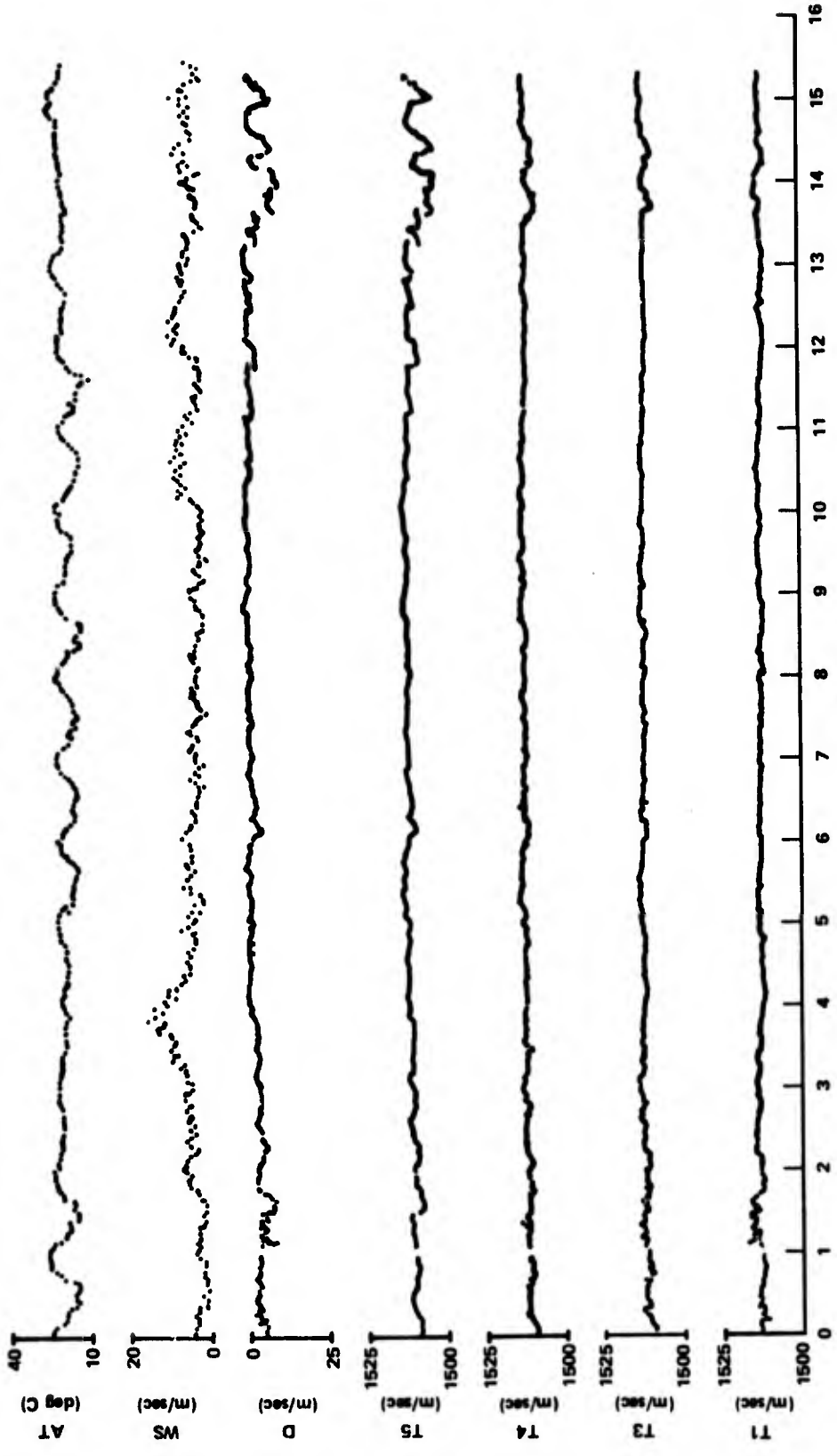

Figure 92. Time History of Oceanographic Measurements, from 1433 on 30 August 1972 to 0942 on 14 September 1972

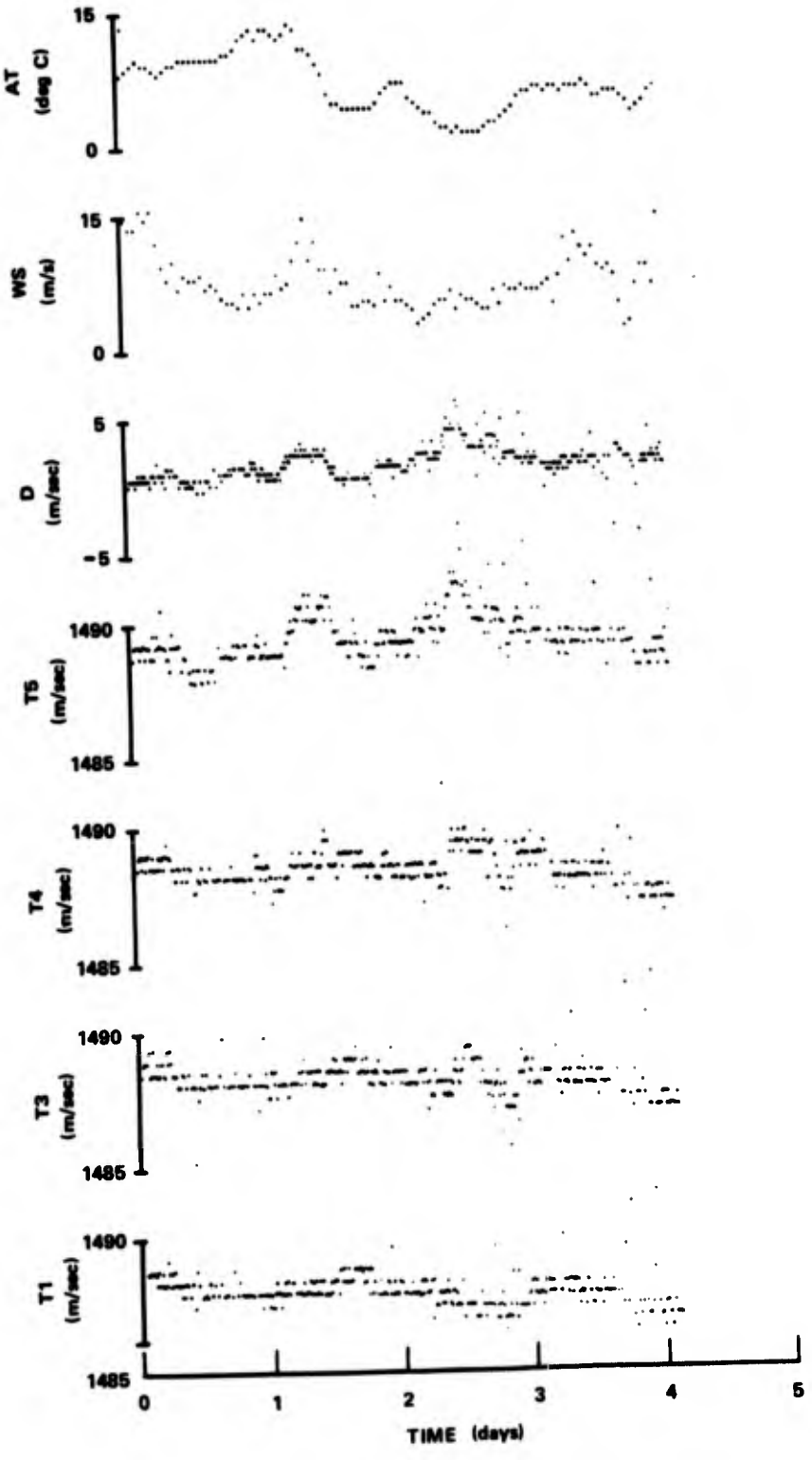

Figure 93. Time History of Oceanographic Measurements, from 1100 on 27 November 1972 to 1210 on 1 December 1972

CONCLUSIONS

Volume I of this report discussed the theory underlying the model presented herein. This volume describes the validation process by which comparisons were made against other models in standard cases and against actual data. At this point someone (probably a nonmodeler) might ask the question, "Do you have a validated model?" An appropriate answer to the question is that, in practice, no underwater acoustic model can ever be validated in any strict sense of the word "validated." This is because comparisons between theory and experiment in ocean acoustics are almost always subjective in nature, and by the nature of the ocean there is always great uncertainty during any test. The classical ideal in an experiment of isolating two parameters is rarely even approached. Although one cannot quarrel with the necessity of following a validation procedure to test a model, it would be naive to think that a definite point could be reached at which one could claim, "This model is validated." It is doubtful that even Barnum would ever make such a claim. The only claim that can be made for this model is that it is useful in a wide variety of ocean environments. In ocean acoustics, this is no small claim!

The strength of the model lies in its ability to predict the sound field, at low frequencies, for very complex situations. The sound field can be predicted for any arbitrary sound velocity profile which can vary with range. The bottom properties such as composition and depth, may also vary with range. The effect of a sloping bottom on propagation and the field caused by backscattering of energy can be determined. Mode conversion can be taken into account in all calculations. The signal transmitted may be assumed to be either CW or pulsed CW of arbitrary length. Propagation can be determined for either a point source to point receiver or determined for an array of transmitting or receiving elements. Information can be obtained so that any array can be weighted so as to enhance individual modes. Finally, the sound field can be calculated for any arbitrary combination of modal components.

However, the model does have several serious weaknesses. First, in extremely complex situations the computer time, hence cost, can become extremely large. One method of reducing the computer time has been proposed in this report. Second, in the model the bottom is approximated as being a semi-infinite, liquid, homogeneous layer. A more complicated multilayered bottom would be particularly useful in predicting propagation at very low frequencies when the bottom layering is known. Finally, the model is strictly deterministic in nature. However, there are situations (reference 31) when a statistical description of scattering is clearly necessary. Since mode conversion is often a scattering-like phenomenon, the inclusion statistically of the effect of material scattering by means of mode conversion would seem to be the next logical, progressive step in the development of the model.

In volume I, the theory was developed for unattenuated modes or equivalently, for the case in which eigenvalues are real. Mode attenuation was included as a small perturbation which did not affect the eigenvalues. Mode conversion effects were calculated by making use of simple orthogonality properties. However, strictly speaking, one should solve for complex eigenvalues. This may yield different

eigenfunctions than when real eigenvalues are assumed. Further, the orthogonality relationships necessary for the mode conversion calculations would be much more difficult to obtain. The exact treatment would require computation of mode conversion effects, using the adjoint mode eigenfunctions. A further approximation in the mode conversion calculations was the neglect of energy converted into the continuous spectrum. Although nothing in the comparisons between theoretical results and measured data has indicated that the approximations used herein are not valid, these difficulties are nevertheless of considerable importance and require more investigation. It therefore remains an open area for future research.

One procedure in the process of model validation is to compare predictions against those of other models in standard cases. This was done for cases in which the stratification was assumed to be constant with range, and agreement was generally excellent. Similar comparisons were not made for cases in which the stratification changed as a function of range, largely because of the unavailability of good standard cases in which the solution is well known for such stratification. There is some work being done on obtaining exact solutions for the geometry of a wedge and, hopefully, in the future similar comparisons can be made for this case.

Another procedure in the process of model validation is to compare predictions against experimental data in a wide variety of environments. Such comparisons were made, and the results were found to be generally encouraging in the assessment of the ability to predict propagation loss as a function of many parameters, such as range and depth. In addition, it was found that parameters of the medium could be determined by using acoustic data and model predictions. Moreover, the model was found to be useful in determining the proper weighting of array elements for the purpose of mode enhancement. However, a large discrepancy, involving data taken in the Baltic Sea, was unresolved and further experiments have been conducted to investigate this problem. In future work, it would be desirable to examine further data for which the stratification of the medium varies with range. In addition it appears desirable to make initial comparisons with data in which a backscattered field is measured, preferably measured separately from the field progressing forward.

REFERENCES

1. C. L. Bartberger and L. L. Ackler, Normal Mode Solutions and Computer Programs for Underwater Sound Propagation, NADC Reports NADC-72001-AE and NADC-72002-AE, 4 April 1973.

2. F. R. DiNapoli, Fast Field Program for Multilayered Media, NUSC Technical Report 4103, 20 August 1971.

3. W. G. Kanabis, Computer Programs to Calculate Normal Mode Propagation and Applications to Analysis of Explosive Sound Data in the BIFI Range, NUSC Technical Report 4319, 6 November 1972.

4. C. W. Spofford, "A Synopsis of the AESD Workshop on Acoustic-Propagation Modeling by Non-Ray-Tracing Techniques 22-25 May, 1973," Washington, D.C., AESD TN-73-05, November 1973.

5. A. V. Newman and F. Ingenito, A Normal Mode Computer Program for Calculating Sound Propagation in Shallow Water with an Arbitrary Velocity Profile, NRL Memorandum Report 2381, January 1972.

6. R. L. Deavenport, 5 February 1975, private conversation.

7. S. McDaniel, 13 January 1975, private conversation.

8. W. G. Kanabis and H. F. Bernier, "Propagation in BIFI Range Using Explosive Sources," NUSL Technical Memorandum 2211-93-68, 25 March 1968.

9. W. G. Kanabis, "BIFI Propagation Tests of 20 January 1968," NUSL Technical Memorandum 2211-185-68, 8 July 1-68.

10. B. Sussman and W. G. Kanabis, "Shallow Water Acoustic Studies," NUSL Technical Memorandum 2211-282-68, 27 November 1968.

11. W. G. Kanabis and H. J. Arens, Determination of Acoustic Parameters Using Normal Mode Theory, NUSC Technical Report 4335, 14 November 1972.

12. W. G. Kanabis and H. J. Arens, Shallow Water Acoustic Tests Using Explosives in the Baltic Sea, NUSC Technical Report 4691, 17 June 1974.

13. W. G. Kanabis and F. R. DiNapoli, "Application of Normal Mode Theory to an Ocean Stratified in Depth and Range," NUSC Technical Memorandum TA11-305-73, 19 October 1973.

14. W. R. Schumacher, "Shallow Water Acoustical Studies: Information Concerning," NUSL Memorandum 2211-18-68, 17 January 1968.

15. D. E. Weston, "Underwater Explosives As Acoustic Sources," Proceedings of the Physical Society, London, August 1960.

16. R. G. Williams, T. Azarovitz, and J. Lamoureux, Seasonal Variations of Temperature and Sound Speed in Block Island Sound, NUSC Technical Report 4131, 30 December 1971.

17. B. Sussman and W. G. Kanabis, The Transmission of 1700-Hz, Acoustic Energy Over the Block Island - Fishers Island (BIFI) Range, NUSC Technical Report 4167, 29 November 1971.

18. B. Sussman and W. G. Kanabis, unpublished data.

19. W. G. Kanabis, Signal Fluctuations in Shallow Water: BIFI 48-Hour Tests, NUSC Technical Report 4441, 10 May 1973.

20. W. G. Kanabis, "Propagation Loss Measurements at 400 Hertz in the BIFI Range Using a Towed Source," NUSC Technical Memorandum 2211-26-71, 27 January 1971.

21. W. G. Kanabis, "Time Smear Analysis of BIFI Signals, "NUSL Technical Memorandum 2211-87-69, 11 April 1969.

22. W. G. Kanabis, "Description of Software of BIFI Automated Data Reduction System," NUSL Technical Memorandum 2211-91-69, 28 March 1969.

23. J. J. Gallagher, "Mass Physical and Acoustic Properties of Subsurface Sediments in Block Island Sound," NUSC Technical Memorandum TA131-62-75 (in preparation).

24. D. A. Quigley, Scientific Analog Data Processing at the Naval Underwater Systems Center, New London Laboratory, NUSC Technical Report 4557, 30 May 1973.

25. O. F. Hastrup and O. V. Oleson, "Sound Propagation in Shallow Water Vol II: Unclassified Papers. Proceedings of a Conference Held at SACLANTCEN on 23-27 September 1974," SACLANTCEN Conference Proceedings No. 14, 15 November 1974.

26. L. A. King, "More Enhancement of Acoustic Signals," NUSC Technical Memorandum TA11-332-74, 15 November 1974.

27. P. E. Seaman, "The Emplantment of the Normal Mode Transmitting Array Tower in Block Island Sound," NUSC Technical Memorandum SA22-456-71, 11 November 1971.

28. L. F. DiRienzo, "Normal Mode Transmitting Array in Block Island Sound," NUSC Technical Memorandum TA12-104-71, 28 June 1971.

29. W. G. Kanabis and J. M. Gorman, unpublished data.

30. N. Amitay, V. Galindo, and C. P. Wu, Theory and Analysis of Phased Array Antennas, Wiley Interscience, New York, 1972.

31. R. H. Mellen, "Sound Propagation in a Randomly Inhomogeneous Medium," NUSC Technical Memorandum PA4-273-73, 2 November 1973.